Universidade Federal Fluminense

Instituto de Física

Programa de Pós-Graduação em Física

Neutron stars and screening mechanisms

Bernardo França de Aguiar

Niterói-RJ

2020

BERNARDO FRANÇA DE AGUIAR

NEUTRON STARS AND SCREENING MECHANISMS

Dissertação de Mestrado apresentada ao Programa de Pós-Graduação em Física da Universidade Federal Fluminense, como parte dos requisitos necessários para a obtenção do Título de Mestre em Física.

Orientadora: Raissa Fernandes Pessoa Mendes

Niterói-RJ

2020

Ficha catalográfica automática - SDC/BIF
Gerada com informações fornecidas pelo autor

D278n De aguiar, Bernardo França
Neutron stars and screening mechanisms / Bernardo França De aguiar ; Raissa Mendes, orientadora. Niterói, 2020.
115 f. : il.

Dissertação (mestrado)-Universidade Federal Fluminense, Niterói, 2020.

DOI: http://dx.doi.org/10.22409/PPGF.2020.m.15992174737

1. Estrelas de Neutrons. 2. Relatividade Geral. 3. Teorias alternativas. 4. Gravitação. 5. Produção intelectual. I. Mendes, Raissa, orientadora. II. Universidade Federal Fluminense. Instituto de Física. III. Título.

CDD -

Bibliotecário responsável: Sandra Lopes Coelho - CRB7/3389

Contents

Resumo

Teorias modificadas de gravitação que oferecem modelos viáveis para energia escura frequentemente se baseiam em mecanismos que escondem ou *blindam* seus efeitos em ambientes com densidades altas. Nesse trabalho, nós exploramos o fato de que, em teorias tensor-escalar, o grau de liberdade escalar não se acopla diretamente à densidade de massa, mas ao traço do tensor de energia-momento e investigamos se pode haver uma falha parcial da blindagem dentro das estrelas de nêutrons mais compactas encontradas na natureza.

Palavras-chave: Blindagem. Estrelas de nêutrons. Testes da Relatividade Geral.

Abstract

Modified theories of gravity that offer viable models for dark energy often rely on mechanisms that screen their effects in high density environments. In this work we explore the fact that in scalar-tensor theories the scalar degree of freedom does not couple to the mass density alone, but to the trace of the energy-momentum tensor and investigate whether there could be a partial unscreening of the scalar field inside the most compact stars found in nature.

Keywords: Screening. Neutron Stars. Tests of General Relativity.

Chapter 1

Introduction

Neutron stars are the densest stellar objects found in the Cosmos, besides black holes and hypothetical exotic objects. They result from the supernova explosion of a massive star, which had a total mass of more than about 10 solar masses, combined with the gravitational collapse that compresses the core past white-dwarf densities to that of atomic nuclei. Assuming that the star is composed only of neutrons supported by their degeneracy pressure (a phenomenon described by the Pauli exclusion principle, just as white dwarfs are supported against collapse by electron degeneracy pressure), other baryonic elements may be present in its composition, such as pions, kaons, meson condensates and other hyperons [1]. Neutron stars are also expected to exhibit different phases of superfluidity/superconductivity. Additionally, the gravitational energy of a neutron star is of the order of its rest energy, which means that the gravitational field of these objects is necessarily determined in the relativistic context, where the effects of space-time curvature must be taken into account.

Neutron stars are extreme objects. They can be a few times more massive than the Sun, but with radii of only 10 - 20 km. The high densities of neutron stars result in a very high surface gravity, with typical values 10^{11} times greater than that of the Earth. To imagine how extreme the situation is: neutron stars have an escape velocity that varies from one third to half the speed of light. Moreover, as the nucleus of a massive star is compressed and collapses into a neutron star, it retains most of the star's angular momentum. However, as it has only a tiny fraction of the radius of its progenitor star, typically a neutron star will have a very high rotation speed. Neutron stars are known to have rotation periods of about 1.4 ms to 30 s [2].

Besides helping to constrain models of nuclear matter composition, knowledge of neutron star mass-radius relations, oscillation modes, moments of inertia, tidal deformabilities, populations, etc., could also help to constrain modified theories of gravity in the most extreme conditions, an interesting possibility that is the subject of the present work.

Although General Relativity is well tested in various situations, there exist several theories that modify it. Like any physical theory, these modified theories of gravity must be tested in order to investigate whether they are viable or not. From a more philosophical point of view, modifying General Relativity is justified if we assume that Nature is not a lottery when talking about the possible ways to describe it; obviously the way we describe it is irrelevant to Nature itself, however, there may be different ways of describing the same physical phenomenon. From an observational point of view, the existence of mysterious dark components that have not yet been directly detected justifies modifications such as MOG [3], which aims to describe the effect of dark matter on the dynamics of galaxies, and Quintessencia [4], which aims to describe the effects of the hypothetical dark energy responsible for the accelerated expansion of the universe. From a theoretical point of view, the lack of a complete quantum gravity theory leads to attempts to alleviate the problem of quantization of gravity by adding other fields and curvature terms to the theory [5]. It is hoped that with the evolution of experiments, such as the detection of gravitational waves, it will be possible to test more accurately these theories and to discard them or not.

Among the multiple ways to modify General Relativity, one of the simplest ones is to introduce additional scalar degrees of freedom, in the so-called scalar-tensor theories [6]. Mechanisms that allow scalar-tensor theories to evade solar system tests, but still display the correct cosmological behavior are called screening mechanisms [7]. Many of the models of screened modified gravity are constructed in such a way that the scalar field minimizes the effective potential that governs its evolution, and explore the consequences that arise when this occurs. In this work, we will deal with two models that present this mechanism: Dilaton [8] and Chameleon [9]. The screening mechanism in the Chameleon model is implemented through the effective mass of the scalar field, which varies with the local density, in such a way that in dense locations the effective mass is large, making the force associated with the field very short-ranged, and therefore not observable, while in the rarefied cosmological scales, the mass is small and the field mediates a long-range

interaction. In the Dilaton model, the mechanism is performed through the effective coupling with matter, which also varies with local density and is very small in dense regions, masking the effect of the force associated with the scalar field.

Once a model presenting a screening mechanism is tuned to general relativity for typical solar system densities, naively one could think that no new phenomenology would arise in much denser environments, such as neutron stars. However, in a relativistic scenario the scalar field equation actually implies a coupling to the trace T of the energy-momentum tensor of matter fields, and not to the mass density alone. For a perfect fluid, $T = 3p - \epsilon$, where p is the pressure and ϵ is the energy density. For non-relativistic matter, $\epsilon \gg p$, and $T < 0$. However, it is conceivable that inside the most compact neutron stars found in nature, a pressure-dominated core, with $3p > \epsilon$, might form [10]. One of the aims of this work is to study how screening mechanisms behave in such ultra-dense regions, and how the presence of the scalar field alters the structural properties, such as mass and radius, of neutron stars. We also study, through radial perturbations, how the scalar field alters the stability of such stars. The original results from this thesis were published in the paper Physical Review D **102**, 024064 (2020) [11].

The thesis is organized as follows. In Chapter 2, an introduction to general relativity and its foundations is presented. We also discuss tests on the solar system and challenges in cosmology, introducing the possibility of using new degrees of freedom, such as the scalar field, to describe the universe. In Chapter 3, ways of modifying General Relativity are presented, we briefly introduce some modified theories of gravity and their consequences, and later discuss scalar-tensor theories in the Jordan and Einstein frames. Finally, we explain the screening mechanism present in the Chameleon and Dilaton models. In Chapter 4 the equations that govern the hydrostatic equilibrium of relativistic stars are derived and integrated numerically; after that, the stability of neutron stars under radial perturbations is studied. Finally, conclusions are drawn in Chapter 5.

Chapter 2

General Relativity

Among many trials and errors, the theory of General Relativity was developed by Albert Einstein between 1907 and 1915. After his work on Special Relativity, Einstein began to seek a new formulation for gravity that would incorporate the principles of relativity. It is widely considered to be one of the most successful intellectual achievements of all times, derived from solid principles, even today it is capable of describing many aspects of gravitational physics. The objective of this chapter is, first, to introduce the fundamental blocks on which the theory of General Relativity is built, such as Einstein's Equivalence Principle, which paved the way for a new interpretation of the nature of gravity, now reinterpreted not as a force but rather as a manifestation of space-time geometry. Second, it discusses tests on the solar system, which not only General Relativity, but any other theory of gravity must pass, introducing also the Parametrized Post-Newtonian formalism, which gives a consistent structure for studying the effects of gravity on the solar system scale. Finally, we give a brief overview of the standard cosmological model, and introduce the possibility of modifications that add a new degree of freedom commonly used to describe the behavior of the universe on a large scale.

2.1 Foundations

Newton's theory of gravitation, the first mathematical description of gravity, can be summarized in two differential equations, one describing the movement of bodies in the gravitational field and the other describing the gravitational field itself:

$$m\ddot{\vec{x}} = \vec{F} = -m_g \vec{\nabla}\phi, \tag{2.1}$$

$$\nabla^2 \phi = 4\pi G\rho, \tag{2.2}$$

where G is the gravitational constant, ϕ is the gravitational potential, ρ is the mass density, m denotes the inertial mass, and m_g denotes the gravitational mass.

Although successful, in 1845, Le Verrier found a small discrepancy between the precession rate of Mercury's perihelion and the prediction of Newton's theory, even after taking into account the effect of the orbits of other planets. Many argued [12] that the existence of a small planet, called Vulcan, was the source of the discrepancy and not some unknown modification of Newton's theory, but such planet has never been observed [13].

One could, at first, modify Newton's theory by adding $1/r^n$ terms to the gravitational potential [14], such that

$$V_{\text{eff}}(r) = \frac{Gm_g}{r}\left[1 + \sum_{n=1}^{\infty} g_n \left(\frac{R}{r}\right)^n\right], \tag{2.3}$$

where the constants g_n and R can be fixed by experiments or by requiring that the theory fits the observable Mercury's perihelion precession. Knowing that the inverse square law is approximately correct and that Mercury's perihelion precession is very small, R must fix the modification scale to be much less than Mercury's orbital radius around the Sun. If the second option to fix the free constants is chosen, a $1/r^2$ modification predicts the perihelion precession of Venus and the Earth in good agreement with observations, however a $1/r^3$ modification is unsuccessful in doing the same [14].

Such *ad hoc* modifications may be able to solve the perihelion problem, but Newton's gravity is still an "action at a distance" theory. The gravitational field propagates instantaneously to every point in space. The concept of "action at a distance" is forbidden after the advent of Special Relativity. There is no absolute motion nor absolute space [15].

An important empirical fact is that the inertial mass m and the gravitational mass m_g are the same. Galileo [16], Newton [17] and several others (see Refs. [18, 19, 20, 21] for examples) proved through experiments, with good precision, the so-called Weak Equivalence Principle (WEP). The violation of WEP, which would occur if some

degree of freedom, for example a mysterious field coupled to matter, contributes differently to the inertial mass than the gravitational mass, can be parametrized by the Eötvos parameter η which measures the difference in free fall acceleration for two bodies of different compositions:

$$\eta = \frac{2|a_1 - a_2|}{|a_1 + a_2|}. \tag{2.4}$$

The best current bound comes from the Eöt-Wash EP-experiment and reads $\eta < 10^{-13}$ [22, 23]. Newton's theory would be perfectly consistent if these masses were different, but this result says something more profound; equality between inertial and gravitational masses suggests a close relationship between gravity and inertia [24].

The Weak Equivalence Principle implies that the motion of free particles in a gravitational field is independent of their masses. Therefore, it is impossible to distinguish between gravity and a uniformly accelerated frame in a small enough region of spacetime. In larger regions of spacetime there will be inhomogeneities in the gravitational field, which will lead to tidal forces that can be detected. Inertial forces can be eliminated if we choose an inertial frame of reference, gravity can also be eliminated, at least locally, if we describe the movement from the point of view of a free-falling observer.

Moreover, mass lost some of its uniqueness as it became clear that mass was simply a manifestation of energy and momentum. Since gravity couples to masses, this mass-energy relation suggests that gravity couples not only to matter but to energy too.

These ideas are condensed into the Einstein Equivalence Principle (EEP), created after Einstein had the famous "happiest thought of my life". Consider the following situations:

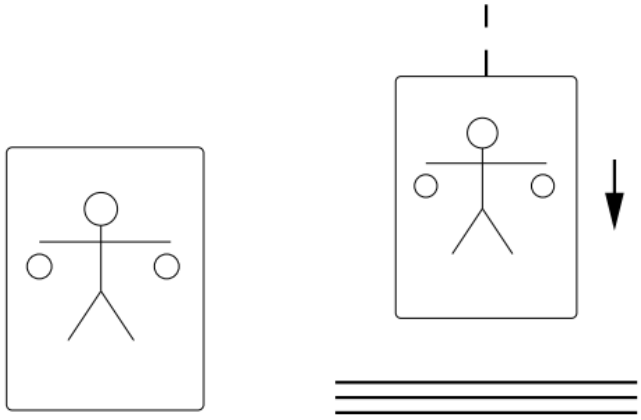

(a) (b)

Figure 2.1: (a) Someone in a small box in space, away from any content of matter, free from the action of any force. This person floats and when he releases two masses, both will remain floating next to him. (b) Consider that such a box is placed in free fall in a homogeneous and constant gravitational field. The person would float along with the two masses, he doesn't feel any force.

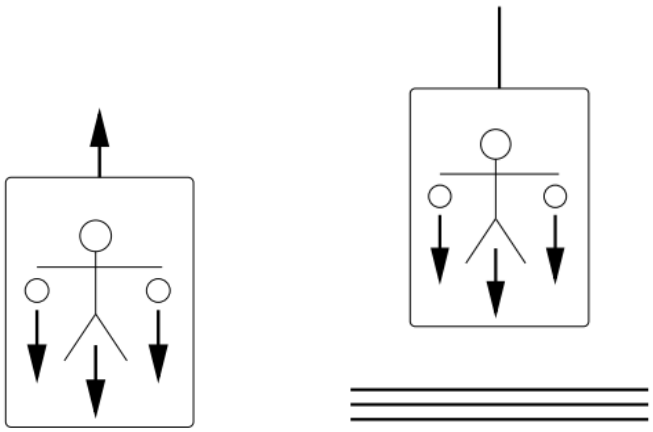

(a) (b)

Figure 2.2: (a) Assume that the box is constantly accelerated upwards. Then, it is obvious that the person will be pressed on the floor of the box with a constant force, and he will see the two masses, which previously floated, fall towards the floor. (b) Consider the same box, but placed stationary in a gravitational field, again the person will be constantly pressed on the floor of the box, in addition to this he will also see the masses falling towards the ground. No experiment can be done inside the box in order to distinguish whether the effects are occurring due to a gravitational field or due to a constantly accelerating movement.

This thought experiment, in other words, can be formalized as follows:

The inertial and gravitational masses are equal and the result of any local non-gravitational experiment in a free-falling frame is independent of the frame's velocity (Lorentz's invari-

ance) and its location in space-time, locally we recover the same laws of special relativity.

The EEP was later extended to contain not only non-gravitational experiments but gravitational experiments as well (in what is called the Strong Equivalence Principle - SEP).

If an accelerated frame can be described as a frame at rest under the action of a gravitational field, and if the laws of nature do not change in the presence of a gravitational field, then there is no reason for a distinction to be made between accelerated frames and inertial frames when the task is to describe nature. The laws of physics are the same for all observers. Now, laws of physics must be written in terms of quantities that are invariant by general coordinate transformations, these objects are tensors.

Even before fully formulating the general theory of relativity, it is possible to predict some effects that the complete theory will have.An example is the deflection of light by massive objects. Consider an observer in an inertial frame and another in an accelerated frame. When sending a beam of light from one point to another, the beam will remain in a straight line for the observer in the inertial frame, while the accelerated observer will see the beam of light being deflected. By the EEP, this effect can then be reinterpreted, but this time understanding that the accelerated observer is actually under the action of a gravitational field. Therefore, in a gravitational field, light must also deflect.

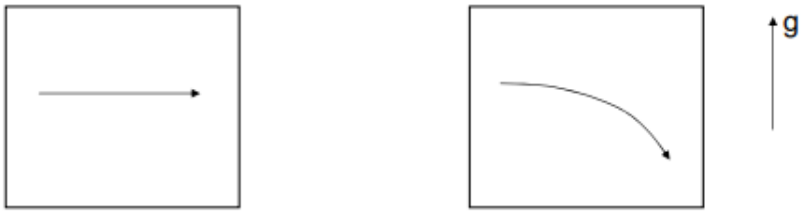

To calculate the magnitude of such an effect, the non-relativistic limit of the geodesic equation can be used, but the value found is half the observed [15]. In order to get the right result, the EP is not enough, the field equations of General Relativity must be used.

Generalizing Newtonian theory taking into account all the previous information is by no means an easy task. One of the first attempts, made by Gunnar Nordström [25], involves generalizing the Poisson equation to

$$\Box\phi = -4\pi GT,$$

$$\frac{\mathrm{d}u_\mu}{\mathrm{d}\tau} = -\partial_\mu \phi,$$

where the Newtonian potential was promoted to a scalar field ϕ and T is the trace of the energy-momentum tensor. This class of scalar theories is well known and studied, the field equations appear to be consistent, however, the constancy of the speed of light implies that the gravitational field should be constant [25].

Nordström tried other modifications, such as

$$\phi \Box \phi = -4\pi G T,$$

$$\frac{\mathrm{d}u_\mu}{\mathrm{d}\tau} = -\partial_\mu \ln \phi - u_\mu \frac{\mathrm{d} \ln \phi}{\mathrm{d}\tau}.$$

Both Nordström's theories satisfy the WEP. However these theories fail to predict the deflection of light passing near a massive body, moreover the second theory predicts an anomalous perihelion precession of Mercury, which disagrees in both sign and magnitude with the observed anomalous precession [26]. Nonetheless, it can be reinterpreted geometrically, which simplifies its structure and resembles the result in which Einstein's work culminated. Einstein showed [27] that the equations of motion could be derived from the geodesic equation

$$\frac{\mathrm{d}^2 x^\mu}{\mathrm{d}\tilde{\tau}^2} + \Gamma^\mu{}_{\alpha\beta} \frac{\mathrm{d}x^\alpha}{\mathrm{d}\tilde{\tau}} \frac{\mathrm{d}x^\beta}{\mathrm{d}\tilde{\tau}} = 0,$$

using a line element of the form $\mathrm{d}s^2 = \phi^2 \eta_{\mu\nu} \mathrm{d}x^\mu \mathrm{d}x^\nu$ where $\Gamma^\mu_{\alpha\beta} = \partial_\alpha \phi \delta^\mu_\beta + \partial_\beta \phi \delta^\mu_\alpha - \eta^{\mu\kappa} \partial_\kappa \phi \eta_{\alpha\beta}$, $\mathrm{d}\tilde{\tau} = \phi \mathrm{d}\tau$ and $\tilde{u}_\nu = \phi u_\nu$. The gravitational field equation takes a interesting form:

$$R = 24\pi G \tilde{T},$$

where $R = -6\phi^{-3} \Box \phi$ is the Ricci scalar computed from the metric above and $\tilde{T} = T/\phi^4$. Although this theory was invalidated by conflicts with observations, it resembles Einstein's results, therefore, it is interesting to question whether such a theory may have influenced the formal and conceptual construction of General Relativity [28].

Using the equivalence principle when investigating the motion of free particles in an accelerated frame it is possible to conclude that gravity can be incorporated into the geometry of space-time. The Christoffel symbols represent the pseudo-force felt by a free

particle in the accelerated frame, and by the equivalence principle, the "gravitational force" felt by a particle in a gravitational field. The metric is the candidate to generalize the gravitational potential. Further investigation shows that the presence of the gravitational field implies a non-Euclidean geometry, since the curvature tensor is not zero. It is known that free particles move through geodesics; in a flat space initially parallel geodesics remain parallel, but that is not the case in a curved space. If acceleration and gravity were globally equivalent, the effect of geodesic deviation would not be seen: in an accelerated frame the relative separation between test particles is unchanged if their relative velocity is initially zero. One can then summarize gravity as the manifestation of the curvature of space-time.

The field equations can be obtained by abandoning the idea of using a scalar field in Minkowski space. Using the previous information, we look for a tensor that involves the metric and its derivatives, in such a way that the field equation has the following form:

$$E_{\mu\nu} = \kappa T_{\mu\nu}, \tag{2.5}$$

where $T_{\mu\nu}$ is the energy-momentum tensor, and $E_{\mu\nu}$ has the following properties:

- $E_{\mu\nu}$ is symmetric since $T_{\mu\nu}$ is symmetric,
- $\nabla_\mu E^{\mu\nu} = 0$, since $\nabla_\mu T^{\mu\nu} = 0$, which implies the geodesic equation,
- $E_{\mu\nu}$ is built only from the metric and its first and second derivatives.

The constant κ can be fixed by demanding that the nonrelativistic limit of the field equations be the Newtonian one.

One heuristic way is to start with Bianchi's identity for the Riemann tensor,

$$\nabla_\lambda R_{\mu\nu\alpha\beta} + \nabla_\mu R_{\nu\lambda\alpha\beta} + \nabla_\nu R_{\lambda\mu\alpha\beta} = 0, \tag{2.6}$$

and doing some manipulations,

$$g^{\lambda\alpha} g^{\nu\beta} \left(\nabla_\lambda R_{\mu\nu\alpha\beta} + \nabla_\mu R_{\nu\lambda\alpha\beta} + \nabla_\nu R_{\lambda\mu\alpha\beta}\right) = 2\nabla^\alpha \left(R_{\mu\alpha} - \frac{1}{2} g_{\mu\alpha} R\right) = 2\nabla^\alpha G_{\mu\alpha} = 0,$$

the Einstein tensor is obtained, and we identify

$$E_{\mu\nu} = G_{\mu\nu} \equiv R_{\mu\nu} - \frac{1}{2} g_{\mu\nu} R. \tag{2.7}$$

In two and three dimensions, if the Ricci tensor is zero it implies that the Riemann tensor will also be zero. So these spaces are necessarily flat in the absence of matter. In four dimensions, the situation is different, the Ricci tensor being zero does not imply that the Riemann tensor is also zero. This means that even in the absence of matter, space-time can be curved [29].

Einstein's equation (2.5) gives us a set of 10 second order nonlinear differential equations. These equations are associated with 4 differential identities due to Bianchi's identities. It is complicated to obtain any analytical solution of these equations, normally some symmetry requirements are imposed in order to reduce the number of equations.

Einstein's equations can be derived in a more elegant way, through the following action

$$S = \frac{1}{16\pi G} \int R\sqrt{-g}\; d^4x + S_M, \tag{2.8}$$

also known as the Einstein-Hilbert action plus a term S_M describing any matter field.

Varying the action with respect to the metric and using that

$$\delta(g^{\alpha\beta} g_{\beta\gamma}) = 0 \Rightarrow \delta g^{\alpha\beta} = -g^{\alpha\gamma} g^{\beta\delta} (\delta g_{\gamma\delta}) \tag{2.9}$$

and

$$\delta R_{\mu\nu} = \nabla_\alpha \delta\Gamma^\alpha{}_{\mu\nu} - \nabla_\nu \delta\Gamma^\lambda{}_{\mu\lambda}, \tag{2.10}$$

one gets for the gravitational sector,

$$\delta S_{EH} = \delta \int \sqrt{-g} d^4x g^{\alpha\beta} R_{\alpha\beta} = \int \left[(\delta\sqrt{-g}) g^{\alpha\beta} R_{\alpha\beta} + \sqrt{-g} (\delta g^{\alpha\beta}) R_{\alpha\beta} + \sqrt{-g} g^{\alpha\beta} \delta R_{\alpha\beta} \right]. \tag{2.11}$$

Using the following identity,

$$\delta\sqrt{-g} = \frac{1}{2}\sqrt{-g} g^{\alpha\beta} \delta g_{\alpha\beta} = -\frac{1}{2}\sqrt{-g} g_{\alpha\beta} \delta g^{\alpha\beta}, \tag{2.12}$$

the result is

$$\delta S_{EH} = \frac{1}{16\pi G}\int \sqrt{-g}d^4x\left(R_{\alpha\beta} - \frac{1}{2}g_{\alpha\beta}R\right)\delta g^{\alpha\beta} + \frac{1}{16\pi G}\int \sqrt{-g}d^4x g^{\alpha\beta}\delta R_{\alpha\beta}, \quad (2.13)$$

where the second term is a surface term.

For the matter fields

$$S_M = \int \mathcal{L}_M\sqrt{-g}\, d^4x \quad (2.14)$$

and variation gives

$$\delta S_M = -\frac{1}{2}\int d^4x\,\sqrt{-g}T_{\mu\nu}\delta g^{\mu\nu}, \quad (2.15)$$

where

$$T_{\mu\nu} = -2\left[\frac{\delta\mathcal{L}_M}{\delta g^{\mu\nu}} - \frac{1}{2}\mathcal{L}_M g_{\mu\nu}\right] = -\frac{2}{\sqrt{-g}}\frac{\delta(\sqrt{-g}\mathcal{L}_M)}{\delta g^{\mu\nu}}, \quad (2.16)$$

So combining the results

$$\delta S = \frac{1}{16\pi G}\int \sqrt{-g}\, d^4x\,[G_{\mu\nu} - 8\pi G T_{\mu\nu}]\,\delta g^{\alpha\beta} = 0 \Rightarrow G_{\mu\nu} = 8\pi G T_{\mu\nu}. \quad (2.17)$$

Einstein's tensor is not the most general tensor that can be constructed from the metric and its first and second derivatives in four dimensions, in fact a term can be added in such a way that the equation continues to satisfy the desired symmetries:

$$E_{\mu\nu} = R_{\mu\nu} - \frac{1}{2}g_{\mu\nu}R + \Lambda g_{\mu\nu}. \quad (2.18)$$

In addition to mathematical motivation, the term was added to the final equation because Einstein was not satisfied with the cosmological solutions he obtained, since he was looking for a stable static cosmological solution [30]. Einstein also hoped that the cosmological constant Λ would make the theory of general relativity embody Mach's principle [31, 32, 33, 34, 35]. The discovery by Hubble that the universe is expanding eliminated the empirical need for a static universe model and consequently put into question the use of the term extra. However, evidence that the universe is not just expanding, but in accelerated expansion, has left open the possibility of using the cosmological constant.

2.2 Solar system tests

Like any physical theory, Einstein's theory has to pass numerous tests. Our solar system, for example, is a fascinating laboratory. Not only Einstein's theory, but any theory of gravitation can be extensively tested in this amazing laboratory. For that, it is first necessary to know the metric outside of, for example, the Sun. In this section, we begin by considering the exact solution describing a spherically symmetric, asymptotically flat, vacuum spacetime — the Schwarzschild solution — and its weak-field approximation and consequences. Next, we discuss the general framework provided by the Parametrized Post-Newtonian Formalism, that helps to constrain deviations from general relativity in a theory-independent manner. From now on, we set $c = 1$ unless stated otherwise.

2.2.1 Schwarzschild solution and its weak-field limit

Solving the coupled differential equations coming from Einstein's equation is not a simple thing if we do not take advantage of the use of symmetries. A first analytical solution was obtained by Karl Schwarzschild in 1916 [36]. The idea was to obtain a solution that described the exterior of objects such as the Earth and the Sun. For modified theories of gravitation, it is often not possible to obtain such a solution analytically [15, 24, 30].

Schwarzschild used a reasonable approximation for objects in the solar system: spherical symmetry and staticity in vacuum. Staticity implies that there there is a preferred choice of time $x^0 = t$ such that the metric components will not depend on t, and that time-space metric components will vanish. Spherical symmetry implies that coordinates $x^2 = \theta$ and $x^3 = \varphi$ can be chosen so that subspaces of constant t and x^1 have line element proportional to $d\Omega^2 = d\theta^2 + \sin^2\theta d\varphi^2$. Moreover, a judicious choice of coordinates can be made so that $g_{12} = g_{13} = 0$. A common choice for x^1 is the areal coordinate r, such that spheres at constant t and r have a surface area of $4\pi r^2$.

In vacuum, Einstein equations reduce to $R_{\mu\nu} - \frac{1}{2}g_{\mu\nu}R = 0$. With the following ansatz,

$$ds^2 = -U(r)dt^2 + V(r)dr^2 + r^2(d\theta^2 + \sin^2\theta d\varphi^2), \tag{2.19}$$

one can find the functions U and V calculating the components of the Ricci tensor and

the Ricci scalar. We have:

$$R_{00} - \frac{1}{2}g_{00}R = \frac{V'}{rV^2} + \frac{1}{r^2} - \frac{1}{r^2V} = 0, \tag{2.20}$$

$$R_{11} - \frac{1}{2}g_{11}R = -\frac{U'}{rUV} + \frac{1}{r^2} - \frac{1}{r^2V} = 0, \tag{2.21}$$

$$R_{22} - \frac{1}{2}g_{22}R = -\frac{U'}{U} + \frac{V'}{V} - \frac{rU''}{U} + \frac{rU'V'}{2UV} + \frac{r(U')^2}{2U} = 0, \tag{2.22}$$

$$R_{33} - \frac{1}{2}g_{33}R = \sin^2\theta\left(R_{22} + \frac{1}{2}R\right) = 0, \tag{2.23}$$

where a prime denotes a radial derivative.

Solving these equations by imposing that the metric reduces to the metric of flat space when $r \to \infty$, expressions for U and V are found:

$$U = V^{-1} = 1 - \frac{C}{r}.$$

Comparison with the weak field metric sets the value of C:

$$C = 2GM. \tag{2.24}$$

The final result is

$$ds^2 = -\left(1 - \frac{2GM}{r}\right)dct^2 + \left(1 - \frac{2GM}{r}\right)^{-1}dr^2 + r^2(d\theta^2 + \sin^2\theta d\varphi^2). \tag{2.25}$$

It is interesting to note that the only free parameter is the total mass of the object, this implies that the metric outside a spherical and static object is completely determined by its mass, regardless of the shape that the energy-momentum tensor takes inside the object.

In order to explore the weak field limit of the Schwarzschild spacetime, it is useful to cast the line element (2.25) in isotropic coordinates defined by

$$r = \rho\left(1 + \frac{GM}{2\rho}\right)^2, \tag{2.26}$$

so that

$$ds^2 = -\frac{(1 - \frac{GM}{2\rho})^2}{(1 + \frac{GM}{2\rho})^2}dt^2 + \left(1 + \frac{GM}{2\rho}\right)^4(d\rho^2 + \rho^2 d\Omega^2). \tag{2.27}$$

The idea is to group the spatial part of the metric [15]. Knowing that the gravitational potential is of the order of

$$|\phi| \lesssim 10^{-6}$$

in the solar system, one can expand the metric in powers of $\phi \sim GM/r$:

$$ds^2 = -\left[1 - \frac{2GM}{r} + 2\left(\frac{GM}{r}\right)^2\right] dt^2 + \left(1 + \frac{2GM}{r}\right)^{-1} [dr^2 + r^2(d\theta^2 + \sin^2\theta d\varphi^2)]. \quad (2.28)$$

where ρ has been changed to r for convenience.

As we will discuss further below, for modified theories of gravity, the metric can be parameterized as follows:

$$ds^2 = -\left[1 - \frac{2Gm}{r} + 2\beta\left(\frac{Gm}{r}\right)^2\right] dt^2 + \left(1 + 2\gamma\frac{Gm}{r}\right)^{-1} [dr^2 + r^2(d\theta^2 + \sin^2\theta d\varphi^2)], \quad (2.29)$$

where β e γ can be related to free parameters of the theory and bounds to these parameters can be used to distinguish between general relativity and modified gravity.

The deflection of light by the Sun can now be calculated. Let us orient the coordinates so that the ray lies in the plane $\theta = \pi/2$ and assume that the incoming ray enters the solar system along the line $\varphi = 0$; moreover, let the Earth be located at $\varphi = \varphi_E$ when the ray reaches it. The goal is to calculate the angle α between the incoming ray and the center of the Sun, as shown in figure 2.3. If the Sun had zero mass, α would be $\pi - \varphi_E$, however the Sun produces a deflection $\delta\alpha$ such that $\alpha = \pi - \varphi_E + \delta\alpha$.

Using the metric (2.28) and the geodesic equation, one obtains [15]

$$\frac{b}{r} = \sin\varphi + \frac{2GM}{b}(1 - \cos\varphi), \quad (2.30)$$

where b is the impact parameter. Notice that the ray returns to $r = \infty$ not at an angle $\varphi = \pi$ but rather at

$$\varphi = \pi + 4\frac{GM}{b}. \quad (2.31)$$

It turns out that the deflection angle measured at Earth is $\delta\alpha = 4\frac{M}{b}$ when the ray comes from infinity parallel to the Sun line. Using the general metric (2.29) one obtains

$$\delta\alpha = 2(1 + \gamma)\frac{GM}{b}. \quad (2.32)$$

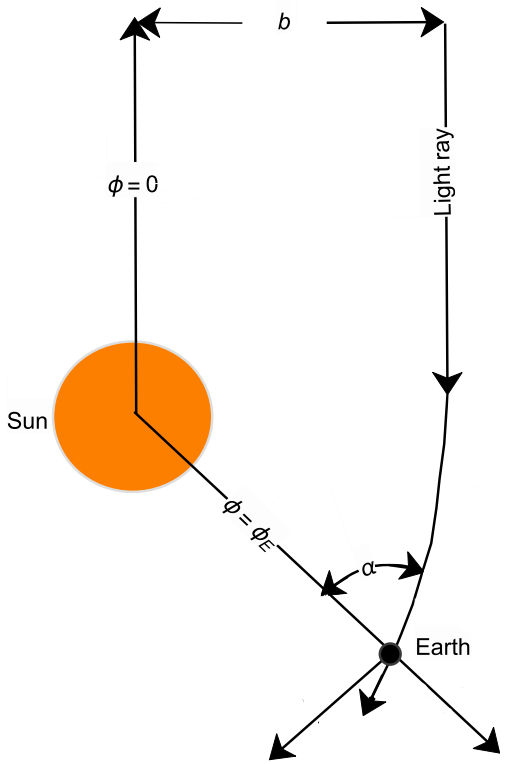

Figure 2.3: Deflection of light by the Sun.

Therefore, the observation of light deflection by the Sun can directly constrain the parameter γ.

For Mercury's perihelion, orienting the coordinates so that the test body moves in the equatorial plane and using the geodesic equation, the result is [15]

$$r = \frac{(1-e^2)a}{1 + e\cos[1 - (\delta\varphi_0/2\pi)\varphi]}, \tag{2.33}$$

where a and e are constants of integration, and $\delta\varphi_0$ is the perihelion shift defined by

$$\delta\varphi_0 = \frac{6\pi GM}{a(1-e^2)}.$$

Note that if $\delta\varphi_0 = 0$, then the orbit would be an ellipse with semi-major axis a and eccentricity e. For the the general metric (2.29) the result is [15]

$$\delta\varphi_0 = \frac{(2 - \beta + 2\gamma)}{3}\frac{6\pi GM}{a(1-e^2)}.$$

Therefore, the parameter β can be constrained by measurements of Mercury's perehelion precession.

2.2.2 The Parametrized Post-Newtonian formalism

Newtonian gravity is a good approximation in the solar system. Since the magnitude of the gravitational potential is of the order of $\phi \lesssim 10^{-6}$, relativistic corrections can be treated in a perturbative way. Here we describe the Parametrized Post-Newtonian (PPN) formalism, which allows the relativistic effects of a general theory, in the weak-field regime, to be calculated consistently. Here we follow the treatment of Ref. [37].

In the solar system, the planetary velocities are related to the potential by the virial relations

$$\phi \sim v^2.$$

As the Sun and the planets are in hydrostatic equilibrium, the pressure p is comparable to $\rho\phi$, in other words

$$p/\rho \sim \phi.$$

Furthermore, from thermodynamics, other forms of energy (compressional energy, radiation, thermal energy, magnetic energy, etc.) are related to pressure by $pV \sim E \sim \rho\Pi V$, and thus Π, the ratio of energy density to rest-mass density, is related to ϕ by $\Pi \sim p/\rho \sim \phi$. These four dimensionless quantities (up to factors of c) are assigned a bookkeeping label ϵ that denotes their "order of smallness":

$$\phi \sim v^2 \sim \frac{p}{\rho} \sim \Pi \sim \mathcal{O}(\epsilon). \tag{2.34}$$

The equation of motion contains both spatial derivatives and time derivatives, and from the Euler equation describing the fluid flow we have

$$\frac{\partial}{\partial t} \sim v \cdot \nabla$$

therefore $\frac{\partial}{\partial t}/\frac{\partial}{\partial x} \sim \mathcal{O}(\epsilon^{1/2})$.

The Lagrangian describing the dynamics of a test-particle in a given metric back-

ground $g_{\mu\nu}$ is given by

$$L = -m\left(-g_{\mu\nu}\frac{dx^\mu}{dt}\frac{dx^\nu}{dt}\right)^{\frac{1}{2}} = -m\left(-g_{00} - 2g_{0j}v^j - g_{ij}v^iv^j\right)^{1/2} \tag{2.35}$$

and in the Newtonian limit, where $g_{ij} = \delta_{ij}+\mathcal{O}(\epsilon)$, $g_{0i} = \mathcal{O}(\epsilon^{3/2})$, and $g_{00} = -1+2\phi+\mathcal{O}(\epsilon^2)$ (see below), this reduces to

$$L = -m(1 - 2\phi - v^2)^{1/2} + \mathcal{O}(\epsilon^2) \approx -m + m\phi + \frac{1}{2}mv^2 + \mathcal{O}(\epsilon^2). \tag{2.36}$$

Therefore, we obtain the expected Newtonian behavior when L is computed up to $\mathcal{O}(\epsilon)$. Post-Newtonian corrections should include all relevant terms up to $\mathcal{O}(\epsilon^2)$. For this purpose, we must include $\mathcal{O}(\epsilon^2)$ terms in g_{00}, the leading $\mathcal{O}(\epsilon^{3/2})$ term in g_{0i} and the term of $\mathcal{O}(\epsilon)$ in g_{ij}:

$$L_{PN} = -m\left(1 - 2\phi - v^2 - g_{00}[\mathcal{O}(\epsilon^2)] - 2g_{0j}[\mathcal{O}(\epsilon^{3/2})]v^j - g_{ij}[\mathcal{O}(\epsilon)]v^iv^j\right)^{1/2}. \tag{2.37}$$

Notice that we are assuming that no half-order terms appear in g_{00} and g_{ij}, and no integer-order terms appear in g_{0i} up to post-Newtonian order. This is partially a consequence of energy conservation in the Newtonian level; notice, for instance that a $O(\epsilon)$ contribution to g_{0i} in Eq. (2.35) would lead to a term that changes sign under time reversal, implying energy dissipation. Effects of energy dissipation by gravitational waves, for instance, would appear at higher post-Newtonian order. We refer to [37] for more details.

In the case of General Relativiy the dynamical field is the metric $g_{\mu\nu}$. Some modified theories of gravity, as will be discussed in Chap. 3, may introduce an additional scalar field ϕ, in other models we have a vector field A_μ or a tensor field $B_{\mu\nu}$ and so on. In what follows we sketch the general procedure to obtain the post-Newtonian metric in a general theory containing (some of) these degrees of freedom.

Setting the cosmological boundary conditions, we assume a flat and isotropic cosmology. With isentropic coordinates, in the rest frame of the present universe, we have,

far away from all post-Newtonian sources,

$$\begin{aligned} g_{\mu\nu} &\rightarrow g^{(0)}_{\mu\nu} = \mathrm{diag}(-c_0, c_1, c_1, c_1) \\ \phi &\rightarrow \phi_0 \\ A_\mu &\rightarrow (A, 0, 0, 0) \\ B_{\mu\nu} &\rightarrow B^{(0)}_{\mu\nu} = \mathrm{diag}(-b_0, b_1, b_2, b_3) \end{aligned} \tag{2.38}$$

Because these asymptotic values may affect the post-Newtonian metric, some cases will require a full cosmological solution.

We then expand the variables in a post-Newtonian series about the asymptotic values:

$$\begin{aligned} g_{\mu\nu} &= g^{(0)}_{\mu\nu} + h_{\mu\nu} \\ \phi &= \phi_0 + \psi \\ A_\mu &= (A + a_0, a_1, a_2, a_3) \\ B_{\mu\nu} &= B^{(0)}_{\mu\nu} + b_{\mu\nu} \end{aligned} \tag{2.39}$$

Generally, the post-Newtonian order of these perturbations are given by

$$\begin{aligned} h_{00} &\sim \mathcal{O}(\epsilon) + \mathcal{O}(\epsilon^2) \\ h_{ij} &\sim \mathcal{O}(\epsilon) \\ h_{0j} &\sim \mathcal{O}(\epsilon^{3/2}) \\ \psi &\sim \mathcal{O}(\epsilon) + \mathcal{O}(\epsilon^2) \\ a_0 &\sim \mathcal{O}(\epsilon) + \mathcal{O}(\epsilon^2) \\ a_i &\sim \mathcal{O}(\epsilon^{3/2}) \\ b_{00} &\sim \mathcal{O}(\epsilon) + \mathcal{O}(\epsilon^2) \\ b_{ij} &\sim \mathcal{O}(\epsilon) \\ b_{0j} &\sim \mathcal{O}(\epsilon^{3/2}) \end{aligned} \tag{2.40}$$

One then substitutes the relations (2.39) into the field equations, keeping only terms that are necessary to obtain a final, consistent post-Newtonian solution.

We start by solving for h_{00} to $\mathcal{O}(\epsilon)$, to obtain the Newtonian limit. Assuming that

$h_{00} \to 0$ far from the system, one obtains

$$h_{00} = 2\alpha U, \tag{2.41}$$

where U is the Newtonian gravitational potential, i.e., a solution of

$$\nabla^2 U = 4\pi G\rho, \tag{2.42}$$

and α is a function of the cosmological parameters and coupling constants that may appear in the field equations. We already saw in last section that $\alpha = 1$ in GR. The metric to lowest order now has the form

$$g_{00} = -c_0 + 2\alpha U, \quad g_{ij} = c_1\delta_{ij}, \quad g_{0i} = 0. \tag{2.43}$$

It is usually general enough to consider a perfect fluid approximation for matter fields, so that the energy-momentum tensor takes the form

$$T^{\mu\nu} = (\epsilon + p)u^\mu u^\nu + pg^{\mu\nu}, \tag{2.44}$$

where $\epsilon = \rho + \rho\Pi$ is the energy density, p is the pressure, and $u^\mu = dx^\mu/d\tau = u^0(1, \vec{v})$ is the four-velocity of fluid elements. To the required order, the energy-momentum tensor, in the perfect fluid approximation, can be expanded as

$$\begin{aligned} T^{00} &= c_0^{-1}\rho(1 + \Pi + 2c_1 U + c_0^{-1}c_1 v^2) + \mathcal{O}(\epsilon^2) \\ T^{0j} &= c_0^{-1}\rho v^j + \mathcal{O}(\epsilon^{3/2}) \\ T^{ij} &= c_0^{-1}\rho v^i v^j + c_1^{-1}p\delta^{ij} + \mathcal{O}(\epsilon^2). \end{aligned} \tag{2.45}$$

To put the metric in the standard Newtonian form, we must make a change of coordinates $x^{\hat{0}} = \sqrt{c_0}x^0$ and $x^{\hat{i}} = \sqrt{c_1}x^i$ and a change of units $\frac{G\alpha}{c_0 c_1} \to G$ to get

$$g_{\hat{0}\hat{0}} = -1 + 2\hat{U}, \quad g_{\hat{i}\hat{j}} = \delta_{ij}, \quad g_{\hat{0}\hat{i}} = 0, \tag{2.46}$$

where $\hat{U} \equiv c_1 U$. This is the Newtonian limit of the metric.

One can extract the expressions of h_{ij} to $\mathcal{O}(\epsilon)$ and h_{0i} to $\mathcal{O}(\epsilon^{3/2})$ using the field equations. In particular, one has to use the perturbative expansion for the Ricci tensor,

given by [37]

$$\begin{aligned} R_{00} = & -\tfrac{1}{2}\nabla^2 h_{00} - \tfrac{1}{2}(h_{jj,00} - 2h_{j0,j0}) + \tfrac{1}{2}h_{00,j}(h_{jk,k} - \tfrac{1}{2}h_{kk,j}) \\ & -\tfrac{1}{4}|\nabla h_{00}|^2 + \tfrac{1}{2}h_{jk}h_{00,jk} \\ R_{0j} = & -\tfrac{1}{2}(\nabla^2 h_{0j} - h_{k0,jk} + h_{kk,0j} - h_{kj,0k}) \\ R_{ij} = & -\tfrac{1}{2}(\nabla^2 h_{ij} - h_{00,ij} + h_{kk,ij} - h_{ki,kj} - h_{kj,ki}) \end{aligned} \tag{2.47}$$

To solve h_{00} to $\mathcal{O}(\epsilon^2)$ one must use the previously calculated solutions for h_{ij}, h_{0j} and h_{00}. The last part consists of making a gauge-transformation to the standard post-Newtonian gauge.

The final result can be cast in the general PPN (Parametrized Post-Newtonian) form

$$\begin{aligned} g_{00} = & -1 + 2U - 2\beta U^2 - 2\xi\Phi_W + (2\gamma + 2\alpha_3 + \zeta_1 - 2\xi)\Phi_1 \\ & +2(3\gamma - 2\beta + 1\zeta_2 + \xi)\Phi_2 + 2(1 + \zeta_3)\Phi_3 \\ & +2(3\gamma + 3\zeta_4 - 2\xi)\Phi_4 - (\zeta_1 - 2\xi)\mathcal{A} \\ g_{0j} = & -\tfrac{1}{2}(4\gamma + 3 + \alpha_1 - \alpha_2 + \zeta_1 - 2\xi)V_j - \tfrac{1}{2}(1 + \alpha_2 - \zeta_1 + 2\xi)W_j \\ g_{ij} = & (1 + 2\gamma U)\delta_{ij}, \end{aligned} \tag{2.48}$$

where γ, β, ξ, ζ_i, α_i are the 10 PPN parameters and U, Φ_1, Φ_2, Φ_3, Φ_4, Φ_w, V, W and $\mathcal{A}$ are potentials properly defined in [37].

Every metric gravitational theory will predict a unique set of post-Newtonian parameters which can easily be compared with experiments and used to constrain the free parameters.

The parameters have different interpretations [37]. General relativity has only two non-zero parameters: $\gamma = \beta = 1$, and experimental bounds are in very good agreement with it. The interpretations and constraints in each parameter are presented in Tables 2.1 and 2.2, adapted from [38].

2.3 Cosmology

The fundamental blocks on which cosmological models are built are based on the following principles [39]:

- There is no special point in the universe; galaxies are evenly distributed in space at

Table 2.1: The PPN Parameters and their interpretations.

Parameter	Interpretations	Value in GR
γ	How much space curvature g_{ij} is produced by unit rest mass.	1
β	How much "nonlinearity" in the superposition law for gravity.	1
ξ	Preferred-location effects.	0
α_1	Preferred-frame	0
α_2	effects.	0
α_3		0
α_3	The failure of conser-	0
ζ_1	vation of energy, mo-	0
ζ_2	mentum and angular	0
ζ_3	momentum.	0
ζ_4		0

Table 2.2: Current limits on the PPN parameters.

Parameter	Effect	Limit
$\gamma - 1$	time delay	2.3×10^{-5}
	light deflection	2×10^{-4}
$\beta - 1$	perihelion shift	8×10^{-5}
	Nordtvedt effect	2.3×10^{-4}
ξ	spin precession	4×10^{-9}
α_1	orbital polarization	10^{-4}
α_2	spin precession	2×10^{-9}
α_3	pulsar acceleration	4×10^{-20}
ζ_1	combined PPN bounds	2×10^{-2}
ζ_2	binary acceleration	4×10^{-5}
ζ_3	Newton's 3rd law	10^{-8}
ζ_4	not independent	—

large scales.

- There is no special spatial direction in the universe; galaxies are evenly distributed in different angular directions at large scales.

In other words, at large scales the universe is both homogeneous and isotropic. Mathematically this means that space-time must be maximally symmetric [24]. These principles allow the construction of simple cosmological models to investigate the evolution of the universe. One can show that in this case, the Ricci tensor and the spatial metric satisfy $R_{jl} = 2k\gamma_{jl}$, and the line element takes the following form:

$$ds^2 = -dt^2 + a(t)^2 \left(\frac{dr^2}{1 - kr^2} + r^2 d\theta^2 + r^2 \sin^2 \theta d\phi^2 \right), \tag{2.49}$$

also known as the Friedmann-Lemaître-Robertson-Walker (FLRW) metric, where k describes different types of spatial geometry and $a(t)$ is determined through the distribution of matter of the universe via the Friedmann equations. For $k = 0$ the universe is said to be spatially flat: the spatial hypersurface has the well-known Euclidean geometry. For $k > 0$ the universe is said to be closed and the spatial hypersurface has a shape that is topologically equivalent to a 3-sphere. For $k < 0$ the universe is said to be open and the geometry is called hyperbolic. By solving the Einstein equations with a cosmological constant and a perfect fluid energy momentum-tensor, given by Eq. (2.44), one finds the Friedmann equations:

$$H^2 \equiv \left(\frac{\dot{a}}{a} \right)^2 = \frac{8\pi G}{3} \epsilon - \frac{k}{a^2} + \frac{\Lambda}{3}, \tag{2.50}$$

$$\frac{\ddot{a}}{a} = -\frac{4\pi G}{3}(\epsilon + 3p) + \frac{\Lambda}{3}, \tag{2.51}$$

where a dot indicates a time derivative. Looking closely to the second equation (2.51), it reveals that $\epsilon + 3p$ acts as the effective gravitational energy, which means that pressure has a gravitational effect.

Conservation of the energy-momentum tensor, $\nabla_\mu T^{\mu\nu} = 0$, results in the continuity equation,

$$\dot{\epsilon} + 3H(\epsilon + p) = 0. \tag{2.52}$$

For a fluid with an equation of state $p = w\epsilon$, where w is a constant, with $w = 0$ for

non-relativistic matter, while $w = \frac{1}{3}$ for radiation, this equation has the solution

$$\epsilon = \epsilon_0 \left(\frac{a_0}{a}\right)^{3(w+1)}, \tag{2.53}$$

where ϵ_0 and a_0 are constants. Therefore ϵ decreases with increasing a: as the universe expands, matter and radiation get diluted.

2.3.1 Challenges in cosmology

One critical challenge of modern physics is to understand the mechanisms behind the apparent accelerated expansion of the universe [40]. In order to have an accelerated expanding universe, $\ddot{a} > 0$. From Eq. (2.51), without the cosmological constant, the dominating fluid must satisfy $p < -\frac{\epsilon}{3} < 0$. It is concluded that it must have a negative pressure or, equivalently, the equation of state needs to satisfy $w < -\frac{1}{3}$. One possible approach, which agrees very well with cosmological observations, is to use general relativity plus a cosmological constant Λ, which effectively acts as a perfect fluid with equation of state $w = -1$. Indeed, observations are completely consistent with the existence of a mysterious energy component – known as *dark energy* – with equation of state $w \approx -1$ and which contributes to roughly 70% of the total energy of the universe [41].

Now, for a flat universe model consisting of pressureless matter and the cosmological constant, equations (2.50) and (2.51) become[1]

$$H^2 = \frac{8\pi G}{3}\epsilon_m + \frac{\Lambda}{3}, \qquad \frac{\ddot{a}}{a} = -\frac{4\pi G}{3}\epsilon_m + \frac{\Lambda}{3}, \tag{2.54}$$

where ϵ_m is composed not only of baryonic matter but also a dark component, known as *dark matter*. Evidence for the existence of dark matter comes from observations that show that many galaxies would separate, not form, or even move as they do if they did not contain a large amount of invisible matter [40]. Since dark matter has not yet been observed directly, if it exists, it must barely interact with ordinary baryonic matter and radiation, except through gravity. Dark matter is expected to be composed of some undiscovered particle, but there are attempts to describe its effects through alternative theories of gravitation, such as MOND [42], which modifies the Newtonian force law and

[1] One should also include radiation, but since radiation contributes very little to the energy budget today it can be neglected at the background level at late times.

MOG [43], which promotes the gravitational constant to a scalar field and introduces, in addition, two other scalar fields and one vector field.

By identifying $f = \ddot{a}$ as a force per unit mass, $R = a$ as the typical lenght scale, and $\rho_m = M/(\frac{4\pi R^3}{3})$ as a mean density, equation (2.54) can be written in an schematic way as

$$f = -\frac{GM}{R^2} + \frac{1}{3}\Lambda R,$$

which is the form of a force law. This demonstrates that the cosmological constant gives rise to a repulsive force whose value increases with distance, the repulsive nature of this force can be responsible for the acceleration of the universe. In the model given by (2.54), the universe will eventually undergo a phase of accelerated expansion where the scale factor becomes $a(t) = a_0 e^{H_0 t}$, since ϵ_m is decreasing with increasing a and eventually $\Lambda \gg \epsilon_m$. An interesting observation is that both are of the same order at the present time, and for this coincidence to occur, a fine tuning must occur in the initial conditions of the universe.

Although the introduction of the cosmological constant in Physics is justified with cosmological arguments, and mathematically [see discussion around Eq. (2.18)], a more physical justification emerged in the late 1960s when it was shown that the zero point vacuum fluctuations must respect Lorentz's invariance and therefore have the form $\langle 0|T_{\mu\nu}|0\rangle = \lambda g_{\mu\nu}$ [4]. A free quantum field can be thought of as an infinite sum of harmonic oscillators. Formally, the vacuum energy of an infinite collection of harmonic oscillators will be infinite. The effective cosmological constant generated by vacuum fluctuations is [44]

$$\frac{\Lambda}{8\pi G} = \langle T_{00}\rangle_{\text{vac}} \propto \int_0^{k_{\max}} \sqrt{k^2 + m^2}\, k^2 dk \ ,$$

and integration results is

$$\frac{\Lambda}{8\pi G} = \langle T_{00}\rangle_{\text{vac}} \propto k_{\max}^4.$$

As we let the cutoff $k_{\max} \to \infty$ the result diverges. However, cosmological observations indicate that the value of the cosmological constant is [45]

$$\rho_\Lambda = \frac{\Lambda}{8\pi G} \leq (10^{-12}\text{GeV})^4.$$

We know that no simple low-energy theory is likely to be exactly true at high

energies, where other particles, and possibly new kinds of forces, may become important. Therefore, if we discard the high moment modes and regularize $\langle T_{00} \rangle_{\text{vac}}$ by imposing a cutoff at the Planck scale, where it is widely believed that conventional field theory breaks down due to quantum gravity effects, we get

$$\rho_\Lambda \sim (10^{18}\text{GeV})^4,$$

which remains extremely large. A smaller cutoff does not improve the situation; for instance, a cutoff at the QCD scale results in

$$\rho_{\text{QCD}} \sim (10^{-3}\text{GeV})^4.$$

Supersymmetry was conjectured in the 1970s [46], and with that, if confirmed to be correct, bosons and fermions of identical mass would contribute equally but with opposite sign to the expected vacuum expectation value of physical quantities. The problem of the cosmological constant could then be solved by an adjusted balance between bosons and fermions in the nature [47]. However, supersymmetry, if it exists, is broken at the density scales prevalent in the universe today and, therefore, the cosmological constant should be expected to disappear at the beginning of the universe, but reappear during late times, when the density scale prevalent in the universe was below ρ_{SUSY}. This is an undesirable scenario, since a non-zero value of Λ at the beginning of the universe is useful from the point of view of inflation, while a very small value of Λ is in accordance with current cosmological observations.

In any case, the ΛCDM (cosmological constant plus cold dark matter) is still the model in best accordance with recent cosmological observations. The best fit for the density parameters $\Omega_i = \frac{\rho_i}{3H^2 M_{\text{Pl}}^2}$, taken from the Planck data [45], is $\Omega_{\text{dark matter}} = 0.222 \pm 0.026$, $\Omega_{\text{baryonic matter}} = 0.0449 \pm 0.0028$ and $\Omega_\Lambda = 0.734 \pm 0.029$. The best fit for the Hubble parameter today is $H_0 = 100h\frac{km}{s\ Mpc}$ with $h = 0.710 \pm 0.025$.

2.3.2 Dark energy and scalar fields

Measuring the equation of state of dark energy is a big effort in observational cosmology today. If an equation of state $w \neq -1$ is ever observed then the cosmological constant is not the correct description of dark energy. So even though a cosmological constant is in

agreement with experiments today, it is nonetheless useful to consider more complicated models in case some day observations will tell us otherwise. We can have two cases here, either is the late time acceleration of the universe due to some new dynamical degrees of freedom or it can be due to some breakdown of general relativity on cosmic scales.

Models that introduce a new degree of freedom in Nature, such as a scalar field, in order to explain dark energy, are often called Quintessence. This name has its origin in ancient Greece, where the local belief said that nature was formed by five fundamental elements: fire, earth, water, wind and a fifth element (in Latin, "quintessentia"), the aether, permeating all the space. In terms of the components present in the cosmological models, the scalar field would be the fifth component, where the other four are: radiation, baryonic matter, dark matter and curvature. Scalar fields which do change in spacetime can be difficult to distinguish from a cosmological constant (in the late universe) because the change may be extremely slow. Promoting dark energy to a scalar field results in interesting properties; with an appropriate choice of self interaction some models avoid fine-tuning in the initial conditions [48]. If, for example, such field is coupled to gravity, as in Brans-Dicke theory, the gravitational constant in such a model can be promoted to a field-dependent "effective constant".

To briefly illustrate the idea behind Quintessence, we start with the Einstein-Hilbert action and add the scalar field. Since observations suggest that dark energy is smoothly distributed in our universe we can assume that the scalar field is homogeneous, so the action is

$$\mathcal{L}_\Phi = -\sqrt{-g}\left[\frac{1}{2}(\partial_\mu\Phi)(\partial^\mu\Phi) + V(\Phi)\right] = \sqrt{-g}\left[\frac{1}{2}\dot{\Phi}^2 - V(\Phi)\right] \tag{2.55}$$

on cosmological scales.

One can obtain the pressure and energy density associated with the scalar field if we compare the energy-momentum tensor of the scalar field with that of a perfect fluid. We get

$$\epsilon_\Phi = \frac{1}{2}\dot{\Phi}^2 + V(\Phi) \tag{2.56}$$

and

$$p_\Phi = \frac{1}{2}\dot{\Phi}^2 - V(\Phi). \tag{2.57}$$

The equation of state, defined as $w = \frac{p}{\epsilon}$, is thus

$$w_\Phi = \frac{\frac{1}{2}\dot{\Phi}^2 - V(\Phi)}{\frac{1}{2}\dot{\Phi}^2 + V(\Phi)}. \tag{2.58}$$

The observed cosmic acceleration today indicates that $\omega_\Phi \approx -1$ which again means that we must require that our field is "rolling slowly" in the sense that $\frac{\dot{\Phi}^2}{2V(\Phi)} \ll 1$. The equation of motion for Φ reads

$$\Box\Phi - \frac{dV}{d\Phi} = 0. \tag{2.59}$$

In a flat FLRW background metric it reduces to

$$\ddot{\Phi} + 3H\dot{\Phi} + \frac{dV}{d\Phi} = 0. \tag{2.60}$$

This is analogous to the classical problem of a particle with position $\Phi(t)$ moving under the action of a potential $V(\Phi)$. The term $3H\dot{\Phi}$ acts as a friction force, "slowing" the temporal evolution of the field. If $m_\Phi \equiv \sqrt{d^2V/d\Phi^2}$ is greater than the frictional term the potential is too steep and the field rolls through the potential too fast, such that ω_Φ will not be approximately -1 today. Over time the field will rest on a value that corresponds to the minimum of the potential, if it has any. Note that $H_0 \sim 10^{-33}$eV, so the mass of the scalar field must be adjusted to an extremely small value for Quintessence models to be viable, much less than the mass of the electron.

If the field is coupled to matter, if the coupling is not extremely small, the long-range nature of the force associated with the field can cause deviations from general relativity in the results of experiments in the solar system. In order to present the correct cosmological dynamics, many Quintessence models also need fine adjustment in the initial conditions, but there is a class of potentials that have the so-called attractor solution, in such a way that a common behavior is obtained for different initial conditions [40]. In this scenario, the fine-tuning problem is not so severe because the density of dark energy declines in a similar way to the density of matter and radiation and its value at the present moment is only a consequence of the age of the universe. Although the solution is not so sensitive to changes in the initial conditions, the free parameters of the theory must be adjusted so that the field has the correct cosmological behavior, acting as the cosmological constant in the present moment.

Chapter 3

Modified gravity

Cosmological observations and fundamental physical questions suggest that general relativity may need to be modified in both the low and high energy regimes. From the high-energy perspective, GR is purely a classical theory and not renormalizable through usual methods of quantum field theory [49]. Modifications to GR can aleviate this problem. For instance, modifications that add quadratic curvature terms to the Einstein-Hilbert action can make it renormalizable [50]. Another interesting feature of such high-energy corrections is that they can make these new theories avoid the formation of singularities [51]. Quantum gravity and unification theories predict the existence of new degrees of freedom in the low-energy regime, thus, modifications of general relativity can be constructed as a toy model to study the phenomenology of a possible quantum gravity theory.

From the low-energy perspective, cosmological and astrophysical observations provide evidence for the existence of mysterious dark components that permeate our universe. One of the many ways to describe dark energy is by introducing the simplest degrees of freedom into general relativity: scalar fields. If such a field couples to matter, its small mass would cause forces of cosmological range to exist, however, such forces were never detected on the solar system scale. If such fields do exist and are responsible for the observed cosmological effects, then there must be some dynamic mechanism that hides the scalar field on solar system scales, but allows the correct cosmological behavior; this mechanism is called screening mechanism [52].

The first section of this chapter gives an overview of different modified theories of gravity, which arise from different motivations and aspects. Next, the class of theories of interest in this work, the scalar-tensor theories, will be exposed. Finally, the screening

mechanism of the Dilaton and Chameleon models will be explained.

3.1 Pathways to modify general relativity

On the model-building side, Lovelock's theorem [53, 54] provides a theoretical guide that indicates which of the assumptions underlying Einstein's theory can be modified. Such a theoretical guide is constructed by examining the fundamental blocks of the theory. In simple terms, the theorem states that GR emerges as the unique theory of gravity under specific assumptions. More precisely, it can be articulated as follows [55]:

The only equation that can be obtained from a four-dimensional action that involves only the metric, its first and second derivatives is Einstein's equation plus a cosmological constant.

This theorem limits the theories that we can build using only the metric, but it does not imply that the Einstein-Hilbert action is the only action that can be constructed using $g_{\mu\nu}$ in four dimensions. Indeed, Einstein's equations also follow from the more general Lagrangian density:

$$\mathcal{L} = \alpha\sqrt{-g}R - 2\lambda\sqrt{-g} + \beta\epsilon^{\mu\nu\rho\lambda}R^{\alpha\beta}{}_{\mu\nu}R_{\alpha\beta\rho\lambda} + \gamma\sqrt{-g}\left[R^2 - 4R^{\mu}{}_{\nu}R^{\nu}{}_{\mu} + R^{\mu\nu}{}_{\rho\lambda}R^{\rho\lambda}{}_{\mu\nu}\right],$$

since the last two terms do not contribute to the Euler-Lagrange equation.

Lovelock's theorem seems to leave little room for modifying General Relativity. However, when analyzed in detail, the theorem contains a number of nontrivial assumptions [55]. Giving up each of these assumptions provides a way to circumvent its conclusions and gives rise to different classes of modified theories of gravity [55]:

- *Violations/limitation of diffeomorphism invariance;*
- *Accept higher-order terms in the derivatives of the metric and non-locality;*
- *Higher dimensions;*
- *Additional fields.*

In what follows we discuss each of these pathways to modify GR and a few representative theories in each class.

Violations of diffeomorphism invariance

Lorentz invariance has been tested with remarkable precision in the standard model sector and is believed to be a necessary symmetry in any theory of gravitation. Violations of Lorentz's invariance are typically introduced through extra fields. A new class of theories can be created assuming that Lorentz invariance is just an emergent symmetry that is broken for high energies in the gravitational sector. Some of these theories were found to possess a better ultraviolet behavior than GR [56].

Vector-tensor theories, such as Einstein-Aether theories [56], have the property that they single out a preferred reference frame and therefore become a theoretical workplace for studying violations of Lorentz symmetry in gravitation. They are based on the theories proposed by Will and Nordtvedt in the 1970s [57]. The gravitationally coupled Lorentz-violating vector field, called the aether, can make theory have interesting effects, such as a normalization of Newton's constant, leave an imprint on perturbations in the early universe, and affect the growth rate of structure in the Universe [58]. Some of these theories are built to reproduce Milgrom's Modified Newtonian Dynamics (MOND) at the non-relativistic limit. MOND was first proposed as a possible alternative to dark matter, as it can explain the anomalous rotational velocities in galaxies, typically understood to implicate an excess of mass due to dark matter. For high accelerations, it satisfies Newton's second law, $\vec{a} = -\nabla\phi$, but in the low acceleration regime Newton's second law is modified to $(|\vec{a}|/a_0)\vec{a} = -\nabla\phi$. The action of the Einstein-Aether theory is generally taken to be [3]

$$S = \frac{1}{16\pi G_N}\int d^4x\sqrt{-g}\left[R + K^{ab}_{mn}\nabla_a u^m \nabla_b u^n + \lambda(g_{ab}u^a u^b + 1)\right],$$

where the tensor K is defined by

$$K^{ab}_{mn} = c_1 g^{ab}g_{mn} + c_2\delta^a_m\delta^b_n + c_3\delta^a_n\delta^b_m + c_4 u^a u^b g_{mn}.$$

Here u is known as the Aether field and c_i are dimensionless adjustable parameters of the theory. The Newtonian limit was examined by Carroll and Lim [59], who used the

ansatz of a static metric, with the Aether vector parallel to the timelike Killing vector and showed that the gravitational constant is modified to

$$G = \frac{G_N}{1 - (c_1 + c_4)/2}.$$

Tests on the solar system put strong constraints on the constants c_i. This is because the PPN parameters in Einstein-Æther theory are nonzero functions of the c_i. Moreover, Einstein-Æther theory predicts the existence of spin-1 and spin-0 gravitational perturbations and not only spin-2 gravitational perturbations like GR. All these propagating modes have speeds that are functions of the c_i, and which differ in general from the speed of light. More stringent constraints on c_i come from binary pulsar data [60, 61].

Another class of theories that limit diffeomorphism invariance is Unimodular Gravity. As old as General Relativity itself, the unimodular condition $\sqrt{-g} = 1$ was originally proposed by Einstein as a way to (partially) fix a coordinate system in GR, nevertheless, the unimodular condition has an interesting implication. The fundamental block on which Unimodular Gravity is built is the invariance under a restricted group of diffeomorphisms that leave the metric determinant unaltered, so that the determinant of the metric can be set equal to a scalar density ω_0,

$$\sqrt{-g} = \omega_0, \tag{3.1}$$

which provides a fixed volume element in spacetime. One way to define Unimodular gravity is to introduce the unimodular condition (3.1) into the Einstein-Hilbert action as a constraint multiplied by a Lagrange multiplier λ,

$$S = \int d^4x\sqrt{-g}\left(\frac{R}{\kappa} - \lambda(\sqrt{-g} - \omega_0)\right) + S_m.$$

The field equation for the metric is the Einstein equation with a $\lambda g_{\mu\nu}$ term. One can use conservation of the energy-momentum tensor to show that λ is a fixed constant and choose it as $\lambda = \Lambda/(2\kappa)$. Therefore, in this scenario, the cosmological constant is just a constant of integration. It is well known [62] that classically Unimodular Gravity produces the same physics as GR with a cosmological constant, but it differs from GR in the quantum regime.

Higher-order derivatives and non-locality

Another way to modify GR is to allow the field equations to contain higher order derivatives of the metric. General relativity is generalized by making the Einstein-Hilbert action a more general function of the Ricci scalar or by adding different scalar curvature invariants to the action. However, this procedure can also introduce instabilities into the theory, such as ghost-like degrees of freedom [63]. Interest in these theories grew when it was shown that the quantization of matter fields in an classical space-time can lead to theories in this class [64]. It is also known that $f(R)$ theories of gravity can have improved normalization properties [50], and that they can lead to a period of accelerated expansion early in the Universe's history. They have also been considered as a possible explanation for the observed late-time accelerated expansion of the Universe [65].

The $f(R)$ generalization of Einstein's equations is derived from an action of the form

$$S = \frac{1}{\kappa}\int dx^4\sqrt{-g}f(R) + S_M, \tag{3.2}$$

where $f(R)$ can be constructed from powers of the Ricci scalar R. By varying (3.2) with respect to the metric, one obtains the field equations

$$f_R R_{\mu\nu} - \frac{1}{2}f g_{\mu\nu} - \nabla_\mu\nabla_\nu f_R + g_{\mu\nu}\Box f_R = \frac{\kappa}{2}T_{\mu\nu}.$$

where $f_R \equiv df/dR$.

The field equations that one obtains from the least action principle associated with Eq. (3.2) depend on the variational principle that one adopts. There are 3 possibilities: the "Palatini approach" where the variation is made, independently, with respect to the metric and connection, the "metric-affine" approach, which follows the same process, with the peculiarity that the matter action is considered to be not only a functional of the metric, but also of the connection, and the "metric variation" where the connection is assumed to be the Levi-Civita one. For further details of the Palatini approach and the metric-affine approach the reader is referred to [66].

An interesting property is that $f(R)$ theories of gravity derived from the metric variational approach can be conformally transformed into a frame in which the field equations become those of General Relativity, with a minimally coupled scalar field. In

the general case one considers a conformal transformation of the form [67]

$$\tilde{g}_{\mu\nu} = f_R g_{\mu\nu},$$

which allows the field equations to be transformed into

$$\tilde{R}_{\mu\nu} - \frac{1}{2}\tilde{g}_{\mu\nu}\tilde{R} = \left(\nabla_\mu\phi\nabla_\nu\phi - \frac{1}{2}\tilde{g}_{\mu\nu}\Box\phi - \tilde{g}_{\mu\nu}V(\phi) + \tilde{T}_{\mu\nu}\right),$$

where $\phi \equiv \sqrt{3/\kappa}\ \ln f_R$ and

$$V(\phi) = \frac{Rf_R - f}{\kappa f_R^2}.$$

In this formulation, the energy-momentum tensor is not conserved. Another way to reformulate the theory in terms of scalar fields, while maintaining conservation of the energy-momentum tensor, is by doing a Legendre transformation. One can write the gravitational sector of the action (3.2) in the equivalent form

$$\mathcal{L} = \sqrt{-g}\left[f(\xi) + f'(\xi)(R - \xi)\right].$$

By making the definition $\phi = f'(\xi)$, assuming that $\phi(\xi)$ is an invertible function, defining also the potential $V(\phi) = \frac{1}{2}[\xi(\phi)\phi - f(\xi(\phi))]$ the Lagrangian density transforms into

$$\mathcal{L} = \sqrt{-g}[\phi R - 2V(\phi)].$$

We will come again to theories of this form, since they will be the main focus of the original contribution of this work.

One particular choice of $f(R)$ that is often studied is the Starobinsky model, where $f = R + \alpha R^2$. In this case, in the Newtonian limit, the line element becomes $ds^2 = -(1-2U)dt^2 + (1+2V)d\vec{x}^2$ with

$$U(r) = \frac{GM}{r}\left(1 + \frac{e^{-m_0 r}}{3}\right),$$
$$V(r) = \frac{GM}{r}\left(1 - \frac{e^{-m_0 r}}{3}\right),$$

where $m_0^2 = (6\alpha)^{-1}$ [68]. Therefore, for small values of α the Yukawa potential is exponentially suppressed and general relativity is recovered. The complete post-Newtonian

expansion can be found at [69].

Another possible way to modify GR is to add non-local fields. Lovelock's theorem implicitly assumes that the energy-momentum tensor enters the field equations linearly. By abdicating this assumption it is possible to construct theories in which the gravitational source is a nonlinear combination of the energy-momentum tensor, such that $\nabla_\mu T^{\mu\nu} = 0$ is still valid [70]. These theories satisfy the WEP and although they are equivalent to GR in vacuum, they differ from GR when coupled to matter. Because of this nonlinear coupling they resolve some of the curvature singularities that afflict fluid collapse and early time cosmology in GR [71].

Higher dimensions

Riemann, Cayley and Grassmann and others were responsible for the first studies on geometry in higher dimensions in the middle of the nineteenth century. The problem is more phenomenological than theoretical: we have the tools to study gravitational theories in higher dimensions since Riemannian geometry is not restricted to $3 + 1$ dimensions. Despite that, gravity does not act as a 10-dimensional force in our experiments. The stability of Earth's orbit is the simplest observation along these lines. The point source Newtonian potential will typically fall as $1/r^{D-3}$ in D dimensions; for $D \neq 4$, it follows that we cannot have stable planetary orbits, therefore gravity should not appear 10-dimensional on solar system scales. The word appear is used because there are models in which a mechanism hides the extra dimensions at certain scales such as the solar system, but which are revealed at shorter and/or greater distances.

Kaluza-Klein theory arose from an attempt to unify General Relativity and electrodynamics on a $4+1$ dimensional space where one of the spatial dimensions is small and compact [72, 73]. A profound question can be asked: how and why were the 3 dimensions of space able to grow large, while the extra dimension remained microscopically small? Unfortunately, a satisfactory answer to this question has not yet emerged. By performing a harmonic expansion of all fields along the extra dimension it is possible to compute an effective $3 + 1$ dimensional theory by integrating out the heavy modes, and then investigate the new degrees of freedom that have emerged and what implications their existence would entail. This idea is widely used by string theorists who compactify 10-dimensional string theories and 11-dimensional supergravity/M-theory on compact manifolds of 6 or

7 dimensions respectively [74]. Each different compactification gives a different effective 4-dimensional theory [75].

These effective theories predict the existence of scalar fields in nature. For example, the low energy gravi-dilaton string-frame effective action, including dilaton-dependent corrections, as given in [76, 77, 78] is:

$$S = \int d^4x\sqrt{-\tilde{g}}\left[\frac{e^{-2\psi(\phi)}}{2l_s^2}\tilde{R} - \frac{Z(\phi)}{2l_s^2}\tilde{g}^{\mu\nu}\tilde{\nabla}_\mu\phi\tilde{\nabla}_\nu\phi - \tilde{V}(\phi)\right] + S_m[\Psi_i, \tilde{g}_{\mu\nu} : g_i(\phi)], \qquad (3.3)$$

where l_s is the string lenght-scale, Ψ_i are the matter fields, $\tilde{R}$ is the Ricci scalar curvature constructed from $\tilde{g}_{\mu\nu}$ and $g_i(\phi)$ represent the "constants" of nature such as the gauge coupling constants, which are now dilaton-dependent. In the scenario of the string dilaton in the strong coupling regime, deviations from general relativity would not be observed, as long as the matter coupling of the dilaton was dragged to zero by the cosmological expansion. This is equivalent to the Damour-Polyakov mechanism, which will be explained later, with a minimum at infinity [79]. In the strong coupling regime, it is proposed in [76], that the dilaton has an exponentially decreasing potential similar to those used in quintessential models, and in [80] it was shown that the dilaton in this potential can be behave like dark energy. In [8] the screening mechanism that is the target of this work is proposed, allowing the dilaton to evade gravitational tests.

3.2 Scalar-Tensor Theories

3.2.1 High-energy and mathematical motivations

The most straightforward path to circumvent Lovelock's theorem consists of adding extra degrees of freedom. This option paves the way for countless possibilities where the metric can be coupled to scalar, vector and tensor fields. Because of the coupling with extra dynamical fields, these theories usually violate the equivalence principle. It is not straightforward to construct theories with extra fields nonminimally coupled to gravity or matter that avoid such problem. Because such degrees of freedom remain undetected to date, a major challenge for these theories has been to tame the behavior of the extra fields, so as to evade current experimental constraints related to their existence. One can, at first, adjust the free parameters of the theory, so the theory does not present deviations

from general relativity, but this does not guarantee the right cosmological behavior.

Scalar-tensor theories were put forward by P. Jordan about 50 years ago [81], by introducing a non-minimal coupling between a scalar field and gravity as described by GR, while the matter Lagrangian does not depend on the scalar field, making sure that the theory respected the weak-equivalence principle. Interpreting the consequences of this coupling leads to the conclusion that the gravitational coupling becomes spacetime-dependent, which can be used to explain why this constant today is so much smaller than the coupling constants of the electro-weak theory and the theory of the strong interactions. Another initial motivation for the introduction of scalar-tensor theories was the search for a theory respecting Mach's principle, which is not completely or explicitly embodied in general relativity [82].

From the high-energy perspective, one compelling reason to take scalar-tensor theories seriously is that they follow naturally, as an effective 4D theory, of string and Kaluza-Klein-like theories, furthermore, the low energy limit of the gravitational sector of bosonic string theory yields a Brans-Dicke theory (defined below) with $\omega_{BD} = -1$ [83, 84]. Currently, the only scalar field detected in Nature is the Higgs field, which was discovered in 2012 at the Large Hadron Collider (LHC).

To see on general grounds why a scalar field arises as a result of the compactification of an extra dimension, consider the 5-dimensional line element

$$ds^2 = \gamma_{\mu\nu} dx^\mu dx^\nu + 2\gamma_{\mu 5} dx^\mu dx^5 + \gamma_{55} dx^5 dx^5, \tag{3.4}$$

where x^μ, with μ running from 1 to 4, represent coordinates along the extended dimensions. Kaluza's idea was to suppose *a priori* that in some coordinates, the metric components $\gamma_{\mu\nu}$ do not depend on the fifth coordinate x^5. By defining

$$g_{\mu\nu} \equiv \gamma_{\mu\nu} - \frac{\gamma_{\mu 5}\gamma_{\nu 5}}{\gamma_{55}},$$

$$\kappa A_\mu = \frac{\gamma_{\mu 5}}{\gamma_{55}},$$

and

$$e^{2\phi} = \gamma_{55},$$

one can show that the 5-dimensional line element (3.4) can be written as $\mathrm{AIHPA}_1 990_{5_2 2_1 1 3_0} ds^2 =$

$g_{\mu\nu}dx^\mu dx^\nu + e^{2\phi}(dx^5 + \kappa A_\mu dx^\mu)^2$.

So, the 5-dimensional Ricci scalar can be written in terms of the 4-dimensional Ricci scalar constructed from $g_{\mu\nu}$:

$$^{(5)}R = {}^{(4)}R - 2e^{-\phi}\Box e^{\phi} - \frac{1}{4}\kappa^2 e^{2\phi}F_{\mu\nu}F^{\mu\nu}.$$

Therefore, the Einstein-Hilbert action in 5 dimensions,

$$S = \int d^5x\sqrt{-\gamma}\frac{^{(5)}R}{16\pi G_5},$$

becomes

$$S = \int d^4x\sqrt{-g}\frac{1}{16\pi G_5 e^{\phi}}\left(R - 2e^{-\phi}\Box e^{\phi} - \frac{1}{4}\kappa^2 e^{2\phi}F_{\mu\nu}F^{\mu\nu}\right)$$

when integrated over x^5. One can identify Newton's constant in 4 dimensions, G_4, as $G_4 = G_5 e^{\phi}$. Therefore the action represents a scalar field coupled to gravity and eletromagnetism.

Another occurrence of scalar-tensor theories, this time from a mathematical point of view, comes from the generalization of the Einstein-Hilbert action using Lyra geometry [85]. A $n-$dimensional Lyra spacetime consists of a smooth manifold equipped with a smooth scalar field ψ and a connection. The Lyra connection is given by

$$\Gamma^{\alpha}_{\mu\nu} = \frac{1}{\psi}\left\{ {\alpha \atop \mu\nu} \right\} + \frac{s+1}{\psi^2}g^{\alpha\kappa}(g_{\nu\kappa}\partial_\mu\psi - g_{\mu\nu}\partial_\kappa\psi),$$

where s is a constant, $\left\{ {\alpha \atop \mu\nu} \right\}$ are the usual Christoffel symbols, and the last term on the right hand side describes torsion. The Lyra connection is metric-perserving $\nabla_\alpha g_{\mu\nu} = 0$. The torsion tensor is given by $T^{\alpha}_{\mu\nu} = \frac{s}{\psi^2}(g^{\alpha}_{\nu}\nabla_\mu\psi - g^{\alpha}_{\mu}\partial_\nu\psi)$, so the connection is torsion-free if $s = 0$. The ψ field acts as a torsion potential. The Lyra curvature tensor and the Lyra curvature scalar are defined as

$$K^{\beta}_{\mu\nu\alpha} = \frac{1}{\psi^2}[\partial_\nu(\psi\Gamma^{\beta}_{\mu\alpha}) - \partial_\mu(\psi\Gamma^{\beta}_{\nu\beta}) + \Gamma^{\gamma}_{\mu\alpha}\Gamma^{\gamma}_{\gamma\nu} - \Gamma^{\gamma}_{\nu\alpha}\Gamma^{\beta}_{\gamma\mu}],$$

$$K = \frac{R}{\psi^3} + \frac{2(s+1)}{\psi^3}(1-n) + \frac{1}{\psi^4}[(s+1)^2(3n-n^2-2) - 2(s+1)(2-n)]\partial^\mu\psi\partial_\mu\psi.$$

Note that neither the curvature tensor nor the curvature scalar coincide with those of

Riemann geometry. The Lyra covariant volume element is $\psi^4\sqrt{-g}d^nx$. The generalization of the Einstein-Hilbert actions is

$$S = \int d^4x\psi^4\sqrt{-g}K,$$

then, using the previous definitions, the action becomes

$$S = \int d^4x\sqrt{-g}\left(\phi R - \frac{\omega}{\phi}g^{\mu\nu}\nabla_\mu\phi\nabla_\nu\phi\right)$$

with $\psi^2 = \phi$ and $\omega = 3(s^2-1)/2$. Again one obtains a scalar-tensor theory of gravity.

3.2.2 Brans-Dicke-type theories

The Jordan-Fierz-Brans-Dicke theory of gravity, commonly referred to as Brans-Dicke theory, is probably the most well-known alternative to Einstein's theory of general relativity. Here we will consider an extended class of models, in which the action, in the so-called *Jordan-frame*, is

$$S = \frac{1}{16\pi G}\int d^4x\sqrt{-\tilde{g}}\left[\Phi\tilde{R} - \frac{\omega(\Phi)}{\Phi}(\tilde{\partial}_\sigma\Phi)^2 - 2\tilde{V}(\Phi)\right] + S_m(\Psi,\tilde{g}_{\mu\nu}). \tag{3.5}$$

The original Brans-Dicke proposal had $\omega(\Phi) = \omega_{BD} = cte$, where ω_{BD} is the Brans-Dicke parameter. The factor of Φ in the denominator of the second term in brackets in Eq. (3.5) is introduced so that ω is dimensionless. The action (3.5) could be obtained almost immediately from the Kaluza-Klein's prescription.

By varying Eq. (3.5) with respect to the metric $g^{\mu\nu}$ and scalar field Φ, using

$$\delta(\Phi\tilde{R}) = \tilde{R}\delta\Phi + \Phi\tilde{R}_{\mu\nu}\delta\tilde{g}^{\mu\nu} + \Phi\tilde{\nabla}_\rho(\tilde{g}^{\mu\nu}\delta\tilde{\Gamma}^\rho_{\mu\nu} - \tilde{g}^{\mu\rho}\delta\tilde{\Gamma}^\sigma_{\sigma\mu}),$$

one obtains the field equations

$$\tilde{R}_{\mu\nu} - \frac{1}{2}\tilde{g}_{\mu\nu}\tilde{R} = \frac{8\pi G}{\Phi}\tilde{T}_{\mu\nu} + \frac{1}{\Phi}[\tilde{\nabla}_\mu\tilde{\nabla}_\nu - \tilde{g}_{\mu\nu}\tilde{\Box}]\Phi + \frac{\omega(\Phi)}{\Phi^2}[\partial_\mu\Phi\partial_\nu\Phi - \frac{1}{2}\tilde{g}_{\mu\nu}(\partial_\alpha\Phi)^2] - \tilde{g}_{\mu\nu}\frac{\tilde{V}(\Phi)}{\Phi}, \tag{3.6}$$

$$\frac{2\omega(\Phi)+3}{\Phi}\tilde{\Box}\Phi = \frac{8\pi G}{\Phi}\tilde{T} - \frac{\omega'(\Phi)}{\Phi}(\tilde{\partial}_\sigma\Phi)^2 + 2\tilde{V}'(\Phi) - 4\frac{\tilde{V}(\Phi)}{\Phi}. \tag{3.7}$$

From equations (3.6) and (3.7), and using the relationship

$$\tilde{\Box}(\tilde{\nabla}_\mu\Phi) - \tilde{\nabla}_\mu(\tilde{\Box}\Phi) = \tilde{R}_{\mu\nu}\tilde{\nabla}^\nu\Phi,$$

one can show that

$$\tilde{\nabla}_\mu\tilde{T}^{\mu\nu} = 0.$$

In the Jordan frame, the energy-momentum tensor of matter is covariantly conserved, so tests particles follow geodesic trajectories in this frame. However, gravity works differently from GR, since the scalar field modulates the strength of the interactions of matter with the metric field through the effective gravitational coupling G/Φ.

Weak-field regime

Let us now consider the weak field limit of this theory. To simplify, here we will consider a static, point source with no internal degrees of freedom. In this case, $v^j = 0$ and the PPN metric (2.48), in spherical coordinates, can be cast as

$$[\tilde{g}_{\mu\nu}] = \begin{pmatrix} -1 + h_{00}^{(1)}(r)\epsilon + h_{00}^{(2)}(r)\epsilon^2 & 0 & 0 & 0 \\ 0 & 1+\epsilon h(r) & 0 & 0 \\ 0 & 0 & (1+\epsilon h(r))\, r^2 & 0 \\ 0 & 0 & 0 & (1+\epsilon h(r))\, r^2\sin^2\theta \end{pmatrix},$$

The energy-momentum tensor of a point source can be written in the perfect-fluid form, $T^{\mu\nu} = \tilde{\rho}\tilde{u}^\mu\tilde{u}^\nu$, where $\rho = M/(\tilde{u}^0\sqrt{-\tilde{g}})\delta(r)$. We also expand the scalar field such that

$$\Phi(r) = \Phi_0 + \epsilon\delta\Phi^{(1)}(r) + \epsilon^2\delta\Phi^{(2)}(r).$$

To 0th order the scalar field equation (3.7) results in

$$V(\Phi_0) = V'(\Phi_0) = 0. \tag{3.8}$$

A nonvanishing $V(\Phi_0)$ (or, more precisely, $V(\Phi_0)/\Phi_0$) plays the role of a cosmological

constant. Since we required the metric to be asymptotically flat (and not asymptotically de Sitter, which would be more appropriate), the first equation of (3.8) implies that the cosmological constant is zero. Of course, one of the main motivations of studying scalar-tensor theories comes from models for dark energy and typically we will not require $V(\Phi_0)$ to vanish. This condition should be interpreted in the present context as valid in an "asymptotic" region far away from the sources, but still much smaller than the cosmological horizon. The second of the equations in (3.8) means that Φ_0 should correspond to an extremum of the potential.

At first order, the scalar field equation (3.7) becomes

$$\delta\Phi^{(1)''}(r) + \frac{2\delta\Phi^{(1)'}(r)}{r} = m_\Phi^2 \delta\Phi^{(1)}(r) - \frac{8\pi G M \delta(r)}{2\omega(\Phi_0)+3}, \tag{3.9}$$

where

$$m_\Phi^2 \equiv \frac{2\Phi_0 V''(\Phi_0)}{2\omega(\Phi_0)+3} \tag{3.10}$$

can be interpreted as the effective mass squared of the scalar field. At this order, only the 0th order approximation for the metric is required. One gets the solution

$$\delta\Phi^{(1)}(r) = \frac{2}{2\omega(\Phi_0)+3}\frac{GM}{r}e^{-m_\Phi r}. \tag{3.11}$$

The 00 component of Eq. (3.6), at first order, gives

$$h''(r) + \frac{2h'(r)}{r} = \frac{8\pi G M\delta(r)}{\Phi_0(2\omega(\Phi_0)+3)} - \frac{8\pi G M\delta(r)}{\Phi_0} - \frac{2m_\Phi^2}{(2\omega(\Phi_0)+3)\Phi_0}\frac{GM}{r}e^{-m_\Phi r},$$

which is solved by

$$h(r) = \frac{2GM}{r\Phi_0}\left(1 - \frac{e^{-m_\Phi r}}{2\omega(\Phi_0)+3}\right). \tag{3.12}$$

The 11 component of Eq. (3.6), at first order, has the following solution

$$h_{00}^{(1)}(r) = \frac{2GM}{r\Phi_0}\left(\frac{e^{-m_\Phi r}}{2\omega(\Phi_0)+3} + 1\right) = 2G_{\text{eff}}(r)\frac{M}{r}. \tag{3.13}$$

with

$$G_{\text{eff}}(r) \equiv \frac{G}{\Phi_0}\left(1 + \frac{e^{-m_\Phi r}}{2\omega(\Phi_0)+3}\right). \tag{3.14}$$

We see that the scalar mass defines a scale m_Φ^{-1}, in which the effective gravitational

coupling varies. Experiments that test the dependence of the gravitational acceleration with r^{-2} can therefore put bounds on m_Φ. In what follows, we will assume, for simplicity, that $m_\Phi \approx 0$, so that the gravitational constant today is given by

$$G_{\rm eff} \approx \frac{G}{\Phi_0}\left(\frac{2\omega(\Phi_0)+4}{2\omega(\Phi_0)+3}\right).$$

Comparison with Eq. (3.12) then yields the PPN parameter γ and one obtains

$$\gamma = \frac{1+\omega(\Phi_0)}{2+\omega(\Phi_0)}. \tag{3.15}$$

To obtain the parameter β one must solve the second order equations. The result is [37]

$$\beta = 1 + \frac{(d\omega/d\Phi)|_{\Phi_0}}{(2\omega(\Phi_0)+4)(2\omega(\Phi_0)+3)^2}. \tag{3.16}$$

We refer to [86] for more complete expressions for arbitrary m_Φ.

Current observations [87] indicate that $\gamma - 1 = (2.1 \pm 2.3) \times 10^{-5}$, which means that $\omega(\Phi_0) > 40000$ for the massless ($V = 0$) case. The best current constraint on the post-Newtonian parameter β comes from Mercury's perihelion shift and is $|\beta - 1| < 3 \times 10^{-3}$ [88]. Both constraints show that while the theory is certainly viable in the limit of large $\omega(\Phi_0)$, the scalar field must be weakly coupled in order to explain current experiments on Earth or in the solar system. Although explaining such high value of $\omega(\Phi_0)$ in the context of the massless Brans-Dicke theory is impossible, Damour and Nordtvedt [89] found that the field equations of the general Brans-Dicke-type theory can lead to an evolution of the function $\omega(\Phi(t))$ towards infinity during the evolution of the universe. Therefore, the value of $\omega(\Phi_0)$ can be explained as a consequence of the age of the universe.

3.2.3 Scalar-tensor theory in the Einstein frame

The action (3.5) can be transformed into a more familiar form by a conformal transformation of the type

$$\tilde{g}_{\mu\nu} = A^2(x) g_{\mu\nu} \equiv \Phi^{-1}(x) g_{\mu\nu}. \tag{3.17}$$

Under the transformation (3.17) one can show that the Christofell symbols, Ricci tensor and Ricci scalar transform as

$$\tilde{\Gamma}^{\alpha}{}_{\mu\sigma} = \Gamma^{\alpha}{}_{\mu\sigma} + \Theta^{\alpha}{}_{\mu\sigma},$$

where

$$\Theta^{\alpha}{}_{\mu\sigma} = \delta^{\alpha}{}_{\mu}\partial_{\sigma}\ln A + \delta^{\alpha}{}_{\sigma}\partial_{\mu}\ln A - \tilde{g}_{\mu\sigma}\partial^{\alpha}\ln A, \tag{3.18}$$

and

$$\tilde{R}_{\mu\nu} = R_{\mu\nu} - 2\nabla_{\mu}\nabla_{\nu}\ln A + 2\nabla_{\mu}\ln A\nabla_{\nu}\ln A - 2g_{\mu\nu}(\nabla\ln A)^2 - g_{\mu\nu}\Box\ln A,$$

$$A^2\tilde{R} = R - 6\nabla_{\mu}\ln A\nabla^{\mu}\ln A - 6\Box\ln A.$$

Using $\sqrt{-\tilde{g}} = A^4\sqrt{-g}$, $A^2 = \Phi^{-1}$, the resulting action is

$$S = \frac{1}{16\pi G}\int d^4x\sqrt{-g}\left\{R - \frac{1}{2\Phi^2}[3+2\omega(\Phi)]\nabla_{\mu}\Phi\nabla^{\mu}\Phi - 2A^4\tilde{V}\right\} + S_m(\Psi, A^2 g_{\mu\nu}).$$

Making the definitions

$$\frac{d\phi}{d\Phi} = \frac{M_{\rm Pl}}{2\sqrt{2}\Phi}(3+2\omega)^{-1/2}, \qquad V \equiv A^4 M_{\rm Pl}\tilde{V}, \tag{3.19}$$

where $M_{\rm Pl} \equiv 1/\sqrt{8\pi G}$ is the reduced Planck mass, the action transforms into the so-called *Einstein frame* representation:

$$S = \int d^4x\sqrt{-g}\left[\frac{M_{\rm Pl}^2}{2}R - \frac{1}{2}g^{\mu\nu}\partial_{\mu}\phi\partial_{\nu}\phi - V(\phi)\right] + S_m[\Psi, A^2(\phi)g_{\mu\nu}]. \tag{3.20}$$

In the absence of matter fields, these scalar-tensor theories can now be clearly seen to be conformally related to Einstein's theory in the presence of a minimally coupled scalar field with a potential. The effect of the nonminimal coupling in the Jordan frame gets translated, in the Einstein frame, to the matter sector. Now, matter fields couple not to the Einstein frame metric $g_{\mu\nu}$, but to the combination $A^2(\phi)g_{\mu\nu}$.

Variation of the action (3.20) with respect to $g^{\mu\nu}$ results in

$$G_{\mu\nu} = 8\pi G\left[T_{\mu\nu} + \nabla_{\mu}\phi\nabla_{\nu}\phi - g_{\mu\nu}\left(\frac{1}{2}\nabla^{\beta}\phi\nabla_{\beta}\phi + V(\phi)\right)\right]. \tag{3.21}$$

By varying the action with respect to ϕ, one obtains

$$\Box\phi = \frac{dV}{d\phi} - \frac{1}{A}\frac{dA}{d\phi}T = \frac{dV_{\rm eff}}{d\phi}. \tag{3.22}$$

Thus, because of its coupling to matter fields, the scalar field is affected by the ambient matter density, and is governed by the effective potential

$$V_{\rm eff} \equiv V(\phi) - \ln A(\phi) T. \tag{3.23}$$

Alternatively, the scalar field equation can be cast as

$$\Box\phi = \frac{d\tilde{V}_{\rm eff}}{d\phi}, \tag{3.24}$$

where

$$\tilde{V}_{\rm eff} \equiv V(\phi) - \frac{A(\phi)^4}{4}\tilde{T} \tag{3.25}$$

is written in terms of $\tilde{T}$, as defined in the Jordan frame.

The energy-momentum tensor $T_{\mu\nu}$, in Einstein's frame, relates to the energy-momentum tensor in Jordan's frame, $\tilde{T}_{\mu\nu}$, as follows:

$$T_{\mu\nu} \equiv -\frac{2}{\sqrt{-g}}\frac{\delta S}{\delta g^{\mu\nu}} = -\frac{2}{\sqrt{-\tilde{g}}}\frac{1}{A^{-4}}\frac{\delta S}{\delta \tilde{g}^{\alpha\beta}}\frac{\delta \tilde{g}^{\alpha\beta}}{\delta g^{\mu\nu}} = A^2(\phi)\tilde{T}_{\mu\nu}. \tag{3.26}$$

Therefore,

$$T^{\mu\nu} = A^6(\phi)\tilde{T}^{\mu\nu} \qquad T^{\mu}{}_{\nu} = A^4(\phi)\tilde{T}^{\mu}{}_{\nu} \qquad T = A^4(\phi)\tilde{T}.$$

In particular, if matter fields are described by a perfect fluid, one has

$$T_{\mu\nu} = (\epsilon + p)\, u_\mu u_\nu + p g_{\mu\nu}, \tag{3.27}$$

and a similar expression holds in Jordan's frame, involving $\tilde{\epsilon}$, $\tilde{p}$ and $\tilde{u}^\mu$. Then, the energy density, pressure, and fluid's four-velocity in the Einstein and Jordan representations are related as follows:

$$\epsilon = A^4(\phi)\tilde{\epsilon}, \qquad p = A^4(\phi)\tilde{p}, \qquad u^\mu = A(\phi)\tilde{u}^\mu. \tag{3.28}$$

Note that the fluid's 4-velocity is normalized in different ways in each frame, $g_{\mu\nu}u^\mu u^\nu = -1$ and $\tilde{g}_{\mu\nu}\tilde{u}^\mu\tilde{u}^\nu = -1$.

By taking the divergence of Eq. (3.21), one obtains the matter equations of motion,

$$\nabla^\nu T_{\mu\nu} = \frac{\beta(\phi)}{M_{\rm pl}} T \nabla_\mu \phi, \tag{3.29}$$

where

$$\beta(\phi) \equiv M_{\rm pl} \frac{d \ln A}{d\phi}. \tag{3.30}$$

Equation (3.29) reveals that test particles describe trajectories which are not geodesics of the Einstein-frame metric $g_{\mu\nu}$, but are instead forced by the scalar field gradient. Indeed, if u^μ is the particle's four-velocity, the scalar-induced acceleration is given by

$$a^\mu \equiv u^\nu \nabla_\nu u^\mu = -P^{\mu\nu} \frac{d \ln A}{d\phi} \partial_\nu \phi, \tag{3.31}$$

where $P^{\mu\nu} \equiv g^{\mu\nu} + u^\mu u^\nu$ is the projector operator onto the subspace orthogonal to u^μ.

3.3 Screening mechanisms

If the scalar field is conformally coupled to matter, some mysterious force associated with it may exist, but such force is not detected in experiments on Earth or in the solar system. We could at first adjust the parameters associated with the scalar field so that the theory shows no deviations from general relativity in our solar system, but this often prevents the desired cosmological behavior. One way to circumvent this problem is offered by the so-called *screening mechanisms*, which allow solar system constrains to be imposed while retaining freedom on cosmological scales so that the scalar field has an interesting cosmological phenomenology.

Evading gravitational problems caused by matter-coupled scalar fields requires the introduction of nonlinear terms in the Lagrangian description. Here we focus on two approaches, which follow essentially the same principle, in which properties of the theory change according to the local density. They are called the *Chameleon* and *Dilaton* (Damour-Polyakov) models. In these approaches one uses the freedom to choose the potential and coupling to matter [functions $V(\phi)$ and $A(\phi)$ in Eq. (3.20)], resulting in an effective potential whose minimum depends on T, the trace of the energy-momentum tensor, which is dominated by the mass density in Newtonian settings ($T \approx -\rho$). Chameleon models have a nonlinear potential, while the coupling $\beta(\phi)$ in Eq. (3.30) is constant.

Damour-Polyakov-inspired Dilaton models have a nonlinear coupling $A(\phi)$ where there is a field value in which the coupling is zero. As mentioned above, the mechanism present in both models, which is capable of hiding the effects of the scalar field in solar system scales, but also allows the correct cosmological behavior, is called the screening mechanism.

To understand, briefly, how a screening mechanism works, one can assume that the scalar field, on a large scale, is approximately constant, $\phi = \phi_0$, which by the scalar field equation (3.24), must correspond to a minimum of the effective potential: $dV_{\text{eff}}/d\phi|_{\phi_0} = 0$. Imposing a constant value asymptotically implies that the scalar field is homogeneously distributed and that potential dominates the energy density/pressure associated with the scalar field, so that the field behaves like dark energy on cosmological scales. Now consider some localized matter distribution, with characteristic mass M and radius R. Setting $\phi = \phi_0 + \delta\phi$ and assuming that gravity is weak ($GM/R \ll 1$) the scalar field equation (3.24) can be approximated to linear order by

$$\nabla^2\delta\phi - m_{\text{eff}}^2(\phi_0)\delta\phi = \rho \left.\frac{d\ln A}{d\phi}\right|_{\phi_0}, \tag{3.32}$$

where $m_{\text{eff}}^2 \equiv d^2V_{\text{eff}}/d\phi^2$ and ρ is the mass-density of the object, which we can assume to be constant for simplicity. The solution to Eq. (3.32) is

$$\delta\phi = \left.\frac{d\ln A}{d\phi}\right|_{\phi_0} \frac{f(M,R)}{r} e^{-m_{\text{eff}}(\phi_0)r}, \tag{3.33}$$

where $f(M,R)$ is some function of the mass and radius determined by matching the solution inside and outside of the body.

In order to suppress the fifth force mediated by the scalar field, which is proportional to the scalar field gradient, as shown in Eq. (3.31), at least one of the following must hold:

(i) $f(M,R) \ll 1$, meaning that not all mass sources the scalar field (the thin-shell effect discussed below);

(ii) The effective mass should be large asymptotically, $m_{\text{eff}}(\phi_0) \gg 1$;

(iii) The coupling to matter must be small: $\beta(\phi) \ll 1$.

In what follows we discuss in more detail how screening works in the prototypical example of the Chameleon model.

3.3.1 Chameleon

The Chameleon model, created by Justin Khoury and Amanda Weltman [90], features a screening mechanism that allows the mass associated with the field to be large in dense regions, making the scalar force extremely short-ranged in solar system scales (and, therefore, undetectable), but allowing the mass of the scalar field to become small enough in low-density regions relevant to cosmology. Additionally, the chameleon model features a thin-shell effect, whereby item (i) discussed above is implemented.

Following the requirement that the effective potential has a minimum, the chameleon model is described by the following conformal factor,

$$A(\phi) = e^{\beta\phi/M_{\rm Pl}}, \tag{3.34}$$

where β is a constant (assumed to be positive), and potential

$$V(\phi) = \mu^4 \left(\frac{\mu}{\phi}\right)^n. \tag{3.35}$$

So the effective potentials given in Eqs. (3.23) and (3.25) are

$$V_{\rm eff} = \mu^4 \left(\frac{\mu}{\phi}\right)^n - \frac{\beta\phi}{M_{\rm Pl}} T, \qquad \tilde{V}_{\rm eff} = \mu^4 \left(\frac{\mu}{\phi}\right)^n - \frac{1}{4} e^{4\beta\phi/M_{\rm Pl}} \tilde{T}.$$

In either case, considering $\phi/M_{\rm Pl} \ll 1$ the minimum of the effective potential is located at

$$\phi_{\rm min} = \left(-\frac{n M_{\rm Pl} \mu^{4+n}}{\beta \tilde{T}}\right)^{\frac{1}{n+1}},$$

with either T or $\tilde{T}$ appearing in the denominator. We see that for some values of n the effective potential has no minimum, such as when $n = -3, -5, -7, \cdots$. In the original work of Weltman and Khoury [90], $n = 1$ was used, and we shall adopt this choice from now on. Another interesting value of n is $n = -4$, for which the potential features a ϕ^4 self-coupling.

Each of the definition for the effective potential give rise to a notion of the Chameleon effective mass, $m_{\rm eff}(\phi) \equiv d^2 V_{\rm eff}/d\phi^2$ or $\tilde{m}_{\rm eff}(\phi) \equiv d^2 \tilde{V}_{\rm eff}/d\phi^2$. For instance, we have that

$$m^2_{\rm eff}(\phi_{\rm min}) \approx \mu^{4+n} \left[n(1+n) \left(\frac{\beta \tilde{T}}{n M_{\rm Pl} \mu^{4+n}} \right)^{\frac{n+2}{n+1}} \right] + \frac{4\beta^2}{M^2_{\rm Pl}} \tilde{T}.$$

From this we see that the effective mass is an increasing function of density (or $|\tilde{T}|$), at least when $n > -1$. On the other hand, note that if the pressure dominates the energy-momentum tensor, such that $\tilde{T} = 3\tilde{p} - \tilde{\epsilon} > 0$, the potential has no minimum for several values of n, including $n = 1$.

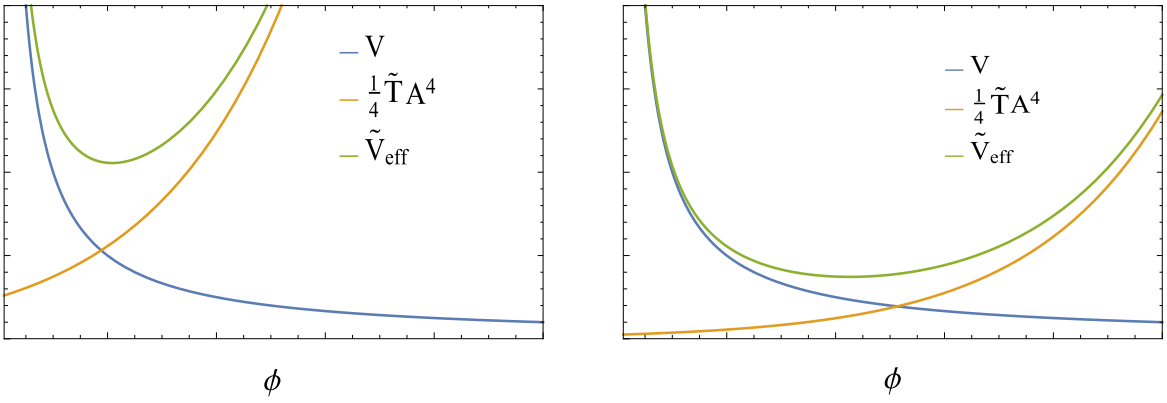

(a) High density

(b) Low density

Figure 3.1: Sketches of the effective potential $\tilde{V}_{\text{eff}}$, bare potential and the conformal coupling for (a) high density and (b) low density matter, both of which with $\tilde{\epsilon} > 3\tilde{p}$. Here $\beta = n = 1$.

Figure 3.6 shows sketches of the effective potential $\tilde{V}_{\text{eff}}$, as well as the separate contributions from the bare potential and the matter coupling. By comparing the two subfigures, it is possible to notice that the higher the density, the lower the value of the field at the minimum. Figure 3.2 sketches the effective mass $\tilde{m}_{\text{eff}}$ and shows that the higher the density the greater the effective mass of the scalar field. In practice, the ratio between the two can be greater than many orders of magnitude. Therefore, in regions such as the solar system, the force associated with the scalar field is suppressed due to a large effective mass causing the force to be short-ranged.

Figures 3.6 and 3.2 consider only non-relativistic matter, for which the trace of the energy-momentum tensor is dominated by the energy density: $\tilde{T} = 3\tilde{p} - \tilde{\epsilon} \approx -\tilde{\epsilon}$. However, in extreme cases, where the pressure dominates the energy-momentum tensor and $\tilde{T} > 0$, the effective potential does not admit a minimum and the effective mass of the scalar field becomes imaginary. Figure 3.3 sketches the effective potential in this case. How the screening mechanism behaves in these cases will be investigated in the next chapter, which contains the original contribution of this thesis.

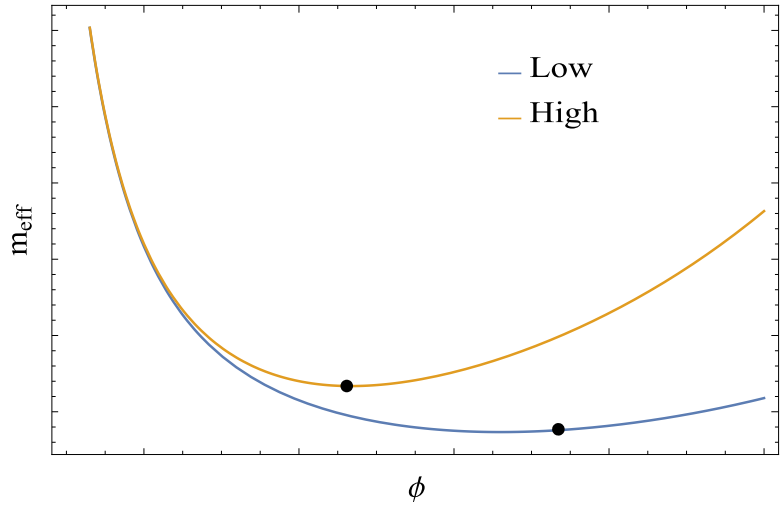

Figure 3.2: The effective mass of the scalar field, for both high and low density non-relativistic matter. The black dot indicates the minimum of the effective potential in both cases.

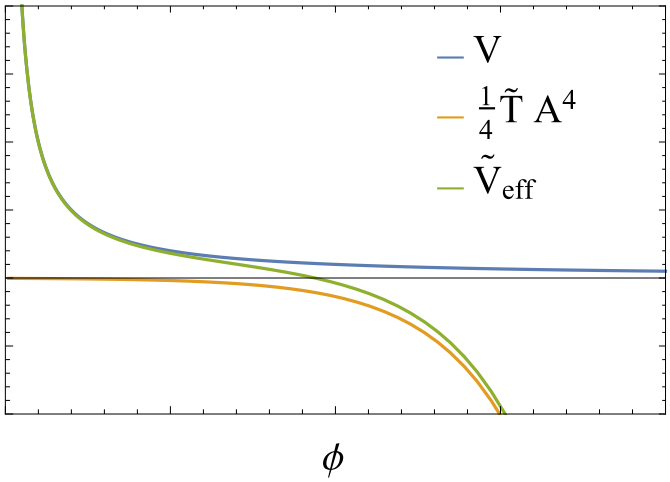

Figure 3.3: Sketch of the effective potential, bare potential and conformal coupling for high densisty matter with $3\tilde{p} > \tilde{\epsilon}$. Here $\beta = n = 1$.

Newtonian approximation: Thin and thick shell solutions

Besides the environmental dependence of the effective mass of the scalar field, an important ingredient of the chameleon screening mechanism is the so-called thin shell effect. Here we consider an analytical approximation that reveals this effect, showing that for objects like the Earth and the Sun, the contribution to the force associated with the scalar field comes from a thin shell close to the surface. We will then compare this solution with the numerical result in the Newtonian regime.

Let us consider an isolated object with radius R and homogeneous density ρ_c, immersed in a background density ρ_b which is also homogeneous. Considering non-relativistic matter, a flat metric and static configurations, the scalar field equation (3.24) becomes

$$\phi''(r) + \frac{2}{r}\phi'(r) = \left[-n\frac{M^{4+n}}{\phi^{n+1}} + \frac{\beta}{M_{\rm Pl}}e^{\frac{\beta\phi}{M_{\rm Pl}}}\rho\right]. \tag{3.36}$$

Note that the equation is written in terms of the density that satisfies the continuity equation in Einstein's frame, defined as $\tilde{\rho}A^3 = \rho$, and obeys

$$\rho = \begin{cases} \rho_c & r < R_c, \\ \rho_b & r > R_c. \end{cases} \tag{3.37}$$

To avoid divergence at the origin, we impose $\phi'(0) = 0$ [$\phi(0) = \phi_i$], and for the force associated with the field to go to zero at infinity, the field gradient must vanish asymptotically, so we need $\phi \to \phi_b = \text{cte}$ as $r \to \infty$. Analyzing Eq. (3.36), we note that it implies that ϕ_b must correspond to a minimum of the effective potential, which is obtained by

$$\left.\frac{dV}{d\phi}\right|_{\phi_b} + \frac{\beta}{M_{\rm Pl}}e^{\frac{\beta\phi_b}{M_{\rm Pl}}}\rho_b = 0. \tag{3.38}$$

If we interpret the scalar field as part of the matter sector, in the same way as in Chapter 1, and compare its contribution to that of a perfect fluid, the asymptotic boundary condition also implies that

$$p_\phi = -\epsilon_\phi, \tag{3.39}$$

asymptotically, where the pressure and density associated with the field are dominated by the potential $V(\phi)$, that is, presenting the correct cosmological behavior.

In interpreting the scalar field equation, a very useful analogy can be made: associating the field to the position and r to time, we can imagine that the particle moves under the inverted effective potential ($-V_{\rm eff}$); the second term on the left side of Eq. (3.36), proportional to $1/r$ acts as a damping term.

The particle initially starts from rest (since $\phi'(0) = 0$) with initial position ϕ_i. In the initial instants (r close to zero), the particle is stuck in its initial position, since the damping factor dominates. As time goes by (r grows) and the damping factor stops dominating, the particle starts to roll over the potential (in, say, $r = R_{\rm roll}$). Upon reaching

the critical time ($r = R_c$), the particle jumps to a potential with another shape, because the density changes, it then starts to climb this potential. If we choose the correct initial value, we can reach the expected asymptotic value (ϕ_b).

Let ϕ_c denote the field value that corresponds to a minimum of the potential inside the star, i.e., such that

$$\left.\frac{dV}{d\phi}\right|_{\phi_c} + \frac{\beta}{M_{\rm Pl}} e^{\frac{\beta\phi_c}{M_{\rm Pl}}} \rho_c = 0. \tag{3.40}$$

Depending on whether ϕ_i is close to or distant from ϕ_c, we will have different outcomes. In what follows, we will treat these two cases separately.

- **Thin shell:** $(\phi_i - \phi_c) \ll \phi_c$

If the initial value is close enough to the minimum of the effective potential, the particle will then be stuck until the friction term is small enough; it will start to roll at a distance $R_{\rm roll}$ close to the object's surface. Therefore, the field will remain approximately constant, that is, close to the initial value:

$$\phi(r) = \phi_1(r) = \phi_c, \qquad 0 \leq r < R_{\rm roll}.$$

After the field begins to distance itself from the minimum, the term $\frac{\beta}{M_{\rm Pl}} e^{\frac{\beta\phi_c}{M_{\rm Pl}}} \rho_c$ starts to dominate the effective potential. If $\beta\phi \ll M_{\rm Pl}$, the scalar field equation between $R_{\rm roll}$ and R becomes

$$\phi''(r) + \frac{2}{r}\phi'(r) \approx \frac{\beta}{M_{\rm Pl}}\rho_c. \tag{3.41}$$

The solution is

$$\phi_2(r) = \frac{\beta\rho_c}{6M_{\rm Pl}} r^2 + \frac{A_1}{r} + A_2, \tag{3.42}$$

where the constants A_1 and A_2 are determined by imposing continuity at $r = R_{\rm roll}$. By imposing $\phi_1(R_{\rm roll}) = \phi_2(R_{\rm roll})$ and $\phi_1'(R_{\rm roll}) = \phi_2'(R_{\rm roll})$ one obtains

$$A_1 = \frac{\beta\rho_c R_{\rm roll}^3}{3M_{\rm Pl}}, \qquad A_2 = \phi_c - \frac{\beta\rho_c R_{\rm roll}^2}{2M_{\rm Pl}}.$$

So the final solution is

$$\phi_2(r) = \frac{\beta\rho_c}{3M_{\rm Pl}} \left(\frac{r^2}{2} + \frac{R_{\rm roll}^3}{r}\right) - \frac{\beta\rho_c R_{\rm roll}^2}{2M_{\rm Pl}} + \phi_c, \qquad R_{\rm roll} < r < R. \tag{3.43}$$

For $r > R$ the density changes to ρ_b and the field climbs the potential. Considering that the field is close to the minimum of the effective potential in the external region of the object, we can approximate the scalar field equation to

$$\phi''(r) + \frac{2}{r}\phi'(r) \approx m_b^2(\phi - \phi_b), \tag{3.44}$$

where $m_b \equiv m_{\rm eff}(\phi_b)$. The general solution is

$$\phi_3(r) = B_1\frac{e^{m_b r}}{r} + B_2\frac{e^{-m_b r}}{r} + \phi_b. \tag{3.45}$$

Imposing that $\phi_3 \to \phi_b$ when $r \to \infty$ and continuity at the surface, we can determine the constants B_1 and B_2:

$$B_1 = 0, \qquad\qquad B_2 = [\phi_2(R) - \phi_b]Re^{m_b R},$$

So the final solution is

$$\phi_3(r) = [\phi_2(R) - \phi_b]\frac{e^{-m_b(r-R)}}{r} + \phi_b, \qquad r > R.$$

By imposing $\phi_2'(R) = \phi_3'(R)$ it is possible to determine $R_{\rm roll}$ exactly. Instead, we use the fact that $R_{\rm roll}$ is close to R, so that $\Delta R \equiv (R - R_{\rm roll})/R \ll 1$, to express $R_{\rm roll}$ in terms of ΔR. Keeping only first order terms in ΔR, we have:

$$\phi_2'(R) = \frac{R\beta\rho_c}{3M_{\rm Pl}}\left(3\Delta R - 3\Delta R^2 + \Delta R^3\right) \approx \frac{R\beta\rho_c}{3M_{\rm Pl}}\Delta R. \tag{3.46}$$

Noting that $\phi_2(R) = \phi_c + O(\Delta R^2)$, we obtain

$$\phi_3'(R) \approx \frac{(1 + m_b R)(\phi_b - \phi_c)}{R}. \tag{3.47}$$

Equating these expressions one can obtain a relationship between ΔR and $(\phi_b - \phi_c)$, and from it determine $R_{\rm roll}$:

$$\Delta R = \frac{4\pi M_{\rm Pl} R(1 + m_b R)(\phi_b - \phi_c)}{3\beta M}. \tag{3.48}$$

where $M = \rho_c(4\pi R^3/3)$ is the mass of the object. The solution $r > R$ can be written as

$$\phi_3(r) = -\frac{3\beta}{4\pi M_{\rm Pl}}\Delta R\frac{Me^{-m_b(r-R)}}{r} + \phi_b, \qquad r > R, \tag{3.49}$$

Finally, we can express the force due to chameleon in a test particle, if the mass of the field is small enough, as follows [see Eq. (3.31)]

$$F_\phi(r) = -m\frac{\beta}{M_{\rm Pl}}\frac{d\phi_3}{dr} = 6\beta^2\Delta R F_{\rm Newton}(r) \quad \text{for} \quad r \ll m_b^{-1}. \tag{3.50}$$

Note that the force is suppressed by a factor $\Delta R \ll 1$ with respect to the Newtonian force $F_{\rm Newton}$, which can be understood as indicating that only a fraction of the object's mass contributes to the fifth force. This is a simple derivation of the *thin shell effect*. These conclusions will be compared with the full numerical solution subsequently.

- **Thick shell:** $\phi_i \gtrsim \phi_c$

In this case, the particle starts to roll as soon as it is released, as the field is sufficiently displaced from the minimum of the potential in the center of the star. We can obtain an approximate solution inside the object by making $R_{\rm roll} \to 0$ for the solution $\phi_2(r)$ in Eq. (3.43), replacing the central value of the field with a value ϕ_i to be determined:

$$\phi_1(r) = \frac{\beta\rho_c}{6M_{\rm Pl}}r^2 + \phi_i, \qquad 0 \le r < R.$$

The exterior solution has the same form as in the previous case, given by Eq. (3.45). Only the integration constants change, which are also obtained by imposing continuity on the surface and a good behavior at infinity:

$$\phi_2(r) = \left(\phi_i - \phi_b + \frac{\beta\rho_c R^2}{6M_{\rm Pl}}\right)\frac{Re^{-m_b(r-R)}}{r} + \phi_b, \qquad r > R.$$

Equating the derivatives on the surface, we obtain a relationship between ϕ_i and ϕ_b,

$$\phi_i = \phi_b - \frac{\beta\rho_c R^2}{6M_{\rm Pl}}\left(1 + \frac{2}{1+m_b R}\right). \tag{3.51}$$

Replacing this relation and simplifying, one gets

$$\phi_2(r) = -\frac{\beta}{4\pi M_{\rm Pl}(1+m_b R)}\frac{M e^{-m_b(r-R)}}{r} + \phi_b, \qquad r > R. \tag{3.52}$$

The fifth force in this case is

$$F_\phi(r) = -m\frac{\beta}{M_{\rm Pl}}\frac{d\phi_2}{dr} = -2\beta^2\frac{GmM}{r^2}(1+m_b r)e^{-m_b r}. \tag{3.53}$$

When $r \ll m_b^{-1}$ this reduces to

$$F_\phi(r) = 2\beta^2 F_{\rm Newton}(r). \tag{3.54}$$

This result shows that the field will contribute with a correction to the gravitational constant $G_{\rm eff} = G(1+2\beta^2)$.

- **Thin versus thick shell solutions**

The thin and thick shell calculations can be used to impose constrains on the free parameters of the theory. One can show [90] that the Eötvos parameter η [see Eq. (2.4)], which is a measure of the difference in relative free-fall acceleration for two different bodies, can be approximated by

$$\eta = 2\frac{|a_1 - a_2|}{|a_1 + a_2|} \approx 10^{-4}\beta^2\Delta R_{\rm Earth}, \tag{3.55}$$

where $\Delta R_{\rm Earth}$ is the thin shell factor of the Earth. Assuming $\beta \sim 1$, current constraints on η imply that

$$\Delta R_{\rm Earth} \lesssim 10^{-7}, \tag{3.56}$$

which can be translated to

$$\mu \lesssim 10^{-3}{\rm eV}, \tag{3.57}$$

for $\beta = n = 1$.

On the other hand, the cosmological constraint is

$$\mu \approx \rho_{DE} \approx 2.40 \times 10^{-3}\text{eV}, \tag{3.58}$$

assuming that the chameleon field should be responsible for the energy density associated with dark energy when evaluated at the minimum of the effective potential. The fact that the energy scales in Eqs. (3.57) and (3.58) coincide indicates that the thin shell effect could in principle provide an effective screening of the chameleon force in solar system scales, while allowing it to play the role of dark energy in cosmological scales.

Newtonian approximation: Numerical integration

The validity of the analytical approach developed in the previous section is confirmed by integrating the scalar field equation numerically. In the following, we take $n = 1$, as in Ref. [90]. The field equation

$$\phi''(r) + \frac{2}{r}\phi'(r) = \left[-\frac{\mu^5}{\phi^2} + \frac{\beta}{M_{\rm Pl}} e^{\frac{\beta\phi}{M_{\rm Pl}}}\rho\right], \tag{3.59}$$

rewritten in terms of the dimensionless parameters defined by

$$\phi = \phi_0\hat{\phi}, \qquad \rho = \rho_0\hat{\rho}, \qquad r = r_0\hat{r},$$

becomes

$$\hat{\phi}''(\hat{r}) + \frac{2}{\hat{r}}\hat{\phi}'(\hat{r}) = \left[-\frac{A}{\hat{\phi}^2} + Be^{C\hat{\phi}}\right], \tag{3.60}$$

with

$$A = \frac{\mu^5 r_0^2}{\phi_0^3}, \qquad B = \frac{\beta r_0^2 \rho_0}{M_{\rm Pl}\phi_0}, \qquad C = \frac{\beta\phi_0}{M_{\rm Pl}}.$$

If we choose $A = B = 1$ and ρ_0 such that $\hat{\rho} = 1$, one obtains

$$\phi_0 = \left(\frac{M_{\rm Pl}\mu^5}{\beta\rho_0}\right)^{\frac{1}{2}}, \tag{3.61}$$

$$r_0 = \left(\frac{\phi_0^3}{\mu^5}\right)^{\frac{1}{2}}. \tag{3.62}$$

Note that the C coefficient depend ons ϕ_0, which, by Eq. (3.61), depends on ρ_0, which has different values inside and outside of the object.

Integration starts at $\hat{r} = 0$ with initial conditions $\hat{\phi}'(0) = 0$ and $\hat{\phi}(0) = \hat{\phi}_i$. In practice, to avoid numerical divergences, we start the integration at a small $\hat{r} = \epsilon$, with initial conditions given by a Taylor expansion of $\hat{\phi}$ close to $\hat{r} = 0$:

$$\hat{\phi}(\epsilon) = \hat{\phi}_i + \hat{\phi}_2\epsilon^2,$$
$$\hat{\phi}'(\epsilon) = 2\hat{\phi}_2\epsilon,$$

where

$$\hat{\phi}_2 = \frac{1}{6}\left(-\frac{1}{\hat{\phi}_i^2} + e^{C_1\hat{\phi}_i}\right). \tag{3.63}$$

Here C_1 denotes the value of C inside the star.

To impose that the field is well-behaved at infinity, so that the chameleon mediated forces vanish asymptotically, we define

$$F(\hat{\phi}_i, \hat{r}_{\rm ext}) = \hat{\phi}(\hat{r}_{\rm ext})|_{\hat{\phi}_i} - \hat{\phi}_b, \tag{3.64}$$

where $\hat{r}_{\rm ext}$ is a sufficiently large value of $\hat{r}$ (ideally $\hat{r}_{\rm ext} \to \infty$), $\hat{\phi}(r_{\rm ext})|_{\hat{\phi}_i}$ is the scalar field value at $\hat{r}_{\rm ext}$ given an initial guess $\hat{\phi}_i$ for its central value, and $\hat{\phi}_b$ denotes the field value at the minimum of the effective potential outside the source. Then one searches for $\hat{\phi}_i$ such that $F(\hat{\phi}_i, \hat{r}_{\rm ext}) = 0$, with $\hat{r}_{\rm ext}$ appropriately chosen. Using the secant method, with an initial guess close to the minimum of the effective potential inside the object, we obtain a confirmation of the analytical approach made previously.

Following [91], let us first consider a Beryllium ball with density $\rho_{\rm Be} = 9\times10^{19} J/m^3$ and radius $R = 40/M$ where $M = 6\times10^3 m^{-1}$, in the air, with density $\rho_{\rm air} = 9\times10^{15} J/m^3$. Choosing $\beta = 1$, the minimum of the effective potential in the interior/exterior and the chameleon mass are

$$\phi_{\rm Be} \approx M, \qquad m_{\rm Be} \approx 8.9 \times 10^3 m^{-1},$$
$$\phi_{\rm air} \approx 100M, \qquad m_{\rm air} \approx 8.9 m^{-1}.$$

The thin shell factor is

$$\Delta R = \frac{4\pi M_{\rm Pl} R(1 + m_{\rm air}R)}{3\beta M}(\phi_{\rm air} - \phi_{\rm Be}) \approx 0.06. \tag{3.65}$$

In Fig. 3.4 we show the scalar field profile obtained numerically, together with the approximation derived in the previous section. The scalar field is nearly constant inside the object and starts to grow near the surface until it reaches its asymptotic value.

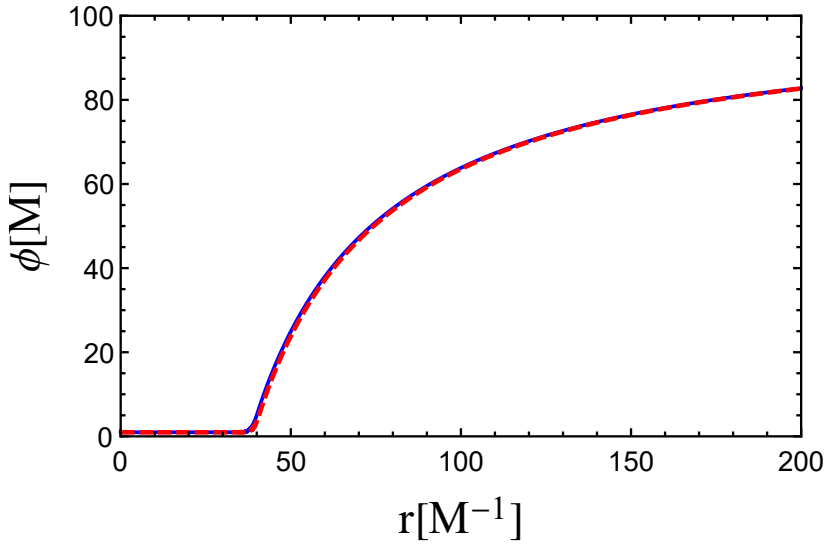

Figure 3.4: Comparison between the numerical and analytical solutions for the scalar field, in the case of a thin shell structure. The solid line represents the numerical solution, the dashed line represents the analytical solution.

A case where there is no thin shell is shown in Fig. 3.5, together with the analytical approximation obtained previously. For this plot we use the same parameters as before, but with $R = 1/M$.

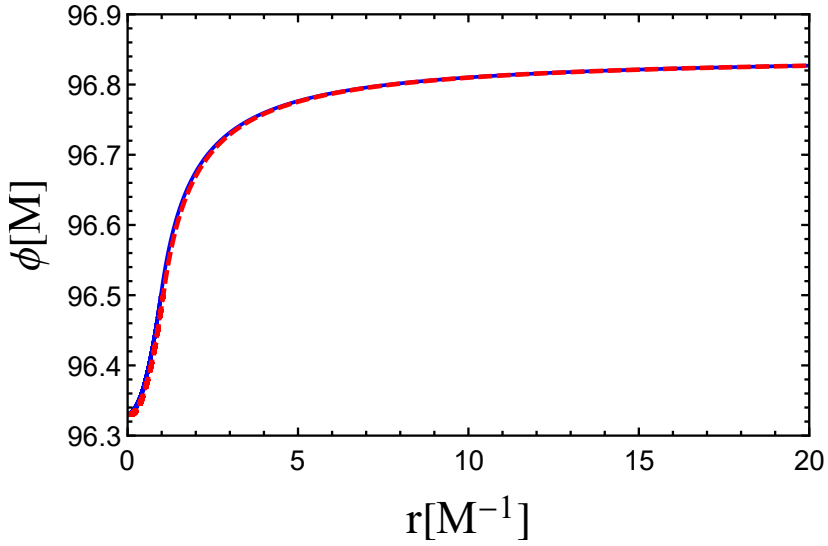

Figure 3.5: Comparison between the numerical and analytical solutions for the scalar field, in the case of a thick shell structure. The solid line represents the numerical solution, the dashed line represents the analytical solution.

3.3.2 Dilaton

The Dilaton model is based on the Damour-Polyakov mechanism, proposed by T. Damour and A. Polyakov in 1994 [79]. This model shows that a massless Dilaton decouples from matter as the field evolves cosmologically. Note that the mechanism was proposed before the discovery of accelerated expansion of the Universe. In the scenario of the screening mechanism, the dilaton matter coupling varies according to the local content of matter, such that in regions as the solar system the coupling is small enough that there is no deviation from general relativity.

The effective string action describing the massless dilaton in four dimensions has the general form in the Jordan frame (with $\kappa_4^2 = 8\pi G$):

$$S = \int d^4x\sqrt{-\tilde{g}}\frac{1}{2\kappa_4^2 e^{2\Phi}}\left(\tilde{R} + 4\tilde{\Box}\Phi - 4(\tilde{\nabla}\Phi)^2\right) + S_m(\Psi, \tilde{g}_{\mu\nu}). \tag{3.66}$$

In the Einstein frame, the action turns to

$$S = \int d^4x\sqrt{-g}\left[\frac{1}{2\kappa_4^2}R - \frac{1}{2\kappa_4^2}g^{\mu\nu}\partial_\mu\phi\partial_\nu\phi\right] + S_m[\Psi, A^2(\phi)g_{\mu\nu}]. \tag{3.67}$$

The equation of motion for the scalar field is

$$\Box\phi = -\kappa_4^2\frac{d\ln A}{d\phi}T. \tag{3.68}$$

In a flat cosmological background it reduces to

$$\ddot{\phi} + 3H\dot{\phi} = \kappa_4^2\frac{d\ln A}{d\phi}T. \tag{3.69}$$

The Damour-Polyakov mechanism assumes that $A(\phi)$ has a minimum at ϕ_0, such that close to the minimum, $A(\phi)$ can be expressed as

$$A(\phi) \approx 1 + \frac{A_2}{2}(\phi - \phi_0)^2,$$

and the scalar field equation becomes

$$\ddot{\phi} + 3H\dot{\phi} = \frac{\kappa_4^2 A_2(\phi - \phi_0)}{1 + \frac{A_2}{2}(\phi - \phi_0)^2}T. \tag{3.70}$$

In radiation dominated era, the trace of energy-momentum tensor is zero, $T = 0$. Therefore, the coupling with matter does not affect the evolution of the scalar field. However, in the matter dominated era $T \approx -\rho_m$, the coupling with matter drags the scalar field to the minimum; therefore as the field evolves it decouples itself from matter.

The environmentally dependent Dilaton introduced in [8] follows a similar principle, but the coupling is dependent on the content of energy and matter. The starting point is an action (3.3), which can be written in the Einstein frame as

$$S = \int d^4x\sqrt{-g}\left[\frac{1}{2\kappa_4^2}R - \frac{k^2(\phi)}{\kappa_4^2}g^{\mu\nu}\partial_\mu\phi\partial_\nu\phi - V(\phi)\right] + S_m[\Psi_i, A^2(\phi)g_{\mu\nu}, g_i], \qquad (3.71)$$

where $k^2(\phi) = 3\beta^2(\phi) - A^2(\phi)Z(\phi)/2c_1^2$; $\beta(\phi) = d\ln\phi/\phi$ and $V(\phi) = A^4(\phi)\tilde{V}(\phi)$. By imposing $A(\phi_0) \approx 1$ at present, where ϕ_0 is the value of ϕ today, and that we are in the strong coupling limit, such that $e^{-\phi_0} \ll 1$, the potential and couplings can be approximated by [8]

$$\tilde{V}(\phi) \approx \tilde{V}_0 e^{-\phi}, \qquad Z(\phi) \approx -\frac{2c_1^2}{\lambda^2} + b_z e^{-\phi}, \qquad g_i^{-2} \approx \tilde{g}_i^{-2} + b_i e^{-\phi},$$

and it was showed [76] that the Dilaton could in principle act as dark energy. Assuming that $b_Z \approx b_i \approx \lambda \approx 1$ and $c_1 \gg 1$, in this approximation, the function $k(\phi)$ is given by

$$k^2(\phi) \approx 3\beta^2(\phi) + \lambda^{-2}.$$

Note that the action defined in (3.3) contains functions $g_i(\phi)$ that represent the 'constants' of nature, which are now Dilaton dependent. Due to the dependence on the scalar field, a contribution of the type

$$\delta S_i = \sum_i \frac{\delta S_m}{\delta g_i}\frac{\delta g_i}{\delta\phi}\delta\phi$$

is proportional to $e^{-\phi}$, which is assumed to be small enough that the contribution from δS_i can be neglected. Then from now on the g_i couplings will be ignored.

If $\hbar = c = 1$ the scalar field ϕ is dimensionless. We define $\tilde{\phi} = M_{\rm Pl}\phi$ so that the theory is comparable to Chameleon:

$$S = \int d^4x\sqrt{-g}\left[\frac{1}{2\kappa_4^2}R - k^2(\tilde{\phi})g^{\mu\nu}\partial_\mu\tilde{\phi}\partial_\nu\tilde{\phi} - V(\tilde{\phi})\right] + S_m[\Psi_i, A^2(\tilde{\phi})g_{\mu\nu}]. \qquad (3.72)$$

Redefining the field again such that $\mathrm{d}\Phi = \sqrt{2}k(\tilde{\phi})\mathrm{d}\tilde{\phi}$, where the dimension of Φ is the

same as $\tilde{\phi}$ because k is dimensionless:

$$S = \int d^4x\sqrt{-g}\left[\frac{1}{2\kappa_4^2}R - \frac{1}{2}g^{\mu\nu}\partial_\mu\Phi\partial_\nu\Phi - V(\tilde{\phi}(\Phi))\right] + S_m[\Psi_i, A^2(\tilde{\phi}(\Phi))g_{\mu\nu}], \tag{3.73}$$

thus the kinetic term is in canonical form. The action is the same as in the Chameleon model, so we don't need to re-obtain the field equations; they are the same as in Chameleon, however, with the potential and coupling implicitly defined:

$$G_{\mu\nu} = 8\pi G\left[\right]T_{\mu\nu} + \nabla_\mu\Phi\nabla_\nu\Phi - g_{\mu\nu}\left(\frac{1}{2}\nabla^\beta\Phi\nabla_\beta\Phi + V(\tilde{\phi}(\Phi))\right)\right], \tag{3.74}$$

$$\Box\Phi = \frac{dV(\tilde{\phi}(\Phi))}{d\Phi} - \frac{d\ln A(\tilde{\phi}(\Phi))}{d\Phi}T = \left(\frac{dV(\tilde{\phi})}{d\tilde{\phi}} - \frac{d\ln A(\tilde{\phi})}{d\tilde{\phi}}T\right)\frac{d\tilde{\phi}}{d\Phi}. \tag{3.75}$$

The conformal coupling is defined as

$$A(\tilde{\phi}) = 1 + \frac{A_2}{2M_{\rm Pl}^2}(\tilde{\phi} - \tilde{\phi}_0)^2, \tag{3.76}$$

so the potential in the Einstein frame reads

$$V(\tilde{\phi}) = \left(1 + \frac{A_2}{2M_{\rm Pl}^2}(\tilde{\phi} - \tilde{\phi}_0)^2\right)^4 \tilde{V}_0 e^{-\tilde{\phi}/M_{\rm Pl}}. \tag{3.77}$$

To understand how the screening mechanism works in the dilaton model, it is necessary to look at the matter coupling

$$\beta(\Phi) = M_{\rm Pl}\frac{d\ln A}{d\Phi} = \frac{1}{\sqrt{2}k(\tilde{\phi})A(\tilde{\phi})}\frac{A_2}{M_{\rm Pl}}(\tilde{\phi} - \tilde{\phi}_0). \tag{3.78}$$

Knowing that the scalar field seeks to minimize the effective potential when it is possible, the central idea is to make the value of the scalar field at the minimum of the effective potential (let us call it $\tilde{\phi}_{\rm min}$) be dragged to the minimum of A (at $\tilde{\phi}_0$) as the density of matter increases, in such a way that the effective coupling with matter, as given by (3.78), decreases.

When evaluated at the minimum of the effective potential, the coupling (3.78) can be written as follows:

$$\beta(\Phi(\tilde{\phi}_{\rm min})) = \frac{1}{\sqrt{2}k(\tilde{\phi}_{\rm min})\left(4 - \frac{A(\tilde{\phi}_{\rm min})^4\tilde{T}}{V(\tilde{\phi}_{\rm min})}\right)}.$$

If we consider non-relativistic matter, with $\tilde{T} \approx -\tilde{\rho}_m$, and assuming that $V(\tilde{\phi})$ is responsible for the late-time acceleration of the universe, then

$$\tilde{\rho}_m A^4/V \approx (\Omega_{\text{baryonic matter}+\Omega_{\text{dark matter}}})/\Omega_\Lambda \approx 0.27/0.73,$$

where it was used that $A \approx 1$ (the scalar field is close to the minimum of A today). Therefore, we have cosmologically $\beta(\tilde{\phi}_{\text{min}}) \approx 0.2$. For non-relativistic matter ($\tilde{T} \approx -\tilde{\rho}_m$), $\beta(\tilde{\phi}_{\text{min}})$ decreases as $\tilde{\rho}_m$ grows, as required for the screening to occur in regions such as the solar system.

It is possible to constraint one of the free parameters of the theory, noting that for non-relativistic matter, $\tilde{T} < 0$ and $\beta(\tilde{\phi}_{\text{min}}) \lesssim 1/(4\sqrt{2})$, so that

$$\frac{(\tilde{\phi}_{\text{min}} - \tilde{\phi}_0)}{M_{\text{Pl}}} \lesssim \frac{1}{4\sqrt{2}A_2}. \tag{3.79}$$

For the minimum of the effective potential to be close to the minimum of A and for the coupling with matter to be small, effectively screening the effects of the scalar field, we must have $A_2 \gg 1$. Note that the discussion made here considers only pressureless matter and can be extended to the case where $\tilde{\epsilon} > 3\tilde{p}$, however in more extreme cases the situation may be different, as will be seen in the next section.

Figures 3.6a and 3.6b sketch the effective potential, bare potential and the conformal coupling for non-relativistic matter with low and high densities. As the density increases the minimum of the effective potential tends to the minimum of the conformal coupling (in the plot we set $\tilde{\phi}_0 = 0$ for simplicity), therefore decreasing the effective coupling β. For relativistic matter, in extreme cases where pressure dominates the energy momentum tensor, the minimum of the effective potential ceases to exist as shown in Figure 3.7, the consequences of this are part of the original result of this thesis and will be investigated in the next section.

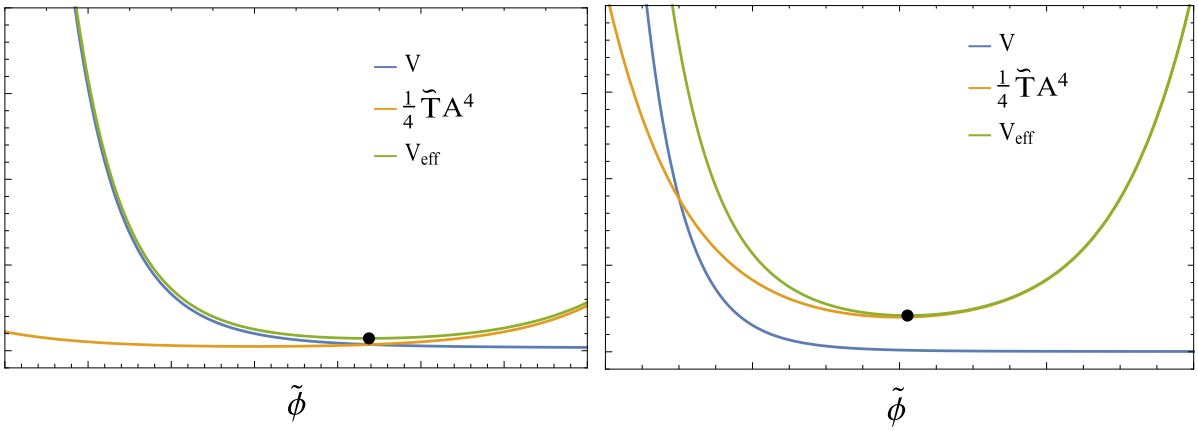

(a) Low density (b) High density

Figure 3.6: Sketches of the effective potential $\tilde{V}_{\text{eff}}$, bare potential and the conformal coupling for (a) low density and (b) high density matter, both of which with $\tilde{\epsilon} > 3\tilde{p}$. The black dot indicates the minimum of the effective potential in each case. Note that the minimum of the effective potential approaches the minimum of A in the high density case.

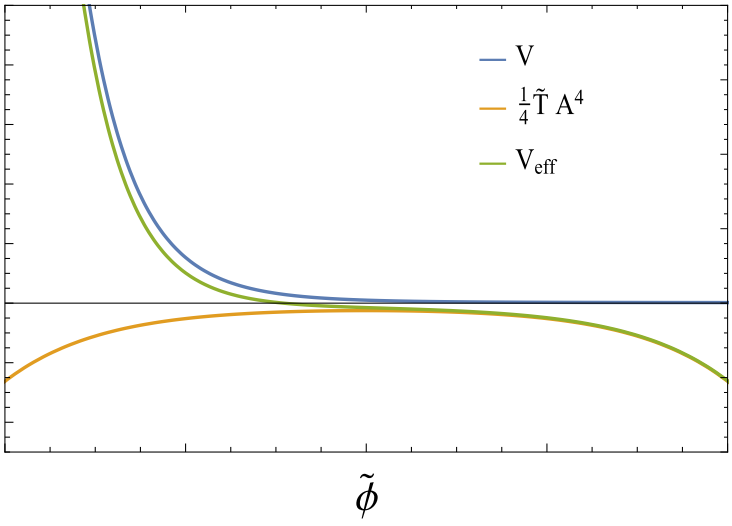

Figure 3.7: Sketch of the effective potential, bare potential and conformal coupling when $\tilde{T} > 0$. Note that the effective potential has no minimum in this case.

Chapter 4

Neutron stars and screening mechanisms

Neutron stars are a possible end state of stellar evolution. As a massive main sequence progenitor evolves, nuclear burning produces an iron-rich core. When all nuclear fuel is exhausted, the core must be supported by the degeneracy pressure. Additional deposits of mass from the burning crust cause the nucleus to exceed the Chandrasekhar limit[1]. Then the electron-degeneracy pressure is overcome, and the nucleus collapses. At these densities, the iron nuclei are divided into alpha particles. As the density increases further, electrons and protons combine to form neutrons via electron capture, releasing neutrinos. When densities reach nuclear density, a combination of strong force repulsion and neutron degeneracy pressure stops the contraction. The outer shell is thrown out by a flow of neutrinos produced in the creation of the neutrons, becoming a supernova. The result of this process is a neutron star. If the remaining object has a mass greater than the neutron star limit (of about 2-3 solar masses), the combination of degeneracy pressure and nuclear forces is insufficient to support it, and it collapses further to become a black hole.

Neutron stars combine a rich (and still poorly understood) microphysics with strong gravitational fields. These elements make neutron stars a fascinating laboratory where it is possible to test not only nuclear physics models, but also modified theories of gravity, helping to investigate how gravity interacts with matter at the highest possible densities.

[1]The Chandrasekhar limit corresponds to a mass of approximately 1.4 solar masses ($M_\odot$), which is the maximum mass of a white dwarf.

In the context of scalar-tensor theories, we already saw how the screening mechanism emerges as a viable option to suppress the effects of the scalar field on solar system scales. The way the screening mechanism behaves in ultra-dense regions is an interesting question, and will be the subject of this chapter. In particular, we will show how sufficiently compact neutron stars can by partially unscreened if they allow for a pressure-dominated phase in their cores, such that $p > \epsilon/3$ (and $T > 0$) in a region of their interior.

We begin, in Sec. 4.1 with a discussion on the nuclear equation of state and the models that we will adopt. Next, the hydrostatic equilibrium equations are derived and integrated numerically, and equilibrium properties of neutron stars are investigated. Finally, the equations that govern the radial perturbations are derived and are also integrated numerically, so that the stability of the solutions found previously can be assessed.

4.1 Equation of state

The equation of state (EOS) condenses all the complex microphysics of the neutron star interior in a relation, say, between pressure and rest-mass density, $\tilde{p} = \tilde{p}(\tilde{\rho})$ [2]. However, the equation of state of nuclear matter within the different layers of a neutron star is not known precisely due to the theoretical difficulties associated with extrapolating the behavior of quantum chromodynamics, superconductivity and superfluidity of matter to that regime. The problem becomes worse due to the empirical difficulties of observing the properties of an object that is hundreds of parsecs away, and the impossibility of producing such dense environments in terrestrial laboratories. Among the many difficulties related to this extrapolation, it is found that, at large enough densities, it is energetically favorable that some of the nucleons combine to form hyperons. However, the presence of hyperons would typically reduce the maximum mass of neutron stars, producing a tension between nuclear physics and astronomical observations in what is known as the hyperon puzzle [92]. Additional difficulties for nuclear models include the proper description of strong hadron-quark phase transitions [93], deconfinement of quarks, or the formation of crystalline structures [94].

Naturally, the physical reliability of any nuclear model is determined by comparing

[2] More generally, this relation can also involve temperature. However, neutrino emission when a neutron star is formed tend to rapidly cool it. Typically it is a good approximation to consider $T \approx 0$.

their astrophysical predictions with the available observations. Measurements of neutron star masses from the observation of binary pulsar systems lead to the conclusion that neutron stars can be as massive as two solar masses, as in pulsars PSR J0348 + 0432, with 2.01 ± 0.04 $M_\odot$ [95], PSR J1614- 2230, with 1.97 ± 0.04 $M_\odot$ [96] and PSR J2215 + 5135, with 2.27 $^{+0.17}_{-0.15} M_\odot$ [97]. A more difficult task is the observational determination of neutron star radii, as it depends on elements, such as the distance from the star, the uncertainties in the modeling of the crust, the absorption of the emitted X-rays by the interstellar medium [98], etc. In fact, the measurement of the radius of neutron stars is the target of new generations of X-ray missions, which have restricted it to the 9.9 - 12 km [99] range. Recently, the LIGO-Virgo Collaborations have reported the first measurement of a neutron star tidal deformability, which can help to estimate their radii [100].

4.1.1 Piecewise-polytropic parametrization

Since the phase of matter in the neutron star core is unknown, many models have been proposed. Current candidates for the EOS include nonrelativistic and relativistic mean-field models; models for which neutron-star cores are dominated by nucleons, by hyperons, by pion or kaon condensates, and by strange quark matter (free up, down, and strange quarks); and one cannot yet rule out the possibility that the ground state of cold matter at zero pressure might be strange quark matter [101, 102, 103, 104].

Here, on the other hand, we will describe a phenomenological parametrization of the nuclear EOS, developed by [105]. The idea is to have a flexible parametrization that can be used to fit different theoretical models.

A polytropic equation of state has the form,

$$p = K\rho_{\rm nuc}c^2 \left(\frac{\rho}{\rho_{\rm nuc}}\right)^{\Gamma}, \tag{4.1}$$

where Γ is the adiabatic index, K is a dimensionless quantity and $\rho_{\rm nuc}$ is a reference density, which we take to be of the order of the nuclear density. The first law of thermodynamics,

$$d\left(\frac{\epsilon}{\rho}\right) = -pd\left(\frac{1}{\rho}\right),$$

has the immediate integral

$$\frac{\epsilon}{\rho c^2} = (1+\alpha) + \frac{K}{\Gamma - 1}\left(\frac{\rho}{\rho_{\rm nuc}}\right)^{\Gamma-1}, \tag{4.2}$$

where α is a constant. The requirement $\lim_{\rho\to 0}\epsilon/(\rho c^2) = 1$ implies $\alpha = 0$, therefore $\frac{\epsilon}{\rho c^2} = 1 + \frac{K}{\Gamma-1}\left(\frac{\rho}{\rho_{\rm nuc}}\right)^{\Gamma-1}$.

Here we adopt a piecewise polytropic parametrization, where the star is divided into parts above a density ρ_0 in which different polytropic phases are used, satisfying Eqs. (4.1) and (4.2), each with its own values of K_i, Γ_i and α_i. Therefore, for $\rho_{i-1} \le \rho \le \rho_i$,

$$p = K_i \rho_{\rm nuc} c^2 \left(\frac{\rho}{\rho_{\rm nuc}}\right)^{\Gamma_i}, \qquad \epsilon = (1+\alpha_i)\rho c^2 + \frac{K_i}{\Gamma_i - 1}\rho_{\rm nuc} c^2 \left(\frac{\rho}{\rho_{\rm nuc}}\right)^{\Gamma_i}. \tag{4.3}$$

For the phases to be connected in a continuous way, one must have

$$K_{i+1} = \frac{p(\rho_i)}{\rho_{\rm nuc} c^2}\left(\frac{\rho_{\rm nuc}}{\rho_i}\right)^{\Gamma_{i+1}} \tag{4.4}$$

and

$$\alpha_i = \frac{\epsilon(\rho_{i-1})}{\rho_{i-1}c^2} - 1 - \frac{K_i}{\Gamma_i - 1}\left(\frac{\rho_{i-1}}{\rho_{\rm nuc}}\right)^{\Gamma_i - 1}. \tag{4.5}$$

Global neutron-star observables, such as the mass, are not very sensitive to the EOS below nuclear saturation density, because the fraction of mass at low densities is small. For the low-density region, we use an analytic form of the SLy EOS that closely matches its tabulated values, with four polytropic pieces. The four regions correspond roughly to a nonrelativistic electron gas, a relativistic electron gas, neutron drip, and the density range from neutron drip to nuclear density.

Table 4.1: The polytropic parameters of each piece of the analytic form of SLy EOS below nuclear density. Here Γ_i and K_i are dimensionless, ρ_i is in g/cm^3. The last dividing density is the density where the low density EOS is matched to the high density EOS and depends on the parameters p_1 and Γ_1 of the high density EOS given in table 4.2.

K_i	Γ_i	ρ_i
1.38254	1.58425	2.44034×10^7
1.29399×10^{-2}	1.28733	3.78358×10^{11}
2.26229×10^{-4}	0.62223	2.62780×10^{12}
4.75734×10^{-3}	1.35692	–

The high-density region is divided into 3 parts, so that phase of the matter in the

Table 4.2: The free parameters Γ_1, Γ_2, Γ_3 and matching pressure p_1 for the SLy, ENG, MPA1 and H4 EOSs. Here Γ_i are dimensionless, p_1 is in dyne/cm^2. The K_i parameters are determined by the relation (4.4).

EOS	Γ_1	Γ_2	Γ_3	$\log(p_i)$
SLy	3.005	2.988	2.851	34.384
ENG	3.514	3.130	3.168	34.437
MPA1	3.446	3.572	2.887	34.495
H4	2.909	2.246	2.144	34.669

core and its stiffness is parameterized by the adiabatic index Γ. The transition from one phase to another is done at $\rho_1 = 10^{14.7}$ g/cm^3, and $\rho_2 = 10^{15.0}$ g/cm^3. Besides the free parameters Γ_1, Γ_2, and Γ_3, the pressure at ρ_1 is also a free parameter in the model. From it K_1 can be determined. K_2 and K_3 can be determined by matching the pressures at ρ_1 and ρ_2 with Eq. (4.4).

The high and low density regions are connected at a density fixed by equating the first polytropic phase of the high density region with the last phase of the low density state EOS:

$$\rho_{tr} = \rho_{\rm nuc}\left(\frac{K_{\rm SLy}}{K_1}\right)^{1/(\Gamma_1-\Gamma_{\rm SLy})} .$$

The scheme is represented in Figure 4.2.

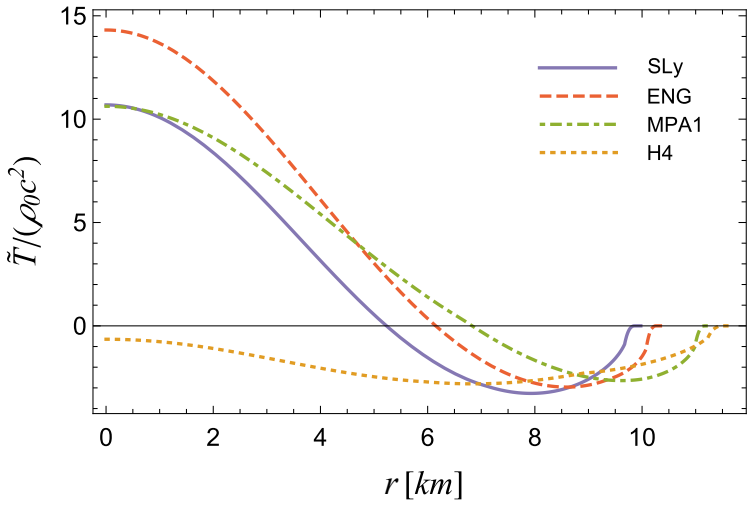

Figure 4.1: Radial profile of $\tilde{T} = 3\tilde{p} - \epsilon$ for the most massive stars allowed by the SLy, ENG, MPA1, and H4 EoS in GR.

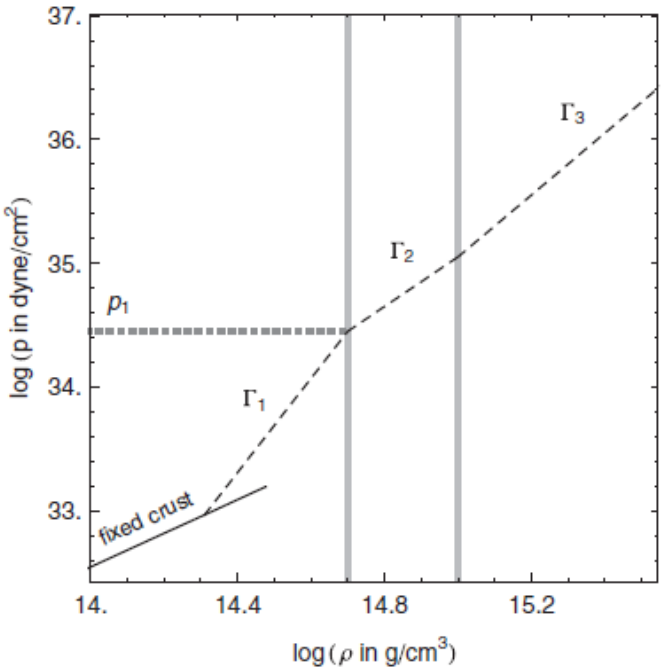

Figure 4.2: Given the crust EOS and the parameters Γ_i and p_1 of the core EOS, the density at which they are joined and the parameters α_i and K_i can be determined. Figure reproduced from Ref. [106].

The EOS used in this work are: SLy, based on a method that uses two potentials to describe the interaction between the particles; ENG and MPA1, based on the Brueckner-Hartree-Fock method, and H4, based on a relativistic mean-field theory with hyperons. The best piecewise polytropic fit to these EOS, as computed in Ref. [106], is shown in Table 4.2.

Figure 4.1 shows the radial profile of the trace of the energy momentum tensor for the most massive stars allowed by the SLy, ENG, MPA1, and H4 EoS in GR. These are obtained by solving the hydrostatic equilibrium equations, to be discussed in the next section. The pressure-dominated phase, with $\tilde{T} = 3\tilde{p} - \tilde{\epsilon} > 0$, which may occur near the nucleus for some EOS is interesting for studying the behavior of the screening mechanism in ultra-dense regions. We will investigate this scenario in the next sections.

4.2 Hydrostatic equilibrium equations

The starting point for obtaining the properties of neutron stars in hydrostatic equilibrium is to obtain the field equations from the theory in question, inside the star. Assuming that the star's matter distribution is spherically symmetric and static, we can use the

following ansatz for the line element [see Eq. (2.19) and the preceding discussion]

$$ds^2 = -e^{\nu(r)}dt^2 + e^{\lambda(r)}dr^2 + r^2(d\theta^2 + \sin^2\theta d\phi^2).$$

The task is summarized in finding the free functions $\nu(r)$ and $\lambda(r)$. The Einstein tensor for the line element above can be computed with the aid of Eqs. (2.20)-(2.23).

Neutron stars are typically well described by a perfect fluid energy-momentum tensor, Eq. (2.44), together with an equation of state which relates p and ϵ. In Einstein's frame, the energy-momentum tensor depends on the field, through Eq. (3.29). So we specify the EOS in terms of Jordan-frame quantities since in this frame the usual thermodynamic relation for energy conservation holds: $d(\tilde{\epsilon}/\tilde{\rho}) = -\tilde{p}d(1/\tilde{\rho})$. The relationships between quantities in Einstein and Jordan frames are given in Eq. (3.28).

Using the tt component of Eq. (3.21), it is possible to obtain an equation for the mass aspect function $m(r)$ defined through

$$e^{\lambda(r)} = \frac{1}{1 - 2m(r)/r}. \tag{4.6}$$

We take $G = 1$ in this section. Assuming that the scalar field is also static and spherically symmetric, $\phi = \phi(r)$, we have:

$$\begin{aligned} G_{tt} = \frac{2e^{\nu(r)}m'(r)}{r^2} &= 8\pi\left(T_{tt} + \partial_t\phi\partial_t\phi - g_{tt}\left(\frac{1}{2}g^{rr}\partial_r\phi\partial_r\phi + V(\phi)\right)\right) \Rightarrow \\ m'(r) &= 4\pi r^2\left[\epsilon(r) + \frac{1}{2}\left(1 - \frac{2m(r)}{r}\right)\phi'(r)^2 + V(r)\right], \end{aligned} \tag{4.7}$$

where was it used that $T_{tt} = \epsilon(r)e^{2\nu(r)}$.

Using the rr component of Eq. (3.21), it is possible to obtain an equation for $\nu(r)$:

$$\begin{aligned} G_{rr} &= 8\pi\left(T_{rr} + \partial_r\phi\partial_r\phi - g_{rr}\left(\frac{1}{2}g^{rr}\partial_r\phi\partial_r\phi + V(\phi)\right)\right) \Rightarrow \\ \nu' &= \frac{1}{\left(1 - \frac{2m(r)}{r}\right)}\left\{\frac{2m(r)}{r^2} + 8\pi r\left[p(r) + \frac{1}{2}\left(1 - \frac{2m(r)}{r}\right)\phi'(r)^2 - V(r)\right]\right\}. \end{aligned} \tag{4.8}$$

where was it used that $T_{rr} = p(r)\left(1 - \frac{2m(r)}{r}\right)$.

To obtain an equation for $p(r)$, taking an easier path, one can use the conservation

of the energy-momentum tensor in the Jordan frame,

$$\tilde{\nabla}_\nu \tilde{T}^{\mu\nu} = \partial_\nu \tilde{T}^{\mu\nu} + \tilde{T}^{\sigma\nu}\tilde{\Gamma}^{\mu}{}_{\sigma\nu} + \tilde{T}^{\sigma\mu}\tilde{\Gamma}^{\nu}{}_{\sigma\nu} = 0, \tag{4.9}$$

where $\tilde{\Gamma}^{\alpha}{}_{\mu\sigma} = \Gamma^{\alpha}{}_{\mu\sigma} + \Theta^{\alpha}{}_{\mu\sigma}$, with $\Theta^{\alpha}{}_{\mu\sigma}$ given in Eq. (3.18). The non-zero components of $\tilde{\Gamma}^{\mu}_{\nu\rho}$ are

$$\tilde{\Gamma}^{t}{}_{tr} = \frac{\nu'(r)}{2} + \frac{d}{dr}\ln A, \qquad \tilde{\Gamma}^{r}{}_{rr} = \frac{rm'(r) - m(r)}{r^2 - 2rm(r)} + \frac{d}{dr}\ln A,$$

$$\tilde{\Gamma}^{\theta}{}_{r\theta} = \tilde{\Gamma}^{\phi}{}_{r\phi} = \frac{1}{r} + \frac{d}{dr}\ln A, \qquad \tilde{\Gamma}^{r}{}_{\theta\theta} = \frac{1}{\sin^2\theta}\tilde{\Gamma}^{r}{}_{\phi\phi} = -(r - 2m(r))\left(1 + r\frac{d}{dr}\ln A\right),$$

$$\tilde{\Gamma}^{r}{}_{tt} = e^{\nu(r)}\left(1 - \frac{2m(r)}{r}\right)\left(\frac{1}{2}\nu'(r) + \frac{d}{dr}\ln A\right).$$

The r-component of Eq. (4.9) then results, after some tedious calculation, in

$$\tilde{p}'(r) = -(\tilde{p} + \tilde{\epsilon})\left(\frac{\nu'}{2} + \frac{d}{dr}\ln A\right). \tag{4.10}$$

Finally, the scalar field equation (3.24), after some manipulation, becomes

$$\phi''(r) + \phi'(r)\left[\frac{2}{r} + \frac{1}{2}\left(\nu'(r) - \lambda'(r)\right)\right] = e^{\lambda(r)}\left[\frac{dV}{d\phi} - \frac{d\ln A}{d\phi}T\right]. \tag{4.11}$$

Putting together the results obtained so far, and recovering factors of c, G and $\hbar$, we have

$$m' = \frac{4\pi r^2}{c^2}\left[A^4\tilde{\epsilon} + \frac{1}{2}\left(1 - \frac{2Gm}{rc^2}\right)(\phi')^2\frac{c^3}{\hbar} + V\right], \tag{4.12}$$

$$\nu' = \left(1 - \frac{2Gm}{rc^2}\right)^{-1}\left[\frac{2Gm}{r^2c^2} + \frac{8\pi G}{c^4}r\left(A^4\tilde{p} + \frac{c^3}{2\hbar}\left(1 - \frac{2Gm}{rc^2}\right)(\phi')^2 - V\right)\right] \tag{4.13}$$

$$\tilde{p}'(r) = -(\tilde{p} + \tilde{\epsilon})\left(\frac{\nu'}{2} + \frac{d}{dr}\ln A\right), \tag{4.14}$$

$$\phi'' + \phi'\left[\frac{2}{r} + \frac{1}{2}\left(\nu' - \lambda'\right)\right] = e^{\lambda}\frac{\hbar}{c^3}\left[\frac{dV}{d\phi} - A^3\frac{dA}{d\phi}(3\tilde{p} - \tilde{\epsilon})\right]. \tag{4.15}$$

These are the equations that describe the hydrostatic equilibrium in scalar-tensor theories with a scalar field non-minimally coupled to matter. Here the fluid quantities in the

Einstein frame have been replaced by those in the Jordan frame.

If one defines dimensionless variables $\hat{r}$, $\hat{m}$, $\hat{p}$, $\hat{\epsilon}$, such that

$$\hat{\epsilon} \equiv \frac{\tilde{\epsilon}}{\rho_{\rm nuc} c^2}, \qquad \hat{p} \equiv \frac{\tilde{p}}{\rho_{\rm nuc} c^2}, \qquad \hat{m} \equiv m \frac{\sqrt{G^3 \rho_{\rm nuc}}}{c^3}, \qquad \hat{r} \equiv r \frac{\sqrt{G \rho_{\rm nuc}}}{c}, \tag{4.16}$$

as well as a dimensionless scalar field $\hat{\phi}$ and potential $\hat{V}$ though

$$\hat{\phi} \equiv \phi \frac{G}{\hbar c}, \qquad \hat{V} \equiv \frac{V}{\rho_{\rm nuc} c^2}, \tag{4.17}$$

then the dimensionless variables satisfy a set of equations identical to (4.12)-(4.15), but with $G = c = \hbar = 1$. Note that $\rho_{\rm nuc}$ does not enter the final equations, and is simply a reference density that let us recover usual dimensionful quantities. In what follows we use $\rho_{\rm nuc} \equiv 1.66 \times 10^{14}$ g/cm^3 as a reference density, which is of the order of the nuclear saturation density.

A subtle detail must be noted: the ϕ field is the redefined field for the case of the dilaton model. To obtain the equations in terms of the field in which the kinetic term is not in canonical form, one must replace ϕ' by $\sqrt{2} k(\phi) \phi'$.

Note that the scalar field and its potential act as an effective source of pressure/density. When the screening mechanism is successful, that is, when the scalar field is able to minimize itself in almost the entire interior of the object, in such a way that $\frac{d \ln A}{d\phi}$ and ϕ' are small, the equations above resemble the case of hydrostatic equilibrium in General Relativity plus a cosmological constant, which here would be identified as the potential. If the screening mechanism is not effective, in such a way that $\frac{d \ln A}{d\phi}$ and ϕ' are large enough, the modifications provided by the scalar field will cause deviations from General Relativity. For $A(\phi) \to 1$, $V(\phi) \to 0$ and $\phi'(r) \to 0$, the equations reduce to those of GR.

In order to explore the structure of neutron stars in theories with screening mechanisms, we aim to solve Eqs. (4.12)-(4.15) numerically. In what follows, we discuss the boundary conditions that should be applied to the problem and the numerical procedure we follow, before reporting our results.

It is worthwhile to mention that neutron stars are typically not static, and a more realistic description should include rotation. Also, the equations we derived rely on the assumption of isotropy, while certain phenomena, such as high-density relativistic

interactions or superfluidity, are able to introduce a certain degree of anisotropy [107]. Moreover, the consideration of anisotropies in the energy-momentum tensor may be also necessary in order to correctly address differentially rotating stars.

4.2.1 Boundary conditions

At $r = 0$, we impose that $m(0) = 0$ and that all variables are regular. So, expanding the equations close to the origin $r \approx 0$,

$$\hat{\phi} \approx \phi_0 + \phi_2 \hat{r}^2 + \ldots, \quad \nu = \nu_0 + \nu_2 \hat{r}^2 + \ldots, \quad \hat{m} = m_3 \hat{r}^3 + \ldots, \quad \hat{p} = p_0 + p_2 \hat{r}^2 + \ldots,$$

where

$$\phi_2 = \frac{1}{6}\left[\left.\frac{dV}{d\phi}\right|_{\phi_0} + A(\phi_0)^3 \left.\frac{dA}{d\phi}\right|_{\phi_0} (\epsilon_0 - 3p_0)\right],$$

$$\nu_2 = -\frac{8\pi}{3}V(\phi_0) + \frac{4\pi}{3}A(\phi_0)^4(3p_0 + \epsilon_0), \qquad m_3 = \frac{4\pi}{3}\left[A(\phi_0)^4\epsilon_0 + V(\phi_0)\right],$$

$$p_2 = -(p_0 + \epsilon_0)\left(\frac{\nu_2}{2} + \frac{\phi_2}{A(\phi_0)}\left.\frac{dA}{d\phi}\right|_{\phi_0}\right),$$

with $\epsilon_0 = \tilde{\epsilon}(p_0)$ being determined by the equation of state. For the dilaton model, the expansion of the scalar field around the origin is different:

$$\tilde{\phi}_2 = \frac{\phi_2}{2k^2(\tilde{\phi}_0)}.$$

As in the Newtonian case, the solutions of interest are those in which the force associated with the field is zero at infinity, $F_\phi \overset{r\to\infty}{\to} 0$, which implies that $\phi \overset{r\to\infty}{\to}$ cte. From Eq. (4.15), this condition implies that the asymptotic value of the field must be the value at the minimum of the effective potential outside the object (ϕ_∞). Thus, asymptotically the field will be homogeneous and the density and pressure associated with it will be dominated by the potential; therefore, the relationship $p_\phi = -\epsilon_\phi$ will be valid.

Note that, in the case of chameleon models characterized by a runaway potential with no extrema [for example, Eq. (3.35) with $n = 1$], it is necessary to assume a background matter density outside the star so that the effective potential has a minimum in this region. In what follows, we assume that outside the star, space is filled with a cosmological fluid, such that $\tilde{p} = -\tilde{\epsilon}$. The reason for doing so is twofold. First, this allows

us to obtain self-consistent solutions for the equilibrium equations [since $d\tilde{p}/dr = 0$ in Eq. (4.14)]. Second, and more importantly, it ensures that the spacetime is asymptotically Schwarzschild-de Sitter, which allows for clearer boundary conditions to be imposed on our metric functions. When dealing with the chameleon model, we set the background energy density to be $\tilde{\epsilon}_\infty = 3.9 \times 10^{-4} \rho_{\rm nuc} c^2$ for computational reasons. On the other hand, there is no technical need to introduce a background matter density outside the star in the dilaton model, since the potential dependence on $A(\phi)$ already ensures it has a minimum. Therefore, in this case we set $\tilde{\epsilon}_\infty = 0$ for simplicity.

Finally, note that the hydrostatic equilibrium equations (4.12)-(4.15) only depend on ν through its radial derivative, so the boundary condition for ν is irrelevant when one is interested in equilibrium solutions. However, the star's oscillation frequencies, which we will compute subsequently, are sensitive to the normalization of this metric function. From the asymptotic behavior of the equations, it is natural to impose that far from the star, the line element must become

$$ds^2 = -\left(1 - \frac{2M}{r} - \Lambda r^2\right) dt^2 + \left(1 - \frac{2M}{r} - \Lambda r^2\right)^{-1} dr^2 + r^2(d\theta^2 + \sin^2\theta d\varphi^2), \quad (4.18)$$

where the cosmological constant is

$$\Lambda = \frac{8\pi}{3}\left[A(\phi_\infty)^4 \tilde{\epsilon}_\infty + V(\phi_\infty)\right]$$

and the gravitational mass M of the star can be estimated from

$$M \approx m(r) - \frac{4\pi}{3} r^3 \left[A(\phi_\infty)^4 \tilde{\epsilon}_\infty + V(\phi_\infty)\right], \quad r \gg R. \quad (4.19)$$

Numerically this differs very little from $m(R)$, where R is the stellar radius, which is obtained from $\tilde{p}(R) = \tilde{p}_\infty$. In practice, we require that $\nu(r) \to (1/2)\ln[1 - 2m(r)/r]$ for $r \gg R$.

4.2.2 Numerical methods

The method we use will be analogous to the Newtonian case. Defining

$$F(\phi_0, \hat{r}_{\rm ext}) = \hat{\phi}(\hat{r}_{\rm ext})|_{\phi_0} - \hat{\phi}_\infty, \quad (4.20)$$

where $\hat{r}_{\rm ext}$ is a sufficiently large value of $\hat{r}$ (ideally $\hat{r}_{\rm ext} \to \infty$), one looks for $\hat{\phi}_0$ such that $F(\phi_0, \hat{r}_{\rm ext}) = 0$. Unlike the Newtonian case, the initial guess is refined before using the secant method. This is done in order to guarantee the convergence of the secant method, since in some cases a severe fine-tuning problem affects the search for the initial condition of the scalar field.

For the Chameleon model, we start with a guess close to the minimum of the effective potential in the center of the star (when it exists) and a fixed value when it does not exist. If the field becomes negative at any time (assuming $\phi_0 > 0$), the integration is aborted and the new initial guess becomes $\phi_0 + \delta$. If the field becomes much larger than a stipulated value, the initial value is changed to $\phi_0 - \delta$. This process continues until the field reaches a satisfactory value at $\hat{r}_{\rm ext} \gg R$, and then the secant method is used to refine the central value of the field.

For the Dilaton model, there are cases where more than one central value of the scalar field satisfies the asymptotic boundary condition. The initial guess is a fixed value where $|\phi_0|$ is large. The integration is done and the boundary value is checked, a new integration is made where the initial value of the field is $\phi_0 + \delta$ and then it is checked whether the scalar field deviates from or approaches the desired boundary condition. If the scalar field approaches the boundary condition, we continue to add δ to the initial value, if not, the initial value is changed to $\phi_0 - \delta$. The procedure is repeated until the boundary condition is reasonable enough for the secant method to be used. The initial value of the scalar field that was obtained in this process is used as a new initial guess, however with an opposite sign, and then it is verified whether there is another solution close to that value (we will see in the next section that this is often the case). After that, the residue space continues to be investigated until an imposed limit is reached, assuming then that there are no more initial values of the field that satisfy the initial condition.

In both cases, the grid of points used is not homogeneous, a 4th order Runge-Kutta method with an adaptive step is used, where the precision is adjusted to be higher inside the star. At each integration step, it is checked whether the pressure is close to the transition region to another polytropic phase; if this is the case, the integration is refined around this point. The same is done on the surface, in order to obtain the stellar radius with better precision. In both cases, the integration step for denser stars had to be limited, as after a certain value, some instabilities arose due to the difference in scale

of variation of the equations that make up the system.

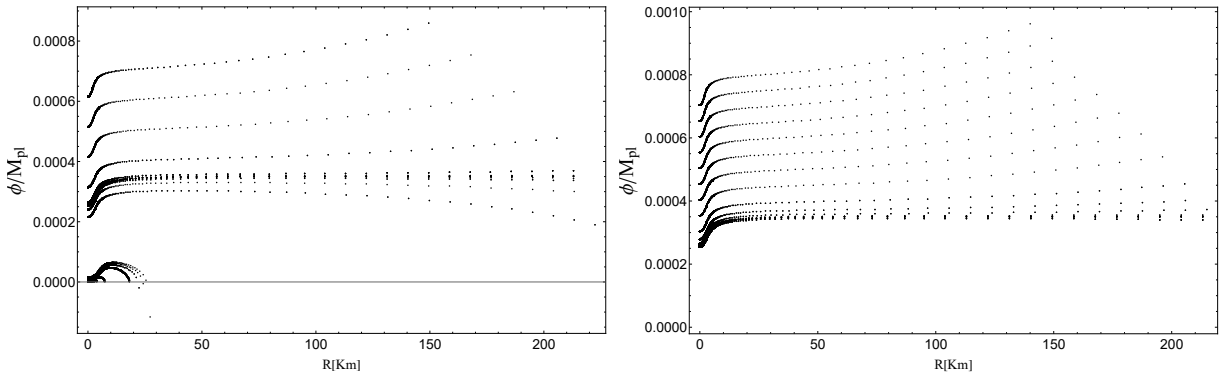

(a) Low initial guess of ϕ_0 (b) High initial guess of ϕ_0

Figure 4.3: Scalar field profiles generated by the code when the initial guess for ϕ_0 is (a) below and (b) above the correct value.

Figures 4.3a and 4.3b show two situations in which the initial guess for ϕ_0 is below and above the correct initial condition. Each curve represents a field profile generated by the code as the procedure described above is implemented. Note that the grid is denser inside the star. As the boundary condition approaches being satisfied, the solution is refined, and then the secant method is used.

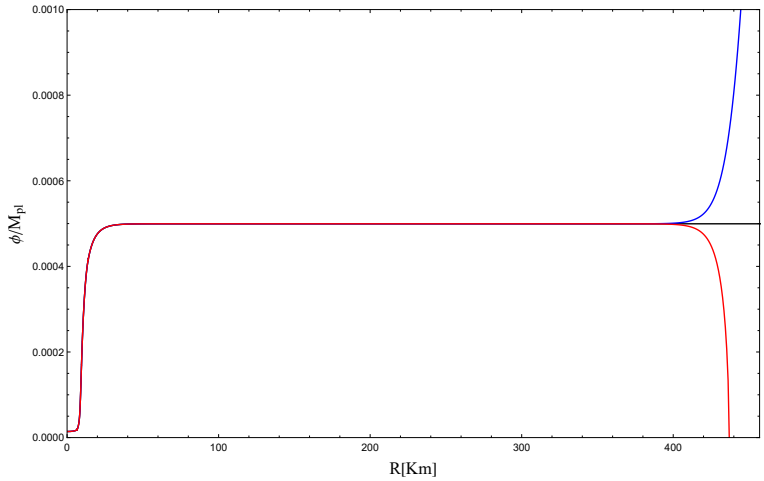

Figure 4.4: Radial profile of the field illustrating the fine-tuning problem in the chameleon model with $\mu = 0.6 \times 10^{-17} M_{\rm Pl}$. The difference between the initial conditions of the three solutions is of the order of 10^{-115}.

Figure 4.4 illustrates the fine-tuning problem in the chameleon model, which becomes worse as μ decreases. The black line indicates the desired solution, with initial condition ϕ_0; the field profile in blue and the field profile in red have initial conditions $\phi_0 \pm 10^{-115}$ respectively.

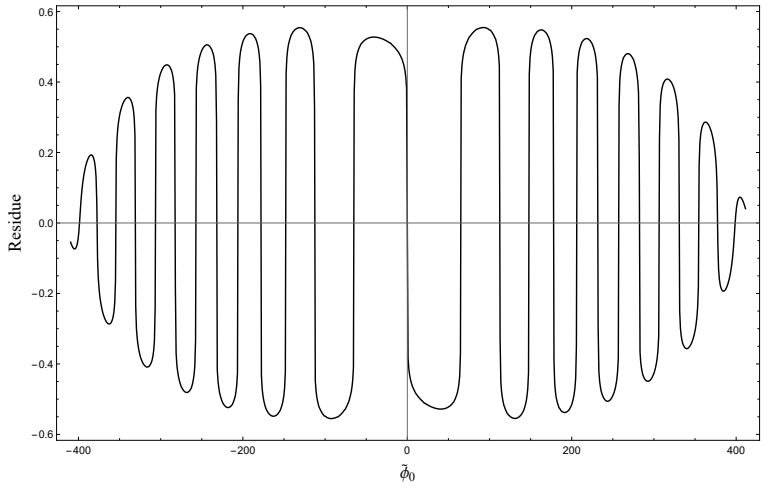

Figure 4.5: Residue as a function of the central value of the scalar field for the Dilaton model with $A_2 = 1000$ and $\lambda = 1$. Multiple solutions can be found in this case.

Finally, Fig. 4.5 shows the residue as a function of the central value of the field in the case of the dilaton model. Multiple solutions can be found. Note that the residue is practically symmetrical, which justifies the method of integration. As the density increases, the number of solutions also grows.

4.2.3 Results

Chameleon

We begin our analysis of relativistic stars in the chameleon model, with potential (3.35) and conformal coupling (3.34). We take $n = 1$ and $\beta = 1$ throughout, but vary the value of μ. Note that, in order to satisfy equivalence principle constraints, $\mu \lesssim 10^{-30} M_{\rm Pl}$ [see Eq. (3.57)]. However, reaching such a small value is prohibitive from the numerical standpoint: Indeed, already for $\mu \lesssim 10^{-17} M_{\rm Pl}$ we find that a high level of fine-tuning is required to obtain solutions with the proper asymptotic behavior. Still, as we discuss below, we believe that our main conclusions would still hold for μ in the realistic range of values.

Figure 4.6 shows the radial profiles for the scalar field and its gradient, for the ENG and H4 equations of state, and $\mu = 7.2 \times 10^{-17} M_{\rm Pl}$. In both cases, for low central densities (bluer colors) the scalar field profile is relatively flat and the star is unscreened — a consequence of the large value of μ adopted in this plot. As the central density increases, a characteristic thin-shell pattern appears, with the scalar field and its gradient suppressed in the stellar interior. This is at the core of the chameleon screening mechanism. Nonethe-

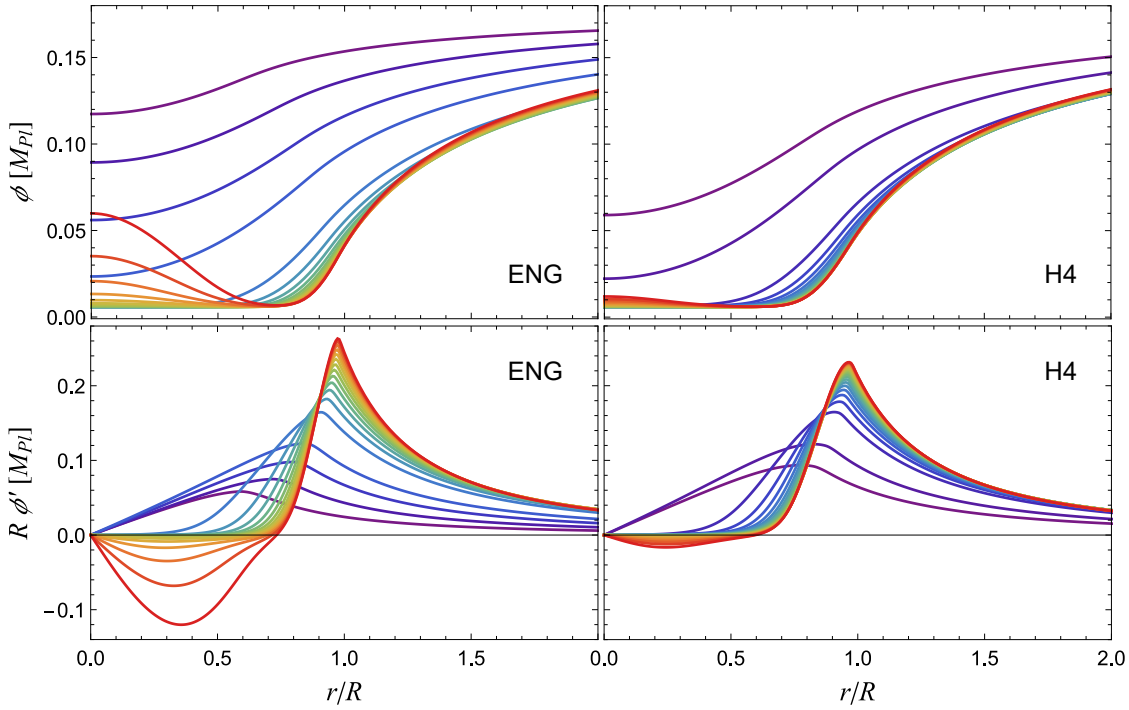

Figure 4.6: *Top panels*: Scalar field as a function of the radial coordinate, for the ENG and H4 EoS. *Bottom panels*: Scalar field gradient as a function of the radial coordinate, for the ENG and H4 EoS. Colors from violet to red indicate increasing central densities (all of which yield stable stars). Here we consider the chameleon model with $n = 1$, $\beta = 1$, and $\mu = 7.2 \times 10^{-17} M_{\rm Pl}$. As the central density increases and the star becomes more compact, we see a partial unscreening of the scalar field in the core of NSs described by the ENG EoS.

less, if the central density is sufficient high (redder colors), stars described by the ENG EoS exhibit a pressure-dominated phase, which re-activates the scalar field in the stellar core. We thus see an amplification of the scalar-mediated fifth force (proportional to $(\phi')^2$) in the stellar interior. However, for all realistic EoS, this pressure-dominated phase does not extend all the way to the stellar surface and the scalar field is again suppressed in the outer layers of the star. As a consequence, the exterior profile for the scalar field and its derivative does not display much difference between the ENG and H4 EoS, the latter of which does not allow a pressure-dominated phase inside any stable star.

Most interestingly, the reactivation of the scalar field in the stellar core can affect the neutron star structure, leaving imprints in observable quantities such as their masses and radii. Figure 4.9 shows mass-radius curves in the chameleon model with $n = 1$, $\beta = 1$, and three values of μ, for the four EoS considered in this work. As μ decreases, the contribution from the potential $V(\phi)$ and the scalar field radial derivative becomes smaller and we see that, for all EOS, the sequences of equilibrium configurations converge

to a limiting curve, which tends to GR at low densities, but diverges at high enough densities.

The increase in effectiveness of the chameleon mechanism as μ decreases, at least when $\tilde{T} < 0$, is illustrated in Figures 4.7 and 4.8. They show the radial profile of the scalar field and its derivative for the same central density, $\tilde{\rho}(0) = 3.5\tilde{\rho}_{\rm nuc}$, with $\mu = 7.2{\times}10^{-17} M_{\rm Pl}$ for (a) of each figure and $\mu/12$ for (b) of each figure. The ratio between the mass of the scalar field in (b) and (a) at $r = 0$ is $\approx 10^4$ and on the stellar surface is $\approx 10^5$. The scalar field mass appears to follow the mass of the star, having the same behavior, presenting a maximum effective mass on the star surface of the maximum mass configuration.

When $\tilde{T} > 0$, for example with $\tilde{\rho}(0) = 9\tilde{\rho}_{\rm nuc}$, the decreasing of μ does not seem to improve the screening mechanism. The ratio between the scalar field masses for $\mu = 7.2 \times 10^{-17} M_{\rm Pl}$ and $\mu/12$ is approximately 1 at the surface, and in fact the situation at the center worsens, since both masses become imaginary, where the ratio between the both scalar field masses squared is $\approx 10^{-8}$.

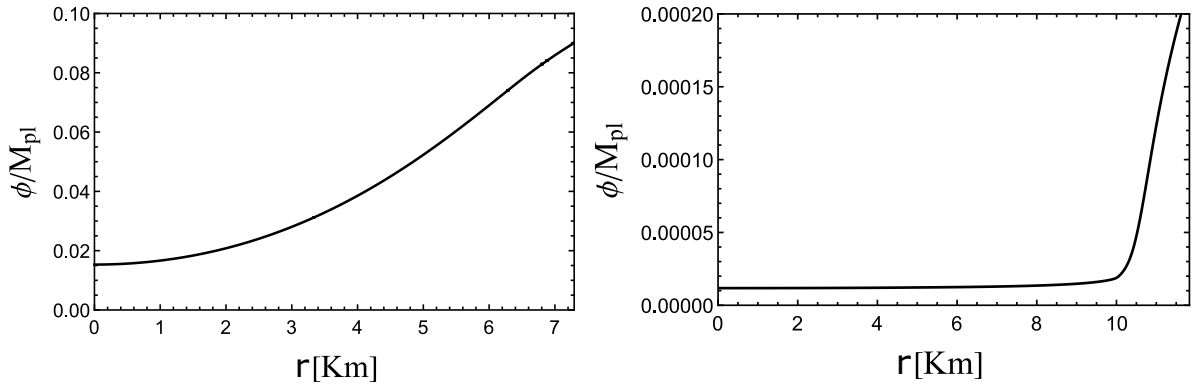

(a) Higher μ (b) Lower μ

Figure 4.7: Scalar field profile for a star with central density $\tilde{\rho}(0) = (3.5)\tilde{\rho}_{\rm nuc}$ in the chameleon model with (a) $\mu = 7.2 \times 10^{-17} M_{\rm Pl}$ and (b) $\mu/12$. As μ decreases, the screening mechanism becomes more efficient.

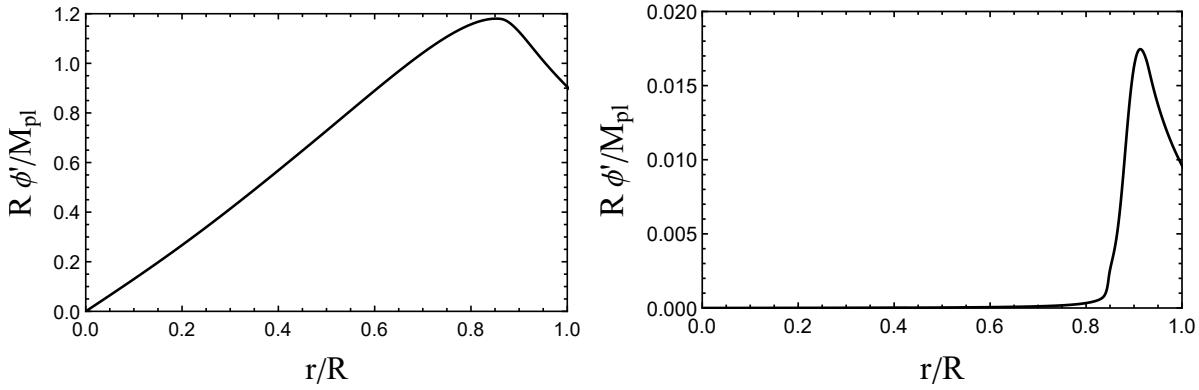

(a) Higher μ (b) Lower μ

Figure 4.8: Radial profile of the scalar field gradient for a star with central density $\tilde{\rho}(0) = (3.5)\tilde{\rho}_{\rm nuc}$ in the chameleon model with (a) $\mu = 7.2 \times 10^{-17} M_{\rm Pl}$ and (b) $\mu/12$. As μ decreases, the screening mechanism becomes more efficient.

The limiting behavior seen in Fig. 4.9 as μ decreases suggests that, if μ was pushed down to realistic values, the masses and radii of NS solutions would not change appreciably with respect to the lowest value of μ considered in Fig. 4.9. Note that deviation from GR starts as soon as the trace of the energy-momentum tensor becomes positive in some region of the stellar interior, as identified by black dots in the plots. The decrease in the maximum mass, for the lowest value of μ displayed in Fig. 4.9, is of 3.2%, 1.7%, and 3.4% for the ENG, SLy, and MPA1 equations of state, respectively. This can be contrasted with the decrease of only 0.016% for the H4 EOS, which displays no pressure dominated phase inside stable stars.

In the next section the stability of these solutions will be discussed.

Dilaton

Let us now turn to the environmentally-dependent dilaton. As a representative example, we choose the ENG EOS and fix the model parameters to $\lambda = 1$, $A_2 = 1000$, and $V_0 = 3.9 \times 10^{-34} \rho_{\rm nuc}$. For this choice of parameters and in the absence of a pressure-dominated phase (i.e., for low central densities), NSs in the dilaton model have very similar structural properties to their GR counterparts, with the scalar field exhibiting a typical thin-shell pattern. However, stars with pressure-dominated cores in the dilaton model can have a widely different behavior, exhibiting the effect of spontaneous scalarization.

In the top panel of Fig. 4.10 we show the central value of the scalar field as a function of the star's central density in the dilaton model. As the central density increases

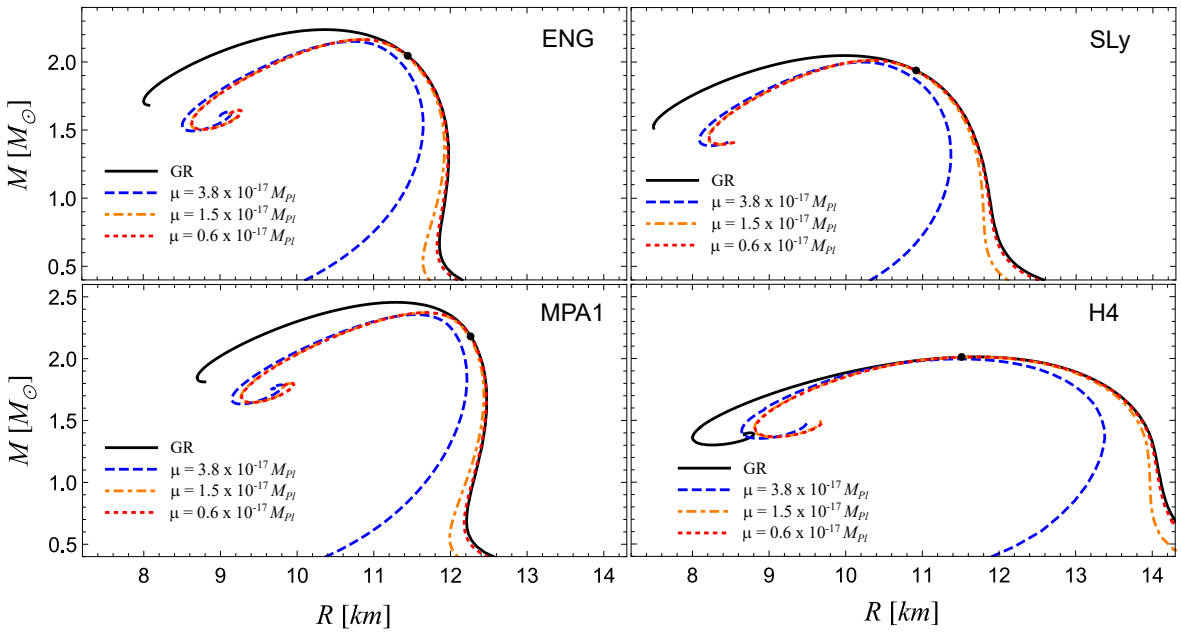

Figure 4.9: Mass-radius curves for the chameleon model, with $n = 1$, $\beta = 1$, and three values of μ. The prediction from general relativity is shown in solid black for comparison. Black dots indicate configurations along the GR curve starting from which $T > 0$ in a region of the stellar interior. For the H4 EoS, a pressure-dominated phase only occurs for dynamically unstable stars.

and a pressure-dominated core begins to form and grow, we observe a sudden amplification of the scalar field content, together with sequential jumps in the number of equilibrium solutions. Figure 4.11 shows the scalar field profiles for the eleven solutions found with a central density of $\tilde{\rho}_c = 10.0\ \rho_{\rm nuc}$. Contrary to the case of the chameleon model, in which the scalar field amplification in stars with pressure-dominated cores was mild (cf. Fig. 4.6), we see that here the scalar field rises orders of magnitude above the asymptotic value (which, for the theory parameters used in the plot, is $\phi_\infty \approx 3.64 \times 10^{-4} M_{\rm Pl}$). This is typical of the scalarization phenomenon [108].

From Fig. 4.11 we see that the new solutions typically exist in pairs, for which structural properties (such as mass and radius) are nearly identical and the scalar field profile is almost the same but with an opposite sign. This stems from the fact that the dilaton model becomes invariant under reflection, $\phi \to -\phi$, if $V_0 \to 0$, and the natural values for V_0 are quite small. The fact that these solutions have a different number of nodes is simply a consequence of the fact that the asymptotic value of the scalar field (such that $dV/d\phi|_{\phi_\infty} = 0$) is positive, and the solution with a negative central value of the scalar field has to cross zero one more time to reach it.

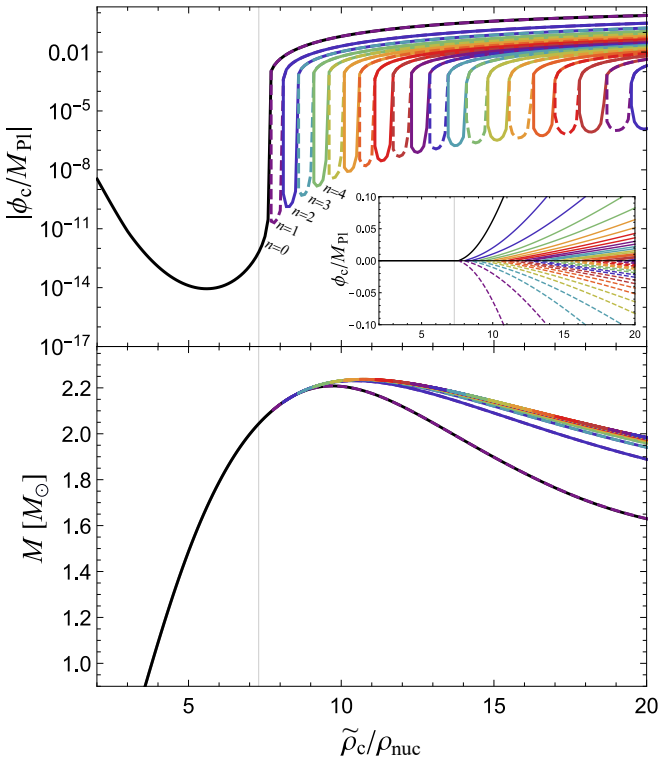

Figure 4.10: Results for the dilaton model with $\lambda = 1$, $A_2 = 1000$, and $V_0 = 3.9{\times}10^{-34}\rho_{\rm nuc}$, and the ENG EoS. The top panel displays the absolute value of the scalar field at the stellar center, $\phi_c \equiv \phi(r = 0)$, as a function of the central density in a log scale, while the inset shows ϕ_c in a linear scale, for the same range of densities. Solutions with a different number n of nodes are represented by various colors and we identify the number n for the five first families. Solid (dashed) curves correspond to solutions with a positive (negative) value of ϕ_c. The critical central density, $\tilde{\rho}_c \approx 7.30\rho_{\rm nuc}$, above which $\tilde{T}(r = 0) > 0$ is displayed as a vertical line. The bottom panel shows the total mass as a function of the central density. Only the first branches are clearly distinguishable, with the high-n solutions accumulating around the GR values.

By analyzing the relationship between $\tilde{T}$ and the effective matter coupling (β) behavior, we see that β is indeed very small in both $\tilde{T}(r = 0) > 0$ and $\tilde{T}(r = 0) < 0$ cases at $r = 0$ and at the stellar surface, being much smaller when $\tilde{T}(r = 0) < 0$. In stars with $\tilde{T}(r = 0) > 0$, the effective matter coupling in the center is smaller in the solution with a mass closer to the mass obtained in GR. However it is approximately the same at the surface for all solutions with different number of nodes of the same central density. This suggests that the value of the scalar field on the surface, and consequently, how far the scalar field is displaced from the minimum of the effective potential outside the star, is somehow related to the value of of $\tilde{T}$ in the center of the star.

In the bottom panel of Fig. 4.10, we show the total mass as a function of the star's central density. Only the first branches of scalarized solutions are clearly distinguishable,

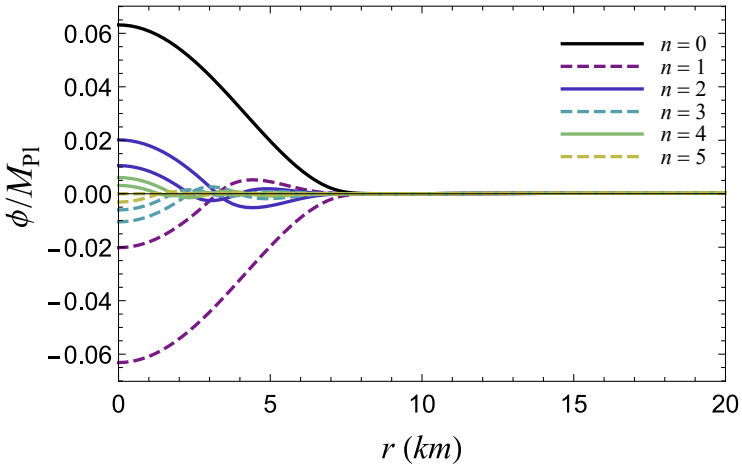

Figure 4.11: Scalar field as a function of the radial coordinate for the eleven equilibrium solutions found with $\tilde{\rho}_c = 10.0\ \rho_{\rm nuc}$ in the dilaton model. The equation of state and model parameters are the same as in Fig. 4.10. The solutions are assorted by the number n of nodes in the scalar field profile, with the same color coding as in Fig. 4.10. All solutions asymptote to $\phi_\infty \approx 3.64 \times 10^{-4} M_{\rm Pl}$. The stellar surface is located approximately at $r = 10.5$ km.

while the high-n solutions accumulate around the GR equilibrium curve. For the branch of solutions with $n = 0$, we find that the maximum mass decreases roughly 1.3% with respect to the GR value. This is a small decrease, comparable to what we found in the chameleon model (cf. Fig. 4.9), although the scalar field activation seems more dramatic in this case.

4.3 Stability of relativistic stars

It is possible to study the evolution of a star close to a given equilibrium solution, with a fixed number of baryons and the same total entropy using perturbation theory. The perturbed configuration is a deformation of the original equilibrium solution, with each fluid element of the equilibrium mapped to a corresponding fluid element in the perturbed configuration by a Lagrangian displacement ξ^μ.

Oscillations of relativistic stars are a rich field, which we will just briefly touch upon. Our main interest will be in the stability of the equilibrium solutions found previously, and, for that purpose, we will focus on radial perturbations.

4.3.1 Radial perturbation equations

Since the radially perturbed configuration retains the spherical symmetry of the background spacetime, the line element can be written as

$$ds^2 = -e^{2\nu(t,r)}dt^2 + e^{2\lambda(t,r)}dr^2 + r^2(d\theta^2 + \sin^2\theta d\varphi^2), \tag{4.21}$$

where

$$\nu(t,r) = \nu_0(r) + \delta\nu(t,r),$$

$$\lambda(t,r) = \lambda_0(r) + \delta\lambda(t,r)$$

with $\nu_0(r)$ and $\lambda_0(r) = -(1/2)\ln[1-2m(r)/r]$ denoting solutions to Eqs. (4.13) and (4.12), respectively. Similarly, we write the perturbed scalar field, perturbed pressure and energy density as

$$\phi(t,r) = \phi_0(r) + \delta\phi(t,r)$$

$$p(t,r) = p_0(r) + \delta p(t,r)$$

$$\epsilon(t,r) = \epsilon_0(r) + \delta\epsilon(t,r)$$

with $\phi_0(r)$ and $p_0(r)$ obeying Eqs. (4.15) and (4.14), respectively.

The perturbed (Einstein-frame) fluid four-velocity is given by

$$\delta u^\mu(t,r) = e^{-\nu_0}(-\delta\nu, d\xi/dt, 0, 0), \tag{4.22}$$

where $\xi(t,r)$ is the radial Lagrangian displacement of a given fluid element. The corresponding Jordan-frame quantities are

$$\delta\tilde{u}^\mu = A(\phi_0)^{-1}(\delta u^\mu - \alpha_0 u^\mu \delta\phi),$$
$$\delta\tilde{p} = A(\phi_0)^{-4}(\delta p - 4\alpha_0 p_0 \delta\phi),$$
$$\delta\tilde{\epsilon} = A(\phi_0)^{-4}(\delta\epsilon - 4\alpha_0\epsilon_0\delta\phi),$$

where we used the shorthand

$$\alpha_0 \equiv \left.\frac{d\ln A}{d\phi}\right|_{\phi_0}. \tag{4.23}$$

Therefore, the perturbed configuration is fully characterized by six functions of

t and r, namely, $\delta\nu$, $\delta\lambda$, $\delta\phi$, ξ, $\delta\tilde{p}$, and $\delta\tilde{\epsilon}$. For adiabatic perturbations, and assuming that the perturbed fluid has the same EoS as the unperturbed configuration, pressure and energy density perturbations can be written in terms of the mass-density perturbation $\delta\tilde{\rho}$ as

$$\delta\tilde{p} = \frac{\Gamma_1 \tilde{p}_0}{\tilde{\rho}_0}\delta\tilde{\rho}, \qquad \delta\tilde{\epsilon} = \frac{\tilde{\epsilon}_0 + \tilde{p}_0}{\tilde{\rho}_0}\delta\tilde{\rho}, \tag{4.24}$$

where

$$\Gamma_1 = \left(\frac{\partial \ln \tilde{p}}{\partial \ln \tilde{\rho}}\right)_s \tag{4.25}$$

is the adiabatic index (defined at constant entropy s).

The equation for rest-mass conservation, $\tilde{\nabla}_\mu(\tilde{\rho}\tilde{u}^\mu) = 0$, can be rewritten in a more useful way as $\nabla_\mu(\rho u^\mu) = 0$, where $\rho \equiv \tilde{\rho}A(\phi)^3$; therefore, it is not necessary to use the metric in the Jordan frame. Expanding this equation to first order in the perturbations results in

$$\frac{\delta\rho}{\rho_0} = -\delta\lambda - \frac{\xi}{\rho_0}\frac{d\rho_0}{dr} - \frac{\partial\xi}{\partial r} - \xi\left(\frac{2}{r} + \frac{d\lambda_0}{dr}\right), \tag{4.26}$$

which in terms of density $\tilde{\rho} = \rho A(\phi)^{-3}$ is

$$\frac{\delta\tilde{\rho}}{\tilde{\rho}_0} = -\delta\lambda - 3\alpha_0\delta\phi - \frac{\partial\xi}{\partial r} - \xi\left(\frac{2}{r} + \frac{d\lambda_0}{dr} + 3\alpha_0\psi_0 + \frac{1}{\tilde{\rho}_0}\frac{d\tilde{\rho}_0}{dr}\right), \tag{4.27}$$

which relates the mass density perturbation to $\delta\lambda$, $\delta\phi$, and ξ.

By inserting the definitions for the perturbed variables in the modified Einstein equation, Eq. (3.21), one obtains equations that govern the evolution of perturbations in the metric components. Expanding Eq. (3.21) to first order in the perturbations, one obtains for the tr component:

$$\frac{\partial\delta\lambda}{\partial t} = 4\pi r\left(-p_0 e^{2\lambda_0}\frac{\partial\xi}{\partial t} + \phi_0'\frac{\partial\delta\phi}{\partial t} - e^{2\lambda_0}\epsilon_0\frac{\partial\xi}{\partial t}\right),$$

which can be readily solved for $\delta\lambda$:

$$\delta\lambda = 4\pi r\phi_0'\left(\delta\phi + \phi_0'\xi\right) - \xi\left(\lambda_0' + \nu_0'\right), \tag{4.28}$$

where

$$\lambda_0' + \nu_0' - 4\pi r(\phi_0')^2 = 4\pi r e^{2\lambda_0}\left(p_0 + \epsilon_0\right)$$

was used.

The rr component of the perturbed field equation is

$$-4\pi r^2(\phi_0')^2\delta\lambda + 4\pi r^2 e^{2\lambda_0}\delta p + 4\pi r^2\phi_0'\frac{\partial\delta\phi}{\partial r} - 4\pi r^2 e^{2\lambda_0(r)}\left.\frac{dV}{d\phi}\right|_{\phi_0}\delta\phi + 2r\nu_0'\delta\lambda + \delta\lambda - r\frac{\partial\delta\nu}{\partial r} = 0,$$

which results, after some simplifications, in

$$\frac{\partial\delta\nu}{\partial r} = 4\pi r\phi_0'\left(\frac{\partial\delta\phi}{\partial r} - \phi_0'\delta\lambda\right) + \left(2\nu_0' + \frac{1}{r}\right)\delta\lambda + 4\pi r e^{2\lambda_0}\delta p - 4\pi r e^{2\lambda_0}\left.\frac{dV}{d\phi}\right|_{\phi_0}\delta\phi. \quad (4.29)$$

Next, by inserting the previous definitions and expanding the scalar field equation to first order in the perturbations, one obtains

$$\begin{aligned}
&-\delta\phi\left.\frac{d^2V}{d\phi^2}\right|_{\phi_0} + 3p_0\beta_0\delta\phi + 3\alpha_0\delta p - \alpha_0\delta\epsilon - \epsilon_0\beta_0\delta\phi \\
&- 2e^{-2\lambda_0}\nu_0'\phi_0'\delta\lambda + e^{-2\lambda_0}\phi_0'\frac{\partial\delta\nu}{\partial r} - \frac{2}{r}e^{-2\lambda_0}\left(2\phi_0'\delta\lambda - \frac{\partial\delta\phi}{\partial r}\right) + e^{-2\lambda_0}\nu_0'\frac{\partial\delta\phi}{\partial r} \\
&+ e^{-2\lambda_0}\left(-\phi_0'\frac{\partial\delta\lambda}{\partial r} + 2\lambda_0'\phi_0'\delta\lambda - 2\phi_0''\delta\lambda\frac{\partial^2\delta\phi}{\partial r^2} - \lambda_0'\frac{\partial\delta\phi}{\partial r}\right) - e^{-2\nu_0}\frac{\partial^2\delta\phi}{\partial t^2} = 0,
\end{aligned} \quad (4.30)$$

that, after some manipulation, yields

$$\begin{aligned}
e^{2\lambda_0-2\nu_0}\frac{\partial^2\delta\phi}{\partial t^2} =& e^{2\lambda_0}\alpha_0(3\delta p - \delta\epsilon) - e^{2\lambda_0}\delta\phi\left(\left.\frac{d^2V}{d\phi^2}\right|_{\phi_0} + (\epsilon_0 - 3p_0)\,\beta_0\right) \\
&+ \phi_0'\partial r\,(\delta\nu - \delta\lambda) + 2\delta\lambda\left(\phi_0'\left(\lambda_0' - \nu_0' - \frac{2}{r}\right) - \phi_0''\right) \\
&+ \left(-\lambda_0' + \nu_0' + \frac{2}{r}\right)\frac{\partial\delta\phi}{\partial r} + \frac{\partial^2\delta\phi}{\partial r^2}.
\end{aligned} \quad (4.31)$$

where the shorthand

$$\beta_0 \equiv \left.\frac{d^2\ln A}{d\phi^2}\right|_{\phi_0}$$

was used.

Finally, the r component of the perturbed equations of motion (3.29),

$$\begin{aligned}
&-3p_0\phi_0'\beta_0\delta\phi - 3p_0\alpha_0\frac{\partial\delta\phi}{\partial r} + p_0\frac{\partial\delta\nu}{\partial r} + p_0 e^{2\lambda_0-2\nu_0}\frac{\partial^2\xi}{\partial t^2} + \rho_0\phi_0'\beta_0\delta\phi - 3\alpha_0\phi_0'\delta p \\
&+ \alpha_0\phi_0'\delta\epsilon + \epsilon_0\alpha_0\frac{\partial\delta\phi}{\partial r} + \epsilon_0\frac{\partial\delta\nu}{\partial r} + \frac{\partial\delta p}{\partial r} + \nu_0'\delta p + \nu_0'\delta\epsilon + \epsilon_0 e^{2\lambda_0-2\nu_0}\frac{\partial^2\xi}{\partial t^2} = 0,
\end{aligned} \quad (4.32)$$

after some manipulation, leads to

$$(p_0+\epsilon_0)\,e^{2\lambda_0-2\nu_0}\frac{\partial^2\xi}{\partial t^2} = -\,(\epsilon_0-3p_0)\,\phi_0'\beta_0\delta\phi - \nu_0'(\delta p+\delta\epsilon) - \frac{\partial\delta p}{\partial r} - (p_0+\epsilon_0)\,\frac{\partial\delta\nu}{\partial r} - \alpha_0\left[(\epsilon_0-3p_0)\,\frac{\partial\delta\phi}{\partial r} + \phi_0'(\delta\epsilon-3\delta p)\right]. \quad (4.33)$$

By inserting Eqs. (4.28) and (4.29) for $\delta\lambda$ and $\delta\nu$, as well as Eqs. (4.24) and (4.27) for δp and $\delta\epsilon$ in Eqs. (4.31) and (4.33) for $\delta\phi$ and ξ, one obtains two coupled differential equations involving $\delta\phi$ and ξ alone (besides background quantities). These are homogeneous equations, and therefore invariant under a simultaneous change in the normalization of ξ and $\delta\phi$, such that $\xi \to A\xi$ and $\delta\phi \to A\delta\phi$. Thus, there is a freedom in choosing the overall normalization of the perturbed quantities.

Next, we assume a harmonic time dependence for the perturbation variables ξ and $\delta\phi$:

$$\xi(t,r) = \xi(r)e^{i\omega t}, \qquad \delta\phi(t,r) = \delta\phi(r)e^{i\omega t}, \quad (4.34)$$

with $\omega \in \mathbb{C}$. Stable modes are characterized by $\Im(\omega) > 0$, while unstable modes have $\Im(\omega) < 0$. With the ansatze (4.34), and defining the vector function $\mathbf{x}(r) = (\xi, \xi', \delta\phi, \delta\phi')^T$, our master equations assume the form

$$\frac{d\mathbf{x}(r)}{dr} = \mathbf{M}(r)\mathbf{x}(r), \quad (4.35)$$

where $\mathbf{M}(r)$ is a 4×4 matrix function of background quantities alone, with the following components

$$M_{11} = M_{13} = M_{14} = 0, \qquad M_{12} = 1, \quad (4.36)$$

$$
\begin{aligned}
M_{21} = \{ & -48\alpha_0^2\Gamma_1 e^{2\nu_0} r^2 \phi_0'^2 \tilde{p}_0 - \big[6e^{2(\lambda_0+\nu_0)} + e^{4\lambda_0+2\nu_0} - 7e^{2\nu_0} + 4e^{2\lambda_0} r^2\omega^2 + 24\pi e^{2\nu_0} r^2 \phi_0'^2 \\
& + 64\pi^2 \left(\Gamma_1+1\right) r^4 V_0^2 e^{4\lambda_0+2\nu_0} + 8\pi r^2 \phi_0'^2 e^{2(\lambda_0+\nu_0)} + 16\pi^2 e^{2\nu_0} r^4 \phi_0'^4 - 4\beta_0 e^{2\nu_0} r^2 \phi_0'^2 \\
& - 16\pi r^2 V_0 e^{2(\lambda_0+\nu_0)} \left(\Gamma_1 \left(e^{2\lambda_0}-3\right) + e^{2\lambda_0} + 4\pi r^2 \phi_0'^2 + 1\right) + e^{2\nu_0}\Gamma_1 \left(5 - 6e^{2\lambda_0} + e^{4\lambda_0}\right. \\
& \left. - \ 16\pi^2 r^4 \phi_0'^4 - 16\pi r^2 \phi_0'^2\right)\big] \tilde{\epsilon}_0 - 32\pi\alpha_0 A_0^4 r^3 \phi_0' e^{2(\lambda_0+\nu_0)} \left(\tilde{p}_0 + \tilde{\epsilon}_0\right) \left[\left(\Gamma_1+3\right)\tilde{p}_0 - \tilde{\epsilon}_0\right] \\
& - 4\alpha_0^2 A_0^4 r^2 e^{2(\lambda_0+\nu_0)} \left(3\tilde{p}_0 - \tilde{\epsilon}_0\right) \left[\left(\Gamma_1+1\right)\tilde{p}_0 + \tilde{\epsilon}_0\right] + 4\pi r\phi_0' \left[\left(2\Gamma_1+1\right)\tilde{p}_0 - \left(\Gamma_1-1\right)\tilde{\epsilon}_0\right] \\
& - 64\pi^2 A_0^8 r^4 \tilde{p}_0^2 e^{4\lambda_0+2\nu_0} \left[\tilde{p}_0 - \left(\Gamma_1-1\right)\tilde{\epsilon}_0\right] - 4\alpha_0^2 e^{2\nu_0} r^2 \phi_0'^2 \left[\left(\Gamma_1+3\right)\tilde{\epsilon}_0 + \left(4\Gamma_1+3\right)\tilde{p}_0\right] \\
& + 16 e^{2(\lambda_0+\nu_0)} r^2 A_0^4 \alpha_0 \tilde{p}_0 \left[\alpha_0\Gamma_1 \left(3\tilde{p}_0 - \tilde{\epsilon}_0\right) - 8e^{2\nu_0} r\Gamma_1 \left(-\alpha_0\phi_0' \left(e^{2\lambda_0} - 8\pi e^{2\lambda_0} r^2 V_0 - 1\right.\right.\right. \\
& \left. + 4\pi r^2 \phi_0'^2 + 2\alpha_0 r\phi_0'\right) \tilde{\epsilon}_0 + \tilde{p}_0 \left(2r\phi_0'^2 \left(\alpha_0^2+\beta_0\right) + \alpha_0 \left(\phi_0' \left(-3e^{2\lambda_0} + 24\pi e^{2\lambda_0} r^2 V_0 + 3\right.\right.\right. \\
& \left. + 4\pi r^2 \phi_0'^2 - 10\alpha_0 r\phi_0'\right) + 2e^{2\lambda_0} r \left.\frac{dV}{d\phi}\right|_{\phi_0} \left.\right)\right)\big] - 16\alpha_0 e^{2\nu_0} r^2 \phi_0' \tilde{p}_0 \Gamma_1' - \tilde{p}_0 \left[6e^{2(\lambda_0+\nu_0)} - 7e^{2\nu_0}\right. \\
& + e^{4\lambda_0+2\nu_0} + 64\pi^2 \left(2\Gamma_1+1\right) r^4 V_0^2 e^{4\lambda_0+2\nu_0} + 24\pi e^{2\nu_0} r^2 \phi_0'^2 + 4e^{2\lambda_0} r^2\omega^2 + 8\pi r^2 \phi_0'^2 e^{2(\lambda_0+\nu_0)} \\
& - 4\beta_0 e^{2\nu_0} r^2 \phi_0'^2 + 16\pi^2 e^{2\nu_0} r^4 \phi_0'^4 + 2e^{2\nu_0}\Gamma_1 \left(-5 + e^{4\lambda_0} - 2r^2 \left(6\pi e^{2\lambda_0} + 2\pi\ + \beta_0\right) \phi_0'^2\right. \\
& + 16\pi e^{2\lambda_0} r^3 \phi_0' \left.\frac{dV}{d\phi}\right|_{\phi_0} \left.\right) + 10e^{2\nu_0} r\Gamma_1' - 2r\Gamma_1'^2 e^{2(\lambda_0+\nu_0)} + 8\pi e^{2\nu_0} r^3 \phi_0'^2 \Gamma_1' \\
& - 16\pi r^2 V_0 e^{2(\lambda_0+\nu_0)} \left(e^{2\lambda_0} + 2\Gamma_1 \left(e^{2\lambda_0} - 6\pi r^2 \phi_0'^2 - 1\right) + 4\pi r^2 \phi_0'^2 - r\Gamma_1' + 1\right)\big] \\
& + 16 e^{2(\lambda_0+\nu_0)} \pi r^2 A_0^4 \left(\tilde{p}_0\tilde{\epsilon}_0 \left(\Gamma_1 - e^{2\lambda_0} - 8\pi\Gamma_1 r^2 \phi_0'^2 + 8\pi e^{2\lambda_0} r^2 V_0 + 4\pi r^2 \phi_0'^2 - 1\right)\right. \\
& + \tilde{p}_0^2 \left(-\Gamma_1 e^{2\lambda_0} - e^{2\lambda_0} + 4\pi\Gamma_1 r^2 \phi_0'^2 + 8\pi \left(\Gamma_1+1\right) e^{2\lambda_0} r^2 V_0 + r\Gamma_1' - 1\right) + 4\pi r^2 \phi_0'^2 \tilde{\epsilon}_0^2\Big) \\
& + 4e^{2\nu_0} r\alpha_0 \left[\tilde{\epsilon}_0 \left(-\phi_0' \left(\Gamma_1 \left(e^{2\lambda_0}-3\right) + 2\left(e^{2\lambda_0} + 4\pi r^2 \phi_0'^2 + 1\right) - 8\pi \left(\Gamma_1+2\right) e^{2\lambda_0} r^2 V_0\right)\right.\right. \\
& + e^{2\lambda_0} r \left.\frac{dV}{d\phi}\right|_{\phi_0} \left.\right) + \tilde{p}_0 \left(\left(\Gamma_1+1\right) e^{2\lambda_0} r \left.\frac{dV}{d\phi}\right|_{\phi_0} + \phi_0' \left(-2e^{2\lambda_0} + 8\pi \left(3\Gamma_1+2\right) e^{2\lambda_0} r^2 V_0 - 2\right.\right. \\
& \left.\left.\left. - 8\pi r^2 \phi_0'^2 + \ \Gamma_1 \left(-3e^{2\lambda_0} + 8\pi r^2 \phi_0'^2 + 9\right) + r\Gamma_1'\right)\right)\big] \ \} \frac{e^{-2\nu_0}}{4\Gamma_1 r^2 \tilde{p}_0}, \qquad (4.37)
\end{aligned}
$$

$$
\begin{aligned}
M_{22} = & \left[-\frac{8\pi e^{2\lambda_0} r V_0 \left(\tilde{p}_0 + \tilde{\epsilon}_0\right)}{\tilde{p}_0} - 16\alpha_0\phi_0' - \frac{2\Gamma_1'}{\Gamma_1} + \frac{e^{2\lambda_0} - 4\pi r^2 \phi_0'^2 + 10\alpha_0 r\phi_0' - 5}{r}\right. \\
& \left. + \frac{\tilde{\epsilon}_0 \left(e^{2\lambda_0} + 4\pi r^2 \phi_0'^2 + 2\alpha_0 r\phi_0' - 1\right)}{r\tilde{p}_0}\right], \qquad (4.38)
\end{aligned}
$$

$$
\begin{aligned}
M_{23} = \frac{1}{2\Gamma_1}\{ &- 8\alpha_0\phi_0'\left[\alpha_0(3\Gamma_1-4)+4\pi\Gamma_1 r\phi_0'\right] + 8\pi A_0^4 e^{2\lambda_0} r\left(\alpha_0+4\pi r\phi_0'\right)\left(\tilde{p}_0-(\Gamma_1-1)\tilde{\epsilon}_0\right) \\
&+ \frac{1}{r\tilde{p}_0}\left[2\alpha_0^2 r\phi_0'\left(3(\Gamma_1-1)\tilde{\epsilon}_0+(12\Gamma_1-19)\tilde{p}_0\right)+\alpha_0\left(1-\Gamma_1\left(-3e^{2\lambda_0}+24\pi e^{2\lambda_0}r^2V_0+3\right.\right.\right. \\
&- \left.\left.\left. 20\pi r^2\phi_0'^2\right)\tilde{\epsilon}_0+\tilde{p}_0\left(-3e^{2\lambda_0}+32\pi\Gamma_1 r^2\phi_0'^2+24\pi e^{2\lambda_0}r^2V_0-20\pi r^2\phi_0'^2-6r\Gamma_1'+3\right)\right)\right. \\
&- 2r\left(\tilde{\epsilon}_0\left(4\pi e^{2\lambda_0}r\left.\frac{dV}{d\phi}\right|_{\phi_0}-\phi_0'\left(2\pi e^{2\lambda_0}-16\pi^2(\Gamma_1+1)e^{2\lambda_0}r^2V_0+2\pi-8\pi^2r^2\phi_0'^2+\beta_0\right.\right.\right. \\
&+ \left.\left.\left. 2\pi\Gamma_1\left(e^{2\lambda_0}+4\pi r^2\phi_0'^2-1\right)\right)+\tilde{p}_0\left(4\pi(\Gamma_1+1)e^{2\lambda_0}r\left.\frac{dV}{d\phi}\right|_{\phi_0}+\phi_0'\left(-4\pi\Gamma_1e^{2\lambda_0}-2\pi e^{2\lambda_0}-2\pi\right.\right.\right.\right. \\
&+ \left.\left.\left.\left. 3\Gamma_1\beta_0-\beta_0+16\pi^2(2\Gamma_1+1)e^{2\lambda_0}r^2V_0+8\pi^2r^2\phi_0'^2+4\pi r\Gamma_1'\right)\right)\right)\right]\}, \qquad (4.39)
\end{aligned}
$$

$$
M_{24} = \frac{1}{\Gamma_1\tilde{p}_0}\left[\alpha_0\left((1-3\Gamma_1)\tilde{p}_0+\tilde{\epsilon}_0\right)+4\pi r\phi_0'\left(\tilde{\epsilon}_0-(\Gamma_1-1)\tilde{p}_0\right)\right] \qquad (4.40)
$$

$$
M_{31} = M_{32} = M_{33} = 0, \qquad M_{34} = 1, \qquad (4.41)
$$

$$
\begin{aligned}
M_{41} = \frac{1}{2}A_0^3e^{2\lambda_0}\left[\right. &- \frac{1}{\Gamma_1}8e^{2\lambda_0}\pi r A_0^5\left(4\pi r\phi_0'\left(\left(2\Gamma_1-1\right)\tilde{\epsilon}_0^2+\left(\Gamma_1^2-2\Gamma_1-1\right)\tilde{p}_0^2-2\tilde{p}_0\tilde{\epsilon}_0\right)\right. \\
&+ \left.\alpha_0\left(\left(2\Gamma_1-1\right)\tilde{\epsilon}_0^2-2\left(\Gamma_1+1\right)\tilde{p}_0\tilde{\epsilon}_0+\left(3\Gamma_1^2-4\Gamma_1-1\right)\tilde{p}_0^2\right)\right) \\
&- \frac{1}{\Gamma_1 r\tilde{p}_0}A_0\left(2\alpha_0^2r\phi_0'\left(\tilde{p}_0+\tilde{\epsilon}_0\right)\left(\left(3\Gamma_1-1\right)\tilde{p}_0-\tilde{\epsilon}_0\right)+\alpha_0\left(-\left(e^{2\lambda_0}-1\right.\right.\right. \\
&- 3\Gamma_1^2\left(e^{2\lambda_0}-4\pi r^2\phi_0'^2-5\right)+8\pi\left(3\Gamma_1^2+2\Gamma_1-1\right)e^{2\lambda_0}r^2V_0+12\pi r^2\phi_0'^2 \\
&- 2\Gamma_1\left(e^{2\lambda_0}+8\pi r^2\phi_0'^2+1\right)\tilde{p}_0^2-2\left(-1+e^{2\lambda_0}+8\pi\left(\Gamma_1-1\right)e^{2\lambda_0}r^2V_0\right. \\
&+ \left.12\pi r^2\phi_0'^2-\Gamma_1\left(e^{2\lambda_0}+8\pi r^2\phi_0'^2+1\right)\right)\tilde{p}_0\tilde{\epsilon}_0+\left(1-e^{2\lambda_0}+8\pi e^{2\lambda_0}r^2V_0\right. \\
&- \left.\left.12\pi r^2\phi_0'^2\right)\tilde{\epsilon}_0^2\right)-4\pi r\left(\Gamma_1^2\phi_0'\left(-e^{2\lambda_0}+8\pi e^{2\lambda_0}r^2V_0+5\ +4\pi r^2\phi_0'^2\right)\tilde{p}_0^2\right. \\
&+ \phi_0'\left(\tilde{p}_0+\tilde{\epsilon}_0\right)^2\left(e^{2\lambda_0}-8\pi e^{2\lambda_0}r^2V_0+4\pi r^2\phi_0'^2-1\right) \\
&- \left.\left.4\Gamma_1\tilde{p}_0\left(\tilde{p}_0+\tilde{\epsilon}_0\right)\left(\phi_0'\left(-e^{2\lambda_0}+8\pi e^{2\lambda_0}r^2V_0+2\pi r^2\phi_0'^2+1\right)+e^{2\lambda_0}r\left.\frac{dV}{d\phi}\right|_{\phi_0}\right)\right)\right) \\
&- 2\phi_0'\alpha_0A_0\left(3\alpha_0\left(\left(1-3\Gamma_1\right)\tilde{p}_0+\tilde{\epsilon}_0\right)+4\pi r\phi_0'\left(\left(4-3\Gamma_1\right)\tilde{p}_0+4\tilde{\epsilon}_0\right)\right)\left.\right], \qquad (4.42)
\end{aligned}
$$

$$
M_{42} = \left[A_0^4e^{2\lambda_0}\left(\alpha_0\left(\left(3\Gamma_1-1\right)\tilde{p}_0-\tilde{\epsilon}_0\right)+4\pi r\phi_0'\left(\left(\Gamma_1-1\right)\tilde{p}_0-\tilde{\epsilon}_0\right)\right)\right], \qquad (4.43)
$$

$$M_{43} = e^{2\lambda_0}\Big[- e^{-2\nu_0}\omega^2 - 8\pi\phi_0'^2 + 64\pi^2 r^2 V_0 \phi_0'^2 + A_0^4 \left((-3\beta_0 + 4\pi r\phi_0' \left(\alpha_0 \left(3\Gamma_1 - 10\right)\right.\right.\right.$$
$$\left.\left.\left. + \ 4\pi \left(\Gamma_1 - 3\right) r\phi_0'\right)\right) \tilde{p}_0 + \tilde{\epsilon}_0 \left(\beta_0 + 8\pi r\phi_0' \left(\alpha_0 + 2\pi r\phi_0'\right)\right)\right) + 16\pi r\phi_0' \left.\frac{dV}{d\phi}\right|_{\phi_0}$$
$$+ A_0^4 \alpha_0 \left(\alpha_0 \left(3 \left(3\Gamma_1 - 5\right) \tilde{p}_0 + \tilde{\epsilon}_0\right) + 4\pi \left(3\Gamma_1 - 4\right) r\phi_0' \tilde{p}_0\right) + \left.\frac{d^2V}{d\phi^2}\right|_{\phi_0} \Big] \tag{4.44}$$

$$M_{44} = \frac{4\pi A_0^4 e^{2\lambda_0} r^2 \left(\tilde{p}_0 - \tilde{\epsilon}_0\right) + e^{2\lambda_0} - 8\pi e^{2\lambda_0} r^2 V_0 + 1}{r}. \tag{4.45}$$

4.3.2 Boundary conditions

At the origin

Around $r = 0$, we demand that $\xi(r)$ and $\delta\phi(r)$ admit a Taylor expansion, therefore, equation (4.35) impose that

$$\xi(r) = \xi_1 r + \xi_3 r^3 + ...$$

$$\delta\phi(r) = \delta\phi_0 + \delta\phi_2 r^2 + ...$$

where ξ_1 and $\delta\phi_0$ are free constants and the remaining coefficients are determined in terms of them and the background quantities.

At junctions between polytropic phases

In Eq. (4.33), the term proportional to $\partial\delta p/\partial r$ depends on $\Gamma_1'(r)$, which, in the piecewise polytropic parametrization, is the derivative of a piecewise constant function $\Gamma_1(r) = \Gamma_i - (\Gamma_i - \Gamma_{i+1})\Theta(r - r_t)$ and therefore is a sum of Dirac delta functions at the radii r_t corresponding to transitions between the various polytropic phases. This implies that $\xi'(r)$ will not be continuous, but will experience a jump at each transition radius. To obtain the magnitude of this discontinuity we integrate Eq. (4.33) from $r_t - \epsilon$ to $r_t + \epsilon$, taking the limit $\epsilon \to 0$. We obtain:

$$\Delta_i(\Gamma_1\zeta') = \Delta_i\Gamma_1\{A(\phi_0)^4 r^2 e^{-\nu_0}[\xi\phi_0'(\alpha_0 - 4\pi r\phi_0') - \delta\phi(3\alpha_0 + 4\pi r\phi_0')]\}|_{r=r_i}\,, \tag{4.46}$$

where

$$\zeta \equiv e^{-\nu_0} A(\phi_0)^4 r^2 \xi$$

and $\Delta_i Q \equiv \lim_{\epsilon\to 0}[Q(r_i+\epsilon) - Q(r_i-\epsilon)]$ denotes the discontinuity of a quantity Q across $r = r_i$.

At the stellar surface

At the perturbed surface, the pressure must vanish. The perturbed stellar surface is located at $R_{\rm new} = R + \xi(R)$, therefore $\tilde{p}(R_{\rm new}) = 0$ implies

$$\tilde{p}_0'(R)\xi(R) + \delta\tilde{p}(R) = 0. \tag{4.47}$$

As in GR, the left-hand side automatically vanishes as long as ξ, $\delta\phi$, and their derivatives are finite at $r = R$. Therefore, it suffices to impose regularity of the perturbed variables at $r = R$.

By dividing Eq. (4.33) by $\tilde{p}_0$, it is possible to conclude that the divergent terms when $\tilde{p}_0 \to 0$ are those proportional to $\tilde{\epsilon}_0/\tilde{p}_0$ and $\tilde{\epsilon}_0^2/\tilde{p}_0$. Analyzing Eq. (4.31), the divergent term is proportional to $\tilde{\epsilon}_0^2/\tilde{p}_0$. For a polytropic equation of state, $\tilde{\epsilon}_0/\tilde{p}_0 \propto \tilde{\rho}_0^{1-\Gamma}$ and $\tilde{\epsilon}_0^2/\tilde{p}_0 \propto \tilde{\rho}_0^{2-\Gamma}$, therefore, it is sufficient to impose that the coefficient of $\tilde{\epsilon}_0/\tilde{p}_0$ vanishes for $1 < \Gamma < 2$. This is equivalent to requiring that

$$\begin{aligned}
B(r) = {} & r\phi_0'^{\,2}\beta_0\xi + \xi\alpha_0\left[\phi_0'\left(2\Gamma\left(2\pi r^2\phi_0'^{\,2} + r\nu_0' + 1\right) + 8\pi r^2 e^{2\lambda_0}V - 4\pi r^2\phi_0'^{\,2} - e^{2\lambda_0} - 2r\nu_0' - 3\right)\right. \\
& \left. + re^{2\lambda_0}\left.\frac{dV}{d\phi}\right|_{\phi_0}\right] + \alpha_0 r\left(\Gamma\phi_0'\xi' + \delta\phi'\right) + (3\Gamma - 4)r\phi_0'\alpha_0^2\left(\delta\phi + \phi_0'\xi\right) + \Gamma r\nu_0'\xi' - \Gamma r\nu_0'^{\,2}\xi \\
& + r\delta\phi\left[\phi_0'(\beta_0 + \alpha_0^2) + (\Gamma - 1)\alpha_0\left(3\nu_0' + 4\pi r\phi_0'^2\right)\right] - 4\pi r\phi_0'\delta\phi\left(4\pi r^2\phi_0'^{\,2} - r(\Gamma+1)\nu_0' - 1\right) \\
& - 8\pi^2 r^3\phi_0'^{\,4}\xi + 8\pi r e^{2\lambda_0}V\xi\left(2\pi r^2\phi_0'^{\,2} - 1\right) + 2\pi r\phi_0'^{\,2}\xi\left[2r(\Gamma+1)\nu_0' - e^{2\lambda_0} + 1\right] \\
& + 2\Gamma\nu_0'\xi + 4\pi r^2\phi_0'\delta\phi' - r\nu_0'^{\,2}\xi - 4\nu_0'\xi - 4\pi r^2 e^{2\lambda_0}\delta\phi\left.\frac{dV}{d\phi}\right|_{\phi_0} - \omega^2 r e^{2\lambda_0 - 2\nu_0}\xi
\end{aligned} \tag{4.48}$$

vanishes when evaluated at $r = R$. This gives us the value of $\xi'(R)$ as a function of $\xi(R)$, $\delta\phi(R)$, $\delta\phi'(R)$ and background quantities. It should be noted that the polytropic index Γ in Eq. (4.48) refers, in our piecewise polytropic approximation for the EOS, to the index in the outermost layer of the star.

Outside the star

Outside the star, we neglect perturbations of the atmosphere in which the star may be immersed, and set $\xi = 0$ for $r > R$. Therefore the perturbed scalar field equation reduces to

$$0 = \delta\phi'' + \delta\phi' \frac{1 + e^{2\lambda_0}\left[1 - 8\pi r^2\left(\tilde{\epsilon}_\infty A^4 + V\right)\right]}{r} - e^{2\lambda_0}\delta\phi\Big[4\tilde{\epsilon}_\infty A^4(\beta_0 + \alpha_0^2) + 12\tilde{\epsilon}_\infty A^4\alpha_0^2 + 16\pi r\phi_0'\left(4\tilde{\epsilon}_\infty A^4\alpha_0 + \left.\frac{dV}{d\phi}\right|_{\phi_0}\right) + 8\pi\phi_0'^2\left(8\pi r^2\left(\tilde{\epsilon}_\infty A^4 + V\right) - 1\right) + \left.\frac{d^2V}{d\phi^2}\right|_{\phi_0} - \omega^2 e^{-2\nu_0}\Big]. \tag{4.49}$$

We impose an outgoing boundary condition for the scalar field perturbation:

$$\delta\phi(t, r_c) \propto e^{i\omega(t - r_c)},$$

where r_c denotes the cosmological horizon. For unstable modes, i.e. when $\omega^2 = -\Omega^2 < 0$, this amounts to demanding that $\delta\phi(r) \to 0$ far away from the star.

4.3.3 Numerical Integration

With the boundary conditions specified above, Eq. (4.35) can be solved numerically by standard methods. Note that, in total, we impose four boundary conditions for our perturbed variables: $\delta\phi'(0) = 0$, $\xi(0) = 0$, $B(R) = 0$ and $\delta\phi \to 0$ as $r \gg R$. Since there is an additional overall normalization freedom, the system is overdetermined, and only admits solutions for a discrete (possibly empty) set of frequencies. In this subsection we discuss the numerical procedure to find such frequencies.

We begin by noting that any solution of a homogeneous system of the type

$$\frac{d\mathbf{x}(r)}{dr} = \mathbf{M}(r)\mathbf{x}(r), \tag{4.50}$$

where $\mathbf{M}(r)$ ias a $n \times n$ matrix and $\mathbf{x}(r)$ is a vector, both functions of r, can be expressed as

$$\mathbf{x}(r) = \sum_{\alpha=1}^{n} c_\alpha \mathbf{x}_\alpha(r)$$

where $\mathbf{x}_\alpha$ is a set of linearly independent solutions and c_α are constants. Unlike the

previous numerical integrations, the integration inside the star is started at $r = 0$ and is done until $r = R_m$; similarly, we integrate from the surface, $r = R$, to $r = R_m$, where R_m is some intermediate radius where both solutions are matched. This is done in order to avoid integration in the direction of divergences. In our case, we have a system with $n = 4$, and two sets of solutions, one coming from the origin, $\mathbf{x}^{\rm in}$, and the other from the surface, $\mathbf{x}^{\rm out}$:

$$\mathbf{x}^{\rm in}(r) = c_1\mathbf{x}_1^{\rm in}(r) + c_2\mathbf{x}_2^{\rm in}(r) + c_3\mathbf{x}_3^{\rm in}(r) + c_4\mathbf{x}_4^{\rm in}(r), \tag{4.51}$$

$$\mathbf{x}^{\rm out}(r) = a_1\mathbf{x}_1^{\rm out}(r) + a_2\mathbf{x}_2^{\rm out}(r) + a_3\mathbf{x}_3^{\rm out}(r) + a_4\mathbf{x}_4^{\rm out}(r), \tag{4.52}$$

where c_i and a_i are constants which are fixed by the boundary conditions and by joining both solutions in R_m.

For the integration starting at $r = 0$, if we choose four linearly independent vectors $\mathbf{x}_i^{\rm in}(0)$ such as

$$\begin{aligned}
\mathbf{x}_1^{\rm in}(0) &= (0, 1, 1, 0)^T, \\
\mathbf{x}_2^{\rm in}(0) &= (0, 1, -1, 0)^T, \\
\mathbf{x}_3^{\rm in}(0) &= (1, 1, 1, 0)^T, \\
\mathbf{x}_4^{\rm in}(0) &= (0, 1, 1, 1)^T,
\end{aligned}$$

then the boundary conditions at $r = 0$, which require that $\xi(0) = 0$ and $\delta\phi'(0) = 0$, imply that $c_3 = c_4 = 0$. Therefore, the solution satisfying the boundary conditions at $r = 0$ can be written as $\mathbf{x}^{\rm in}(r) = c_1\mathbf{x}_1^{\rm in}(r) + c_2\mathbf{x}_2^{\rm in}(r)$, where $\mathbf{x}_1^{\rm in}(r)$ and $\mathbf{x}_2^{\rm in}(r)$ are obtained by integrating Eq. (4.35) from $r = 0$ with the initial conditions above, and taking care of the derivative jumps implicated by Eq. (4.46).

Similarly, for the integration starting from the surface, we can find four linearly independent vectors, say

$$\begin{aligned}
\mathbf{x}_1^{\rm out}(R) &= (1, \xi'(R), 1, -1)^T, \\
\mathbf{x}_2^{\rm out}(R) &= (1, \xi'(R), -1, 1)^T, \\
\mathbf{x}_3^{\rm out}(R) &= (1, \xi'(R), 1, 1)^T, \\
\mathbf{x}_4^{\rm out}(R) &= (1, 0, 1, 1)^T.
\end{aligned}$$

where $\xi'(R)$ is obtained in each case by solving $B(R) = 0$, defined in Eq. (4.48), with the values of $\xi(R)$, $\delta\phi(R)$ and $\delta\phi'(R)$ specified in each vector above. Since $\mathbf{x}_4^{\rm out}(R)$ does not satisfy the boundary condition at $r = R$, a_4 must be zero. So the solution satisfying the boundary condition $B(R) = 0$ at $r = R$ is written as $\mathbf{x}^{\rm out}(r) = a_1\mathbf{x}_1^{\rm out}(r) + a_2\mathbf{x}_2^{\rm out}(r) + a_3\mathbf{x}_3^{\rm out}(r)$, with $\mathbf{x}_i^{\rm out}(r)$ obtained from the numerical integration of Eq. (4.35) from $r = R$ inwards, again taking care of the jumps implied by Eq. (4.46).

By matching the solutions $\mathbf{x}^{\rm in}(r)$ and $\mathbf{x}^{\rm out}(r)$ at some intermediate radius, say $r = R/2$, one obtains four algebraic conditions from

$$c_1\mathbf{x}_1^{\rm in}(R/2) + c_2\mathbf{x}_2^{\rm in}(R/2) = a_1\mathbf{x}_1^{\rm out}(R/2) + a_2\mathbf{x}_2^{\rm out}(R/2) + a_3\mathbf{x}_3^{\rm out}(R/2)$$

that must be satisfied by the five arbitrary constants c_1, c_2, a_1, a_2, and a_3. Since the overall normalization of $\mathbf{x}(r)$ is arbitrary, it can be fixed by requiring that $\delta\phi(0) = 1$, which implies $c_2 - c_1 = 1$. This closes the system and enables the computation of the interior solution unequivocally, given a value of ω^2.

Outside the star, only Eq. (4.49) is integrated, this is done with the conditions for $\delta\phi(R)$ and $\delta\phi'(R)$ coming from the solution to the inner integration. We evolve the scalar field equation outside the star, and implement a shooting procedure to find the values of $\omega^2 = -\Omega^2 < 0$ such that condition $\delta\phi(r) \to 0$ as $r \to \infty$ is verified. In this shooting procedure, similarly to the search for the initial condition for equilibrium solutions, the residue space, which in this case is just $\delta\phi(r_{\rm ext})|_{\omega^2} = 0$ far away from the star ($r_{\rm ext} \gg R$), is investigated until it is close enough to zero for the secant method to be used. In the Dilaton model, the value obtained for the frequency is used as an initial guess for the integration of the case in which the initial condition of the field has an opposite sign, thus, the integration time to obtain the frequencies for the thousands of solutions is reduced considerably.

4.3.4 Results

Chameleon

Using the method delineated above, we investigate the radial stability of the equilibrium solutions found previously for the chameleon model. We find no evidence of unstable modes for configurations lying prior to the turning point in the mass-radius diagrams of

Fig. 4.9. As in GR, a marginally stable mode, with $\Omega \approx 0$, is found for the maximum-mass solution, and unstable modes are found for denser configurations, with the instability timescale $\tau \equiv \Omega^{-1}$ decreasing as the central density of the solution increases. Figure 4.12 displays the inverse of the instability timescale τ^{-1} as a function of the total mass for the ENG EoS. The corresponding equilibrium solutions are those lying to the left of the turning point in the mass-radius diagram of the upper-left panel of Fig. 4.9. For the chameleon model as well as in GR, radial instability sets in at the turning point of sequences of equilibria; the magnitude of τ is set by the NS dynamical timescale, $\sqrt{R^3/GM}$, which is of the order of milliseconds.

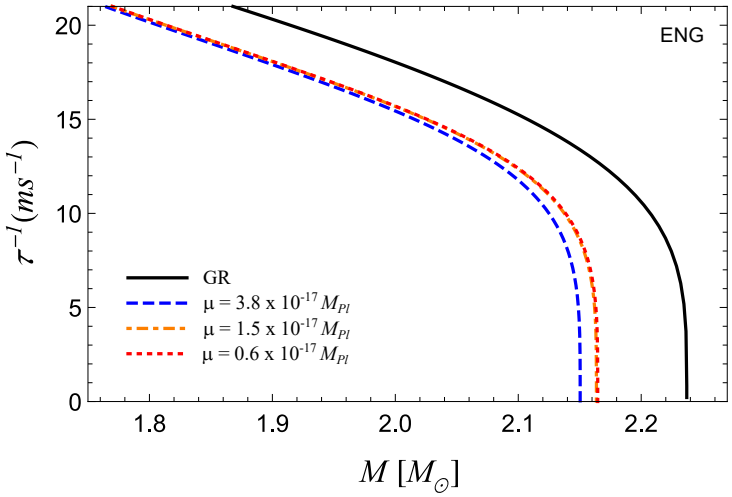

Figure 4.12: Inverse of the instability timescale as a function of total mass for NS solutions described by the ENG equation of state, both in GR and in the chameleon model, with $n = 1$, $\beta = 1$ and the three values of μ specified in the plot. The maximum mass configuration presents a marginally stable mode, while denser configurations are radially unstable.

Our analysis makes it clear that stable, partially unscreened NS configurations can exist in the chameleon model, at least for some realistic EoS. This is in contrast with the conclusion arrived at in Refs. [109, 110] by a less rigorous argument, and raises the interesting possibility of using measurements of the most massive, most compact NSs to further constrain these models.

Dilaton

Since in the dilaton model a wealth of equilibrium solutions were found, an important question that follows is whether and which of them are stable. First, we consider their

dynamical stability under radial perturbations, searching for unstable radial modes (with time dependence $\exp(\Omega t)$, $\Omega > 0$), as described previously. Figure. 4.13 shows the inverse of the instability timescale $\tau^{-1} = \Omega$ as a function of the total mass, for the first few branches of solutions displayed in Fig. 4.10. For each of these branches, we find that the maximum mass configuration is marginally stable (exhibiting a mode with $\Omega \approx 0$) and unstable modes exist for solutions with larger central densities. We find no evidence of unstable modes for solutions with central densities smaller than that of the maximum mass configuration. Branches where the scalar field has a large number n of nodes have an instability timescale very close to the GR values; the same happened for their equilibrium properties (see Fig. 4.10).

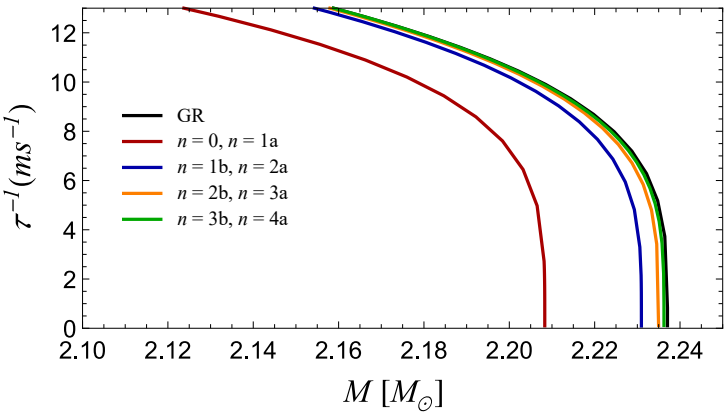

Figure 4.13: Inverse of the instability timescale as a function of total mass for NS solutions in GR and in the dilaton model. The EoS and model parameters are the same as in Fig. 4.10. For readability, we display only the first families of solutions. For a given number of nodes $n > 0$, two branches of solutions are typically found: We denote by "a" ("b") the branch with the largest (smallest) value of $|\phi_c|$. The instability timescale for solutions with $n = 0$ and $n = 1$a (and so on; see plot legend) is indistinguishable in the plot. For each of these branches, the maximum mass configuration presents a marginally stable mode, while denser configurations are radially unstable.

In order to further access the stability of the new solutions present in the dilaton model, we have computed the binding energy $E_b \equiv M_b - M$ as a function of the baryon mass M_b for different branches of equilibrium solutions. For a fixed value of M_b, the solution with $n = 0$ and the one with $n = 1$ and the largest value of $|\phi_c|$, have total masses that are indistinguishable within our numerical accuracy. We find that they are energetically favored over the remaining solutions, since they possess the highest binding energy for fixed baryon mass.

As a final remark, it is worthwhile to mention that, in principle, the validity of the

dilaton model is restricted to values of $\tilde{\phi} - \tilde{\phi}_0$ close to zero. Although the field is indeed small inside equilibrium solutions for low density stars (cf. Fig. 4.10), it can acquire large values inside scalarized solutions, which could call for a study of a more complete model.

Chapter 5

Conclusions

General relativity was created more than a century ago, and since its creation it has been tested and confirmed by several experiments. The theory predicts the existence of black holes, gravitational lenses and gravitational waves, many of these predictions at the time of its creation were believed to be undetectable, after all, it was unimaginable to measure a displacement of 10^{-21}m, as was done by gravitational wave detectors at the present time. In the solar system, the theory passes all tests with praise, solving the problem of the anomalous precession of Mercury's perihelion. Despite the successes, there are several alternative theories of gravity that modify General Relativity by introducing new degrees of freedom to the theory. Such modifications and their predictions are confronted with various experiments in the cosmological and astrophysical regimes.

In this thesis, a class of scalar-tensor theories that presents a screening mechanism was studied. Such mechanism was proposed in order to make the theory evade tests on solar system scales, effectively hiding the scalar field, but allowing the correct cosmological behavior. In Chapter 2 a brief introduction to general relativity was made, exemplifying tests in the solar system and cosmological studies. In Chapter 3, various ways of modifying general relativity were exposed and the screening mechanism was explained. In Chapter 4, the original contribution of this thesis was exposed, where we discuss the effect of the scalar field on the structure and stability of neutron stars.

In the Chameleon model, we saw that, as the potential approaches realistic values, neutron star observables (such as mass and radius) of the low and medium central density stars in the theory tend to those of general relativity. For extreme cases, where $T > 0$ in some region of the star, the observables differ from those of general relativity, no

matter how much the potential decreases. The mass of the scalar field becomes imaginary in the region where $T > 0$. By investigating radial stability, we find no evidence of unstable modes for configurations lying prior to the turning point in the mass-radius diagrams (see Fig. 4.9). As in GR, a marginally stable mode is found for the maximum-mass solution, and unstable modes are found for denser configurations. Therefore, we show that, in contrast with the conclusion arrived at Refs. [109, 110], stable partially unscreened neutron star configurations can exist in the chameleon model.

For the Dilaton model, with $T < 0$ in the center of the star, neutron star observables differ from general relativity by less than 1%. The coupling with matter is in fact very small at $r = 0$, in both $T(r = 0) < 0$ and $T(r = 0) > 0$ cases. As soon as $T > 0$ in some region of the star, more than one initial value of the field satisfying the boundary conditions appears. The solution with no nodes differs from general relativity; however, as the number of nodes increases, the masses and radii of the solutions tend to the general relativity case. In cases where $T > 0$ in some region inside the star, the effective coupling with matter is smaller in the center of the solution with mass and radius closest to General Relativity, but the effective coupling on the surface is approximately the same for all equilibrium solutions of the same central density. In both models, for all EOS, the maximum mass is less than the maximum mass obtained in general relativity. Investigating the radial stability, we find no evidence of unstable modes for solutions with central densities smaller than that of the maximum mass configuration, as in GR. For each of the new branches of solutions, we find that the maximum mass configuration is marginally stable and unstable modes exist for solutions with larger central densities. We also find that large number n of nodes solutions have an instability timescale very close to the GR values.

An interesting development of the present work is to extend the study of radial perturbations—explored here with focus on stability issues—to the stable case, describing neutron star oscillations. In the Newtonian context, it was recently suggested [111] that helioseismology may be a good probe for fifth force effects. In the relativistic scenario, it was shown [112] that, in some scalar-tensor theories that exhibit the scalarization effect, neutron star oscillation frequencies can differ significantly from GR even when structural properties are similar, due to the presence of new families of modes (see also Ref. [113]). In particular, this could leave signatures in the post-merger waveform of a binary NS

merger (see Ref. [114] for an example), which could be observable by next-generation gravitational wave detectors [115].

Bibliography

[1] P. Haensel, A.Y. Potekhin, and D.G. Yakovlev. *Neutron stars 1: Equation of state and structure*. Springer, 2007.

[2] Feryal Özel and Paulo Freire. Masses, Radii, and the Equation of State of Neutron Stars. *Annu. Rev. Astron. Astrophys.*, 54(1):401–440, sep 2016.

[3] Timothy Clifton, Pedro G. Ferreira, Antonio Padilla, and Constantinos Skordis. Modified gravity and cosmology. *Physics Reports*, 513(1-3):1–189, March 2012.

[4] Varun Sahni and Andrzej Krasiński. Republication of: The cosmological constant and the theory of elementary particles (by ya. b. zeldovich). *General Relativity and Gravitation*, 40(7):1557–1591, March 2008.

[5] K. S. Stelle. Renormalization of higher-derivative quantum gravity. *Physical Review D*, 16(4):953–969, August 1977.

[6] Israel Quiros. Selected topics in scalar–tensor theories and beyond. *International Journal of Modern Physics D*, 28(07):1930012, May 2019.

[7] Philippe Brax. Screening mechanisms in modified gravity. *Classical and Quantum Gravity*, 30(21):214005, oct 2013.

[8] Philippe Brax, Carsten van de Bruck, Anne-Christine Davis, and Douglas Shaw. Dilaton and modified gravity. *Physical Review D*, 82(6), September 2010.

[9] Justin Khoury and Amanda Weltman. Chameleon Fields: Awaiting Surprises for Tests of Gravity in Space. *Phys. Rev. Lett.*, 93(17):171104, oct 2004.

[10] Dylan M. Podkowka, Raissa F. P. Mendes, and Eric Poisson. Trace of the energy-momentum tensor and macroscopic properties of neutron stars. *Phys. Rev. D*, 98(6):064057, sep 2018.

[11] Bernardo F. de Aguiar and Raissa F. P. Mendes. Highly compact neutron stars and screening mechanisms: Equilibrium and stability. *Physical Review D*, 102(2), July 2020.

[12] W. M. Smart. On the motion of the perihelion of mercury. *Monthly Notices of the Royal Astronomical Society*, 82(1):12–19, November 1921.

[13] Mari E. W. Williams. Physics and its concepts - n. t. roseveare, mercurys perihelion from le verrier to einstein. oxford: Oxford university press, 1982. pp. viii 208. ISBN 0-19-858174-2. £20.00. *The British Journal for the History of Science*, 17(2):225–226, July 1984.

[14] James D. Wells. When effective theories predict: the inevitability of mercury's anomalous perihelion precession, 2011.

[15] Charles W. Misner, K.S. Thorne, and J.A. Wheeler. *Gravitation*. W. H. Freeman, San Francisco, 1973.

[16] Galileo Galilei. Discourses and mathematical demonstrations concerning two new sciences, 1638.

[17] Isaac Newton. The principia: Mathematical principles of natural philosophy, 1999.

[18] Irwin I. Shapiro, Charles C. Counselman, and Robert W. King. Verification of the principle of equivalence for massive bodies. *Physical Review Letters*, 36(11):555–558, March 1976.

[19] Some experiments on the proportionality of mass and weight. *Proceedings of the Royal Society of London. Series A, Containing Papers of a Mathematical and Physical Character*, 104(728):588–610, December 1923.

[20] A determination of the ratio of mass to weight for a radioactive substance. *Proceedings of the Royal Society of London. Series A, Containing Papers of a Mathematical and Physical Character*, 84(571):325–344, October 1910.

[21] T. M. Niebauer, M. P. McHugh, and J. E. Faller. Galilean test for the fifth force. *Physical Review Letters*, 59(6):609–612, August 1987.

[22] S. Schlamminger, K.-Y. Choi, T. A. Wagner, J. H. Gundlach, and E. G. Adelberger. Test of the equivalence principle using a rotating torsion balance. *Phys. Rev. Lett.*, 100:041101, Jan 2008.

[23] T A Wagner, S Schlamminger, J H Gundlach, and E G Adelberger. Torsion-balance tests of the weak equivalence principle. *Classical and Quantum Gravity*, 29(18):184002, aug 2012.

[24] Sean M. Carroll. *Spacetime and Geometry: An Introduction to General Relativity*. Cambridge University Press, 2019.

[25] John D. Norton. Einstein, nordstrom and the early demise of scalar, lorentz-covariant theories of gravitation. *Archive for History of Exact Sciences*, 45(1):17–94, 1992.

[26] G.G. Nyambuya. An attempt at a revival of nordström's first theory of gravitation. *New Astronomy*, 67:16–21, February 2019.

[27] A. Einstein and A.D. Fokker. *Die Nordströmsche Gravitationstheorie vom Standpunkt des absoluten Differentialkalküls*. Ann. d. Phys, 1914.

[28] Gonzalo J. Introduction to modified gravity: From the cosmic speedup problem to quantum gravity phenomenology. In *Aspects of Todays Cosmology*. InTech, September 2011.

[29] Robert M. Wald. *General Relativity*. University of Chicago Press, 1984.

[30] Ray Inverno. *Introducing Einstein's relativity*. Clarendon Press Oxford University Press, Oxford England New York, 1992.

[31] Albert Einstein. *Cosmological Considerations in the General Theory of Relativity*. Princeton University Press, 1917.

[32] Christopher Smeenk. Einstein's role in the creation of relativistic cosmology. In *The Cambridge Companion to Einstein*, pages 228–269. Cambridge University Press, May 2014.

[33] Cormac O'Raifeartaigh, Michael O'Keeffe, Werner Nahm, and Simon Mitton. Einstein's 1917 static model of the universe: a centennial review. *The European Physical Journal H*, 42(3):431–474, July 2017.

[34] Willem de Sitter. On the relativity of inertia. Remarks concerning Einstein's latest hypothesis. *Koninklijke Nederlandse Akademie van Wetenschappen Proceedings Series B Physical Sciences*, 19:1217–1225, March 1917.

[35] Matteo Realdi and Giulio Peruzzi. Einstein, de sitter and the beginning of relativistic cosmology in 1917. *General Relativity and Gravitation*, 41(2):225–247, July 2008.

[36] K. Schwarzschild. On the gravitational field of a mass point according to einstein's theory. 1999.

[37] Clifford M. Will. *Theory and Experiment in Gravitational Physics*. Cambridge University Press, September 2018.

[38] Clifford M. Will. The confrontation between general relativity and experiment. *Living Reviews in Relativity*, 17(1), June 2014.

[39] Steven Weinberg. *Gravitation and cosmology : principles and applications of the general theory of relativity*. Wiley, New York, 1972.

[40] Varun Sahni. 5 dark matter and dark energy. In *The Physics of the Early Universe*, pages 141–179. Springer Berlin Heidelberg, December 2004.

[41] A. Zonca *et al.* Planck2013 results. i. overview of products and scientific results. *Astronomy & Astrophysics*, 571:A1, October 2014.

[42] M. Milgrom. A modification of the newtonian dynamics as a possible alternative to the hidden mass hypothesis. *The Astrophysical Journal*, 270:365, July 1983.

[43] J W Moffat. Scalar–tensor–vector gravity theory. *Journal of Cosmology and Astroparticle Physics*, 2006(03):004–004, March 2006.

[44] Sean M. Carroll. Dark energy and the preposterous universe, 2001.

[45] Planck Collaboration and A. Zonca *et al.* Planck 2018 results. vi. cosmological parameters, 2018.

[46] Hironari Miyazawa. Baryon number changing currents. *Progress of Theoretical Physics*, 36(6):1266–1276, December 1966.

[47] Steven Weinberg. The Cosmological Constant Problem. *Rev. Mod. Phys.*, 61:1–23, 1989.

[48] Ivaylo Zlatev, Limin Wang, and Paul J. Steinhardt. Quintessence, cosmic coincidence, and the cosmological constant. *Phys. Rev. Lett.*, 82:896–899, Feb 1999.

[49] A Zee. *Quantum field theory in a nutshell.* Princeton University Press, Princeton, N.J, 2010.

[50] K. S. Stelle. Renormalization of higher-derivative quantum gravity. *Phys. Rev. D*, 16:953–969, Aug 1977.

[51] The singularities of gravitational collapse and cosmology. *Proceedings of the Royal Society of London. A. Mathematical and Physical Sciences*, 314(1519):529–548, January 1970.

[52] Justin Khoury. Chameleon field theories. *Classical and Quantum Gravity*, 30(21):214004, October 2013.

[53] David Lovelock. The einstein tensor and its generalizations. *Journal of Mathematical Physics*, 12(3):498–501, March 1971.

[54] David Lovelock. The four-dimensionality of space and the einstein tensor. *Journal of Mathematical Physics*, 13(6):874–876, June 1972.

[55] Emanuele Berti, Enrico Barausse, Vitor Cardoso, Leonardo Gualtieri, Paolo Pani, Ulrich Sperhake, Leo C Stein, Norbert Wex, Kent Yagi, Tessa Baker, C P Burgess, Flávio S Coelho, Daniela Doneva, Antonio De Felice, Pedro G Ferreira, Paulo C C Freire, James Healy, Carlos Herdeiro, Michael Horbatsch, Burkhard Kleihaus, Antoine Klein, Kostas Kokkotas, Jutta Kunz, Pablo Laguna, Ryan N Lang, Tjonnie G F Li, Tyson Littenberg, Andrew Matas, Saeed Mirshekari, Hirotada Okawa, Eugen Radu, Richard O'Shaughnessy, Bangalore S Sathyaprakash, Chris Van Den

Broeck, Hans A Winther, Helvi Witek, Mir Emad Aghili, Justin Alsing, Brett Bolen, Luca Bombelli, Sarah Caudill, Liang Chen, Juan Carlos Degollado, Ryuichi Fujita, Caixia Gao, Davide Gerosa, Saeed Kamali, Hector O Silva, João G Rosa, Laleh Sadeghian, Marco Sampaio, Hajime Sotani, and Miguel Zilhao. Testing general relativity with present and future astrophysical observations. *Classical and Quantum Gravity*, 32(24):243001, dec 2015.

[56] Petr Hořava. Quantum gravity at a lifshitz point. *Phys. Rev. D*, 79:084008, Apr 2009.

[57] Ted Jacobson. Einstein-aether gravity: A Status report. *PoS*, QG-PH:020, 2007.

[58] Clifford M. Will and Jr. Nordtvedt, Kenneth. Conservation Laws and Preferred Frames in Relativistic Gravity. I. Preferred-Frame Theories and an Extended PPN Formalism. , 177:757, November 1972.

[59] Sean M. Carroll and Eugene A. Lim. Lorentz-violating vector fields slow the universe down. *Phys. Rev. D*, 70:123525, Dec 2004.

[60] Kent Yagi, Diego Blas, Enrico Barausse, and Nicolás Yunes. Constraints on einstein-æther theory and hořava gravity from binary pulsar observations. *Phys. Rev. D*, 89:084067, Apr 2014.

[61] Kent Yagi, Diego Blas, Nicolás Yunes, and Enrico Barausse. Strong binary pulsar constraints on lorentz violation in gravity. *Physical Review Letters*, 112(16), April 2014.

[62] M. Henneaux and C. Teitelboim. The Cosmological Constant and General Covariance. *Phys. Lett. B*, 222:195–199, 1989.

[63] Richard Woodard. Avoiding dark energy with 1/r modifications of gravity. In *Lecture Notes in Physics*, pages 403–433. Springer Berlin Heidelberg.

[64] R. Utiyama and Bryce S. DeWitt. Renormalization of a classical gravitational field interacting with quantized matter fields. *J. Math. Phys.*, 3:608–618, 1962.

[65] Alexei A. Starobinsky. A New Type of Isotropic Cosmological Models Without Singularity. *Adv. Ser. Astrophys. Cosmol.*, 3:130–133, 1987.

[66] Thomas P. Sotiriou and Valerio Faraoni. $f(r)$ theories of gravity. *Rev. Mod. Phys.*, 82:451–497, Mar 2010.

[67] John D. Barrow and S. Cotsakis. Inflation and the conformal structure of higher-order gravity theories. *Physics Letters B*, 214(4):515–518, December 1988.

[68] E. Pechlaner and R. Sexl. On quadratic lagrangians in general relativity. *Communications in Mathematical Physics*, 2(1):165–175, December 1966.

[69] Timothy Clifton. Parametrized post-newtonian limit of fourth-order theories of gravity. *Phys. Rev. D*, 77:024041, Jan 2008.

[70] Paolo Pani, Thomas P. Sotiriou, and Daniele Vernieri. Gravity with Auxiliary Fields. *Phys. Rev. D*, 88(12):121502, 2013.

[71] Máximo Bañados and Pedro G. Ferreira. Eddington's theory of gravity and its progeny. *Phys. Rev. Lett.*, 105:011101, Jul 2010.

[72] OSKAR KLEIN. The atomicity of electricity as a quantum theory law. *Nature*, 118(2971):516–516, October 1926.

[73] Gunnar Nordström. On the possibility of unifying the electromagnetic and the gravitational fields. 2007.

[74] Mariana Graña. Flux compactifications in string theory: A comprehensive review. *Physics Reports*, 423(3):91–158, January 2006.

[75] Leonard Susskind. The anthropic landscape of string theory, 2003.

[76] M. Gasperini, F. Piazza, and G. Veneziano. Quintessence as a runaway dilaton. *Physical Review D*, 65(2), December 2001.

[77] T. Damour, F. Piazza, and G. Veneziano. Violations of the equivalence principle in a dilaton-runaway scenario. *Physical Review D*, 66(4), August 2002.

[78] Michael B. Green, John H. Schwarz, and Edward Witten. *Superstring Theory.* Cambridge University Press, 2009.

[79] T. Damour and A.M. Polyakov. The string dilation and a least coupling principle. *Nuclear Physics B*, 423(2-3):532–558, July 1994.

[80] Thibault Damour, Federico Piazza, and Gabriele Veneziano. Runaway dilaton and equivalence principle violations. *Phys. Rev. Lett.*, 89:081601, Aug 2002.

[81] C. Brans and R. H. Dicke. Mach's principle and a relativistic theory of gravitation. *Phys. Rev.*, 124:925–935, Nov 1961.

[82] Peter G. Bergmann. Comments on the scalar-tensor theory. *International Journal of Theoretical Physics*, 1(1):25–36, May 1968.

[83] C. G. Callan, D. Friedan, E. J. Martinec, and M. J. Perry. Strings in background fields. *Nuclear Physics B*, 262(4):593–609, December 1985.

[84] E.S. Fradkin and A.A. Tseytlin. Quantum string theory effective action. *Nuclear Physics B*, 261:1 – 27, 1985.

[85] Gerhard Lyra. ber eine modifikation der riemannschen geometrie. *Mathematische Zeitschrift*, 54(1):52–64, March 1951.

[86] Andreas Schärer, Raymond Angélil, Ruxandra Bondarescu, Philippe Jetzer, and Andrew Lundgren. Testing scalar-tensor theories and parametrized post-newtonian parameters in earth orbit. *Physical Review D*, 90(12), December 2014.

[87] B. Bertotti, L. Iess, and P. Tortora. A test of general relativity using radio links with the Cassini spacecraft. , 425(6956):374–376, September 2003.

[88] Jean-Philippe Uzan. Varying constants, gravitation and cosmology. *Living Reviews in Relativity*, 14(1), March 2011.

[89] Thibault Damour and Kenneth Nordtvedt. General relativity as a cosmological attractor of tensor-scalar theories. *Phys. Rev. Lett.*, 70:2217–2219, Apr 1993.

[90] Justin Khoury and Amanda Weltman. Chameleon fields: Awaiting surprises for tests of gravity in space. *Physical Review Letters*, 93(17), October 2004.

[91] Justin Khoury and Amanda Weltman. Chameleon cosmology. *Physical Review D*, 69(4), February 2004.

[92] Debarati Chatterjee and Isaac Vidaña. Do hyperons exist in the interior of neutron stars? *Eur. Phys. J. A*, 52(2):29, 2016.

[93] Katerina Chatziioannou and Sophia Han. Studying strong phase transitions in neutron stars with gravitational waves. *Phys. Rev. D*, 101:044019, Feb 2020.

[94] N.K. Glendenning. Phase transitions and crystalline structures in neutron star cores. *Phys. Rept.*, 342:393–447, 2001.

[95] John Antoniadis, Paulo C. C. Freire, Norbert Wex, Thomas M. Tauris, Ryan S. Lynch, Marten H. van Kerkwijk, Michael Kramer, Cees Bassa, Vik S. Dhillon, Thomas Driebe, Jason W. T. Hessels, Victoria M. Kaspi, Vladislav I. Kondratiev, Norbert Langer, Thomas R. Marsh, Maura A. McLaughlin, Timothy T. Pennucci, Scott M. Ransom, Ingrid H. Stairs, Joeri van Leeuwen, Joris P. W. Verbiest, and David G. Whelan. A massive pulsar in a compact relativistic binary. *Science*, 340(6131), 2013.

[96] Fronefield Crawford, Mallory S. E. Roberts, Jason W. T. Hessels, Scott M. Ransom, Margaret Livingstone, Cindy R. Tam, and Victoria M. Kaspi. A survey of 56 midlatitude EGRET error boxes for radio pulsars. *The Astrophysical Journal*, 652(2):1499–1507, dec 2006.

[97] M. Linares, T. Shahbaz, and J. Casares. Peering into the dark side: Magnesium lines establish a massive neutron star in PSR j22155135. *The Astrophysical Journal*, 859(1):54, may 2018.

[98] Feryal Özel and Paulo Freire. Masses, radii, and the equation of state of neutron stars. *Annual Review of Astronomy and Astrophysics*, 54(1):401–440, 2016.

[99] R Gamba, J S Read, and L E Wade. The impact of the crust equation of state on the analysis of GW170817. *Classical and Quantum Gravity*, 37(2):025008, dec 2019.

[100] LIGO and Virgo Collaborations. GW170817: Measurements of Neutron Star Radii and Equation of State. *Phys. Rev. Lett.*, 121(16):161101, oct 2018.

[101] Gordon Baym, Tetsuo Hatsuda, Toru Kojo, Philip D Powell, Yifan Song, and Tatsuyuki Takatsuka. From hadrons to quarks in neutron stars: a review. *Reports on Progress in Physics*, 81(5):056902, mar 2018.

[102] Mark Alford, Matt Braby, M.W. Paris, and Sanjay Reddy. Hybrid stars that masquerade as neutron stars. *Astrophys. J.*, 629:969–978, 2005.

[103] Charles Alcock, Edward Farhi, and Angela Olinto. Strange Stars. , 310:261, November 1986.

[104] Phillippe Jetzer. Boson stars. , 220(4):163–227, November 1992.

[105] Jocelyn S. Read, Benjamin D. Lackey, Benjamin J. Owen, and John L. Friedman. Constraints on a phenomenologically parametrized neutron-star equation of state. *Phys. Rev. D*, 79:124032, Jun 2009.

[106] Jocelyn Read, Benjamin Lackey, Benjamin Owen, and John L. Friedman. Constraints on a phenomenologically parametrized neutron-star equation of state. *Phys. Rev. D*, 79(12):124032, jun 2009.

[107] Rudolf Kippenhahn. *Stellar structure and evolution.* Springer, Berlin New York, 2013.

[108] Thibault Damour and Gilles Esposito-Farèse. Nonperturbative strong-field effects in tensor-scalar theories of gravitation. *Phys. Rev. Lett.*, 70(15):2220–2223, apr 1993.

[109] Eugeny Babichev and David Langlois. Relativistic stars in f (R) and scalar-tensor theories. *Phys. Rev. D*, 81(12):124051, jun 2010.

[110] Philippe Brax, Anne-Christine Davis, and Rahul Jha. Neutron stars in screened modified gravity: Chameleon versus dilaton. *Phys. Rev. D*, 95(8):083514, apr 2017.

[111] Ippocratis D. Saltas and Ilídio Lopes. Obtaining Precision Constraints on Modified Gravity with Helioseismology. *Phys. Rev. Lett.*, 123(9):091103, aug 2019.

[112] Raissa F. P. Mendes and Néstor Ortiz. New Class of Quasinormal Modes of Neutron Stars in Scalar-Tensor Gravity. *Phys. Rev. Lett.*, 120(20):201104, may 2018.

[113] Jose Luis Blázquez-Salcedo, Fech Scen Khoo, and Jutta Kunz. Ultra long lived quasinormal modes of neutron stars in r^2 gravity, 2020.

[114] Laura Sagunski, Jun Zhang, Matthew C. Johnson, Luis Lehner, Mairi Sakellariadou, Steven L. Liebling, Carlos Palenzuela, and David Neilsen. Neutron star mergers as a probe of modifications of general relativity with finite-range scalar forces. *Phys. Rev. D*, 97(6):064016, mar 2018.

[115] Andoni Torres-Rivas, Katerina Chatziioannou, Andreas Bauswein, and James Alexander Clark. Observing the post-merger signal of gw170817-like events with improved gravitational-wave detectors. *Phys. Rev. D*, 99:044014, Feb 2019.